

Artificial Broadcasts as Galactic Populations: II. Comparing Individualist and Collective Bounds on Broadcast Populations in Single Galaxies

BRIAN C. LACKI¹

¹*Breakthrough Listen, Department of Astronomy, University of California Berkeley, Berkeley CA 94720*

ABSTRACT

The search for extraterrestrial intelligence includes efforts to constrain populations of artificial broadcasts in other galaxies. Previous efforts use individualist methods, searching for single broadcasts with high signal-to-noise ratio. These would be detected as observables with extreme values. This approach is limited to very bright broadcasts and also is subject to confusion, where a large number of broadcasts blend together to form a noise continuum. The mean value of the total emission provides an additional collective bound: the luminosity of the transmitters is no higher than the galaxy’s observed luminosity. Using the framework developed in Paper I, I evaluate how confusion affects individualist searches. I then compare individualist and collective approaches for radio broadcasts from the Milky Way, M31, and three Virgo Cluster elliptical galaxies. For current observations, confusion blurs narrowband radio broadcasts together in the Virgo ellipticals when there is one broadcast per gigahertz per 1000 stars. The collective bound implies fewer than $\sim 10^6 (\bar{\ell}/10^{13} \text{ W})^{-1}$ L-band broadcasts per star gigahertz GHz in the Milky Way and is about 10 and 400 times stronger in M31 and M59, respectively. Applying the collective bound to the far-infrared–radio correlation yields constraints on radio broadcast populations in star-forming galaxies throughout the Universe. The collective bound allows us to rule out large regions of broadcast population parameter space even for distant galaxies. It also imposes constraints on gamma-ray, neutrino, and gravitational-wave broadcasts in the nearest galaxies.

Keywords: Search for extraterrestrial intelligence – Technosignatures – Galaxy luminosities – Astronomical techniques – Radio astronomy — Spatial point processes

1. INTRODUCTION

A central debate in the search for extraterrestrial intelligence (SETI; Tarter 2001; Worden et al. 2017) is whether interstellar travel boosts the number of broadcasting societies. Although realistic travel times between the stars are long, they are miniscule compared to the age of the Galaxy. If ETI societies can reliably replicate through interstellar travel and any have the motivation, then the Galaxy could be covered within about a hundred million years (e.g., Jones 1981; Wright et al. 2014b; Carroll-Nellenback et al. 2019). Essentially, the Galaxy would experience a “phase transition” between unpopulated wilderness and a “metasociety” of densely packed ETIs (Paper I, Lacki 2024 in press; compare Kuiper & Morris 1977 and Ćirković & Vukotić 2008). The apparent lack of evidence for so widespread ETIs in the Milky Way and its implications is the subject of much debate (Brin 1983; Webb 2015; Ćirković 2018; Forgan 2019; Lingam & Loeb 2021).

Less attention has focused on the technosignature properties of other galaxies if this reasoning is correct, aside from searches for megastructure populations (Annis 1999; Voros 2013; Wright et al. 2014b; Zackrisson et al. 2015). If ETIs are rare but establish a vast number of societies when they occur, then some galaxies may be heavily populated while others are uninhabited. This should carry over to their technosignatures – some galaxies would be entirely barren of them, while others would be brimming with the signs of billions of inhabited worlds. A negative SETI result for one galaxy might mean nothing for another (Paper I).

This paper considers the constraints we can set on broadcasts from an individual galactic metasociety. Thus far, radio and optical SETI surveys treat broadcasts as potential rare anomalies that must be sifted out from natural sources, noise, and local interference, employing strategies that look for *individual* candidates that stick out from this background (e.g., Oliver & Billingham 1971; Howard et al. 2004; Enriquez et al. 2017). The individualist approach exploits extreme values in the broadcast population statistics. This paper introduces a complementary *collective* approach of using the integrated luminosity of the population: all the

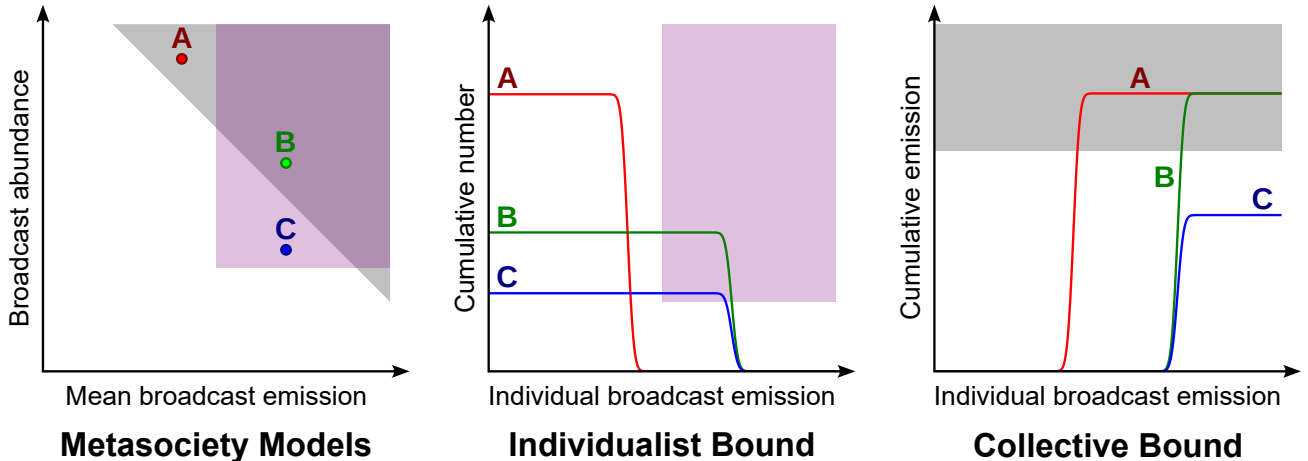


Figure 1. A sketch of how individualist and collective bounds probe the broadcast luminosity distribution in different ways. On left is a standard luminosity vs. abundance plot for broadcasts, as seen in many SETI papers. There is a single individualist bound (purple), a result from a typical SETI search, which rules out model metasocieties B and C. A collective bound (grey) rules out model metasocieties A and B. The middle (individualist) and right (collective) panels show the relevant cumulative distributions. Any distribution that touches the shaded regions is ruled out. The individualist bound is a very sensitive probe of the cumulative number of broadcasts *brighter* than a luminosity sensitivity, but it has no sensitivity below that, even if there are very many broadcasts as in model A. Not shown are the effects of confusion, which happens when broadcasts are so numerous as to blend together. The collective bound is weakly sensitive to populations of all luminosities but is unable to constrain model C, where there is a moderate number of very bright broadcasts. Note that the collective bound’s “power” is the same for models A and B, despite A having far more broadcasts, because those broadcasts are much dimmer.

broadcasts in the galaxy put together cannot outshine the galaxy’s observed total emission (Figure 1).

Constraints based on aggregate emission are a general strategy for noticing and setting limits on new or unknown phenomena (e.g., [Greggio & Renzini 1990](#); [Draine & Lazarian 1998](#)), particularly in astroparticle physics (as in [Spekkens et al. 2013](#); [Geringer-Sameth et al. 2015](#)). In SETI, they let us trade abundance with brightness – a given aggregate luminosity can be achieved by a few very bright broadcasts or a great many faint ones – and allow us to constrain faint transmissions even in distant galaxies. The collective emission of an ETI population can also be relatively insensitive to the detailed properties of individual transmissions thanks to the central limit theorem. We can use the collective bound to set limits on signals that do not remotely resemble the classical pulses or carrier waves ([Kardashev 1964](#); [Caves & Drummond 1994](#); [Lacki 2015a](#)), even ones that look like white noise, obviating the need for a “magic frequency” or “magic basis.” Finally, they are not subject to confusion: when an observation covers many broadcasts, they can all blend together into a noisy background with none individually detectable. It is this quasi-continuum that collective bounds best constrain.

Indeed, the collective approach follows in the footsteps of searches for [Kardashev \(1964\)](#) Type III societies in other galaxies. This branch of SETI seeks the collective effects of millions of inhabited solar systems on the galaxy as a whole, like the waste heat or stellar obscu-

ration from populations of megastructures. Obviously no such ubiquitous population exists in the Milky Way ([Jugaku & Nishimura 2004](#); [Carrigan 2009](#); [Suazo et al. 2022](#)), but this does not preclude Type III societies in other galaxies ([Wright et al. 2014b](#)).

I present a comparison of the relative strengths and weaknesses of the individualist and collective bounds for radio broadcasts in individual galaxies, including a discussion on confusion. Although the focus here is on galaxy-wide populations, collective bounds could be applied to individual stars or planets, even in the absence of interstellar travel. For example, Earth has a multitude of radio transmitters ([Sullivan et al. 1978](#)), which could become so numerous and wideband as to be hopelessly confused – yet Earth could still appear anomalous if it is far too radio-bright for a terrestrial planet.

1.1. Outline of Paper II

The formalism of Paper I is reviewed in Section 2, and then applied to the measured aggregate emission of metasocieties in Section 3. The next three sections deal with the individualist, signal-to-noise-based constraints on ETI broadcasts and how they are weakened by confusion: general considerations in Section 4, then the signal-to-noise ratio for radio broadcasts in Section 5 and optical broadcasts in Section 6. The collective bound is explained in Section 7. I consider the relative merits of individualist surveys and the collective bounds for some nearby galaxies in Section 8. Section 9 expands the discussion of the collective bound to distant galaxies across

the spectrum. The conclusions, in Section 10, are followed by several appendices with detailed derivations.

2. REVIEW OF CONCEPTS

Paper I developed a treatment of ETI populations, but this section reviews basic results used in this paper. At the heart of the formalism is the idea of describing broadcasts and their host societies with random variables. Random variables are a very flexible concept – even a deterministic quantity can be viewed as a random variable with a degenerate distribution. It is likely that at least some properties of technosignatures are unpredictable to us. The time and circumstances in which an ETI evolves on a planet, the exact times it chooses to broadcast and for how long, and the random locations of stars in a galaxy are all contingent, and are among the motivations for a statistical treatment.

Table 1 is a key to the most commonly used variables and notation in the paper.

2.1. *Objects: From the universe to broadcasts*

The framework interprets populations as nodes on a tree, each level representing a different type of object. Parent objects may host child objects, which form a population of the child level’s type. In variables, each type of object is denoted by an uppercase level (J, K, and L for arbitrary types to describe general relations). The object trees are random but can be characterized statistically. The tree is rooted in the model universe (type U), which contains all other objects, and then has four levels of objects below it. The universe contains galaxies (object type G), which in this work are assumed to totally confine ETIs, even with interstellar travel.¹

ETIs have the capacity to reproduce themselves, their infrastructure and environments, and their technosignatures. A *metasociety* (object type M) is a collection of ETIs generally sharing a common origin or influence, and can comprise one or many worlds. All of the societies originating from a single origin through replication share a metasociety. Depending on the scenario, we may treat the galaxy as having one unified metasociety or many small ones (see Paper I). Metasocieties embody the “phase transition” of a galaxy going from uninhabited to fully populated.

A *society* (object type C) is a localized ETI with its infrastructure, capable of producing technosignatures. A natural interpretation is that of a single world or planetary system, although isolated facilities in interstellar space making broadcasts can also count as societies.

¹ If there is enough communication or travel between galaxies to allow for intergalactic metasocieties, that could allow for homogenization, in which case the constraints that apply for one galaxy could apply to its neighbors. However, it could also mean that all galaxies near the Milky Way are atypical and that their technosignature properties do not reflect those of the Universe at large.

A *broadcast* (object type B) is an emission of radiation produced as the technosignature of a society. These include deliberate attempts at communication with other (meta)societies, leakage, and even noncommunicative releases of energy. Broadcasts are characterized by their time and frequency ranges, among other properties.

The objects, as nodes on the tree, can be treated in two ways. Sometimes we want to consider objects that are known or postulated to exist, like the Milky Way or the Arecibo message. These are realized objects, and their properties have fixed values. They are labeled either using an obvious designation for the object in question (e.g., MW for the Milky Way), or by the lowercase letter for the object’s type (e.g., m for a generic realized metasociety). Often, however, we will consider objects whose properties are general random variables. These are random objects, labeled by the uppercase letter for the object’s type (e.g., M for a random metasociety). Variables can describe both realized and random objects, and both types can be considered hosts of descendant objects, so most relations that work for one kind work for the other (see Paper I for technicalities).

The tree structure accounts for the influences between the objects, with influences running from parent to child instead of between “siblings.” A key assumption of this work is that the properties of all the children objects of a parent are independent of each other, conditionalized on the properties of the host. For example, the active times of broadcasts from a single society are not independent, because if we know when one happens, we have an idea when the society was active and a guess for when it made other broadcasts. But if we already know when the society was active, knowing the time of one broadcast provides no new information. The basic motivation for this is that it lets us treat the effects of shared history or influence between objects while using assumptions of (conditional) independence to simplify analysis. Thus, all the broadcasts in a society may be at a single designated frequency; this is viewed as a property of the society that all the broadcasts independently draw on, rather than a dependent shared property of the broadcasts. This conditional independence allows us to invoke certain results like the central limit theorem, which applies to the sum of all the emission from individual broadcasts, and then applies again to the sum of the emission from all the societies.

2.2. *Haystacks and point processes*

The intrinsic properties of each object J are given by a tuple of parameters w_J . Programs like SETI that seek out rare objects in a vast abstract space of possibilities often refer to seeking these out as “needles in a cosmic haystack” (Wright et al. 2018; see also Harwit 1981; Djorgovski et al. 2013. In allusion to this, the parameter space of all tuples for each object type J is its *haystack*, denoted W^J . For example, the broadcast haystack’s dimensions include the bandwidth, duration,

Table 1. Summary of notation used

Notation	Explanation
$\mathbb{I}[E]$	Indicator variable for event E , is 1 if the event occurs and 0 otherwise
$F[X](x), \Psi[X](x)$	Cumulative distribution function (CDF) and probability density function (PDF) for random variable X , evaluated at x
$\langle X \rangle$	Mean of random variable X ; by default, is a simple mean
$\mathbb{V}[X], \mathbb{V}^{1/2}[X]$	Variance and standard deviation of random variable X ; by default, are the simple operations
$\mathbb{M}[X]$	Median of random variable X
x, y	Generic window
μ, \circ, π, s	Windows for a mode, observation, pointing, and survey, respectively
$t(t)$	Window picking all objects active at a given time t
S_y^x, N_y^x	Set of x -type windows that make up y , and the number of windows in that set
$T_x, \Theta_x, B_x, \Upsilon_x, \Delta_x, \Pi_x, \Omega_x, V_x$	Quantities defining a window x : its duration, starting time, bandwidth, central frequency, effective drift rate (used in dedrifting), set of polarizations covered, sky field covered, physical volume sampled
(x, K)	Selection that picks objects hosted by K according to window x
w_J	Parameter tuple describing object J ; the space of all such tuples is the J -haystack W^J
$\Psi_{x,K}^J$	Distribution (intensity) of w_J over W^J for the population that would be selected by (x, K)
$\Sigma_{x,K}^J, N_{x,K}^J$	Sample of J -type objects drawn by (x, K) and the number of objects in that sample
$\kappa_{x J}$	Generic singleton random variable describing an object J , with the quantity integrated over the window x ; when no window is given, the ∞ window is assumed by default
$K_{x,K}^J$	Generic aggregate random variable describing the sum of $\kappa_{x J}$ for all objects selected by (x, K)
$\kappa_{x J}^{[y,K]}$	Random variable $\kappa_{x J}$ regularized to only include values likely to occur in a sample drawn by (y, K) ; an aggregate variable can be regularized too.
$\mathbb{O}[\kappa_{x J}]_{y,K}$	Selection-relative operation of $\kappa_{x J}$: describes the distribution when considering the entire population of objects drawn by the selection (y, K) , instead of for a single object J . Operations that can stand in for \mathbb{O} include the CDF, PDF, minima, maxima, mean, and variance. An aggregate variable can be substituted for $\kappa_{x J}$. When no window is given, it is inherited from the variable (x here).
$\mathbb{O}[\kappa_{x_i J}]_y$	Multiwindow operation \mathbb{O} , ranging over all windows x_i in y
$\mathcal{I}_{\mathfrak{M};x}$	Instrumental response; normalized to 1 and assumed to depend only on sky position
$N_{x,g}^*$	Number of stars covered by window x in galaxy g
Ξ_M^C	Abundance of societies per star in metasociety M
$\Xi_M^B(t, \nu), Z_M^B(t, \nu)$	Mean number of broadcasts per star active at time t and frequency ν in metasociety M , and similarly for the mean number per unit frequency per star
$N_{x,M}^{B;n}$	Count of broadcasts in $\Sigma_{x,M}^B$, weighted by instrumental response to n th power
$\tau_B, \vartheta_B, \beta_{t B}, u_B, \delta_B, \epsilon_B, \varpi_B, \mathbf{r}_B$	The quantities defining a broadcast: its duration, starting time, instantaneous bandwidth, central frequency, drift rate, effective isotropic energy release, polarization properties, and position
$\hat{e}_{x B}, \hat{e}_{x B}, \hat{q}_{x B}, \hat{\ell}_{x B}$	The effective isotropic emission of a broadcast coincident with window x
$\zeta_{p B}(p), \zeta_{x B}$	Fraction of broadcast emission in polarization p ; fraction in polarizations covered by window x
$\xi_{c;o B}$	Quantity summarizing certain properties related to broadcast coherence (Appendix B.3)
$\xi_{\delta;x,M}^B$	Describes narrowband broadcast drift rate distribution, equals $\langle \tau_{x B}^2 \rangle_M / (T_x \langle \tau_{x B} \rangle_M)$
$\chi_{\varrho;x B}$	Transmittance factor: fraction of ϱ emission from broadcast B that remains after extinction
$y_{\varrho;J}$	Dilution factor for ϱ emission from object J , equals $1/(4\pi d_{\varrho;J}^2)$
$Y_{x,M}^{B;n}$	Weighted sum of $y_{\varrho;B} \chi_{\varrho;x B}$ for all broadcasts drawn by (x, M)
$u_{x B}, h_{x B}, \mathfrak{g}_{x B}, \mathfrak{f}_{x B}$	Fluence accumulated over window x from broadcast B
$\mathfrak{U}_{o,M}^B$	Generic type of fluence accumulated over observation o from all broadcasts in metasociety M
\mathfrak{U}_o	Measurement of total fluence over o from galaxy g
$\mathfrak{m}_{x B}, \mathfrak{e}_{x B}, \mathfrak{q}_{x B}$	Emission accumulated by an instrument over window x from broadcast B
$\mathfrak{M}_{x,M}^B, \mathfrak{E}_{x,M}^B, \mathfrak{Q}_{x,M}^B$	Emission accumulated by an instrument over window x from all broadcasts in metasociety M
$\mathfrak{m}_{x n}, \mathfrak{e}_{x n}, \mathfrak{q}_{x n}$	Background collected by instrument over window x
$\mathfrak{M}_x, \mathfrak{E}_x, \mathfrak{Q}_x$	Total emission accumulated by an instrument over window x , both signal and noise
$\mathfrak{s}[\mathfrak{m}_{o B}], \mathfrak{s}[\mathfrak{e}_{o B}], \mathfrak{s}[\mathfrak{q}_{o B}]$	Expected mean signal-to-noise ratio of a broadcast in observation o ; a scaling variable
$\mathfrak{S}[\mathfrak{M}_o], \mathfrak{S}[\mathfrak{E}_o], \mathfrak{S}[\mathfrak{Q}_o]$	Expected maximum signal-to-noise ratio expected for measurements

NOTE—See Paper I for a comprehensive explanation of the notation. Emission variables are listed for generic emission, energy, photons, and, when present, power.

starting time, energy release, and polarization properties, among others.

Any population of objects is modeled as a point process on the appropriate haystack. A point process is basically a random set of points in a space (for details, see Kingman 1993; Daley & Vere-Jones 2003; Baddeley 2007; Chiu et al. 2013; Haenggi 2013). The entire population of J-objects hosted by a single ancestor K on the tree is the point process denoted Σ_K^J (a realized object can be substituted for K). N_K^J is a random variable counting the number of objects in Σ_K^J .

A distribution (or “intensity”) of objects on the haystack gives the mean number of objects. For the J-type objects sharing the ancestor K, the distribution is denoted Ψ_K^J . The mean number of objects in a subset $A \subset W^J$ is,

$$\langle N_K^J(A) \rangle = \int_A \Psi_K^J(\mathbf{w}_J | \mathbf{w}_K) d\mathbf{w}_J. \quad (1)$$

In general, the distribution depends on the properties of the ancestor K, which are specified by the tuple \mathbf{w}_K . This lets all the child objects share statistical properties. If the ancestor is a realized object k, then \mathbf{w}_K is fixed to \mathbf{w}_k , and the only remaining dependence of the distribution is on \mathbf{w}_J itself.

A Poisson point process is one in which the number of points in any region has a Poisson distribution and non-overlapping regions are independent (Kingman 1993). It is appropriate when objects appear independently of each other according to a single well-defined intensity. In this paper, the broadcasts of a realized society and the societies of a realized metasociety are modeled as Poisson point processes: the properties of the immediate “parent” of each subpopulation fully specify the intensity. But when considering the descendant objects of a higher-level ancestor, the distribution of objects itself is random, because it is a random sum of distributions from each of the parents hosted by that ancestor. A Cox point process is just this sort of random superposition of Poisson point processes (Kingman 1993). In this paper, the broadcasts of a metasociety (or galaxy) are modeled generally as a Cox point process.

2.3. Selections

The two basic steps from the statistical description of a population to an observed quantity are selection and measurement. Selection draws a sample. Measurement generates an observable quantity from the gross properties of the sample, introducing noise variance from background noise and microscopic fluctuations in radiation.

Selections are central to the framework (Paper I). They sieve through the vast panoply of objects in all the universe’s history, reflecting the limited scope of our programs. A selection (\mathbf{x}, K) consists of a window \mathbf{x} and a host object K.

Windows filter objects solely according to their tuples’ positions in the haystack. They include the probability

that an object at a given location will be selected, essentially the completeness of the selection. A common type of window selects things according to fundamental quantities like time ($\mathbf{t}(t)$) and frequency ($\mathbf{v}(\nu)$). Other examples of windows include observations (o) and surveys (s). Windows also can filter emission and other quantities, defining bounds of integration: for example, the energy fluence of a broadcast intercepted during one observation can be much smaller than the energy fluence over the entire survey, or all of history. If no window is specified for a random variable, the special ALL-window ∞ is used by default, picking every object and all emission regardless of parameters.

The host specifies a subpopulation of objects to be selected: objects that are not descendants of the host on the “tree” are not included. The host object is specified by its index; when none is given for a random variable, the universal host u (or U) is assumed by default. In order for an object to be selected by (\mathbf{x}, K) , its tuple must be a member of Σ_K^J .

The random set of J-type objects passed by a selection (\mathbf{x}, K) is the random sample $\Sigma_{\mathbf{x}, K}^J$. A J-type object passes this selection if its tuple would be included by the window \mathbf{x} , and the object also happens to be a descendant of K. The selection window modifies the distribution of objects within the host to $\Psi_{\mathbf{x}, K}^J$, which gives the mean number of sampled objects:

$$\langle N_{\mathbf{x}, K}^J \rangle = \int_{W^J} \Psi_{\mathbf{x}, K}^J(\mathbf{w}_J | \mathbf{w}_K) d\mathbf{w}_J. \quad (2)$$

2.4. Random variables and selection-dependent properties

Singleton variables are random variables describing single objects, like the energy released by an individual broadcast during an observation. The notation for singleton variable κ for object J has the form $\kappa_{\mathbf{x}|J}$, with the variable itself a lowercase character. Generally, the singleton variable is integrated within the bounds of some window \mathbf{x} ; a singleton variable κ_J missing its quantity window integrates without external restriction.

Aggregate variables are the sum of singleton variables for a subpopulation of objects drawn by a selection:

$$K_{\mathbf{x}, K}^J = \sum_{\mathbf{w}_J \in \Sigma_{\mathbf{x}, K}^J} \kappa_{\mathbf{x}|J}. \quad (3)$$

Number variables $N_{\mathbf{x}, K}^J$ are special cases of aggregate variables for which $\kappa_{\mathbf{x}|J} = 1$. The distinction between an aggregate variable and a singleton variable is, in the end, one of interpretation. The sum of a quantity among all the objects hosted in a parent can be viewed as a variable associated with the parent itself: $\kappa'_{\mathbf{x}|K} \leftrightarrow K_{\mathbf{x}, K}^J$. This interconversion lets us transfer definitions between singleton and aggregate variables.

The distribution of $\kappa_{\mathbf{x}|J}$ is fully determined by its parameter tuple \mathbf{w}_J , but the value it actually takes can

be otherwise random. So while the effective isotropic luminosity of a broadcast, ℓ_B , is an innate property, the number of photons we count from inevitably has shot noise that we cannot predict. The simple mean of a random variable is defined:

$$\langle \kappa_{x|J} \rangle \equiv \langle \kappa_{x|J} | \mathbf{w}_J \rangle. \quad (4)$$

The simple variance follows from the definition of variance: $\mathbb{V}[\kappa_{x|J}] \equiv \langle \kappa_{x|J}^2 | \mathbf{w}_J \rangle - \langle \kappa_{x|J} | \mathbf{w}_J \rangle^2$. The definitions apply analogously for aggregate variables. Campbell's formula lets us find the simple mean of an aggregate variable, applying to any point process:

$$\langle K_{x,K}^J \rangle = \int_{W^J} \langle \kappa_{x|J} \rangle \Psi_{x,K}^J(\mathbf{w}_J | \mathbf{w}_K) d\mathbf{w}_J \quad (5)$$

(e.g., Kingman 1993; Baddeley 2007).

But we may instead want to know the statistics over all possible objects drawn from a sample – say, the mean number of photons we collect from a random broadcast sampled by a survey. Given a selection (y, K) , the selection-relative probability density function (PDF) of a variable is

$$\Psi[\kappa_{x|J}]_{y,K}(x) \equiv \frac{1}{\langle N_{y,K}^J \rangle} \int_{W^J} \Psi_{y,K}^J(\mathbf{w}_J) \Psi[\kappa_{x|J}](x) d\mathbf{w}_J, \quad (6)$$

where $\Psi[\kappa_{x|J}](x)$ is the unbiased PDF for $\kappa_{x|J}$ at x , implicitly conditionalized on \mathbf{w}_J . The statistical properties of objects and populations can change depending on how they are selected: selections introduce bias. The selection-relative mean is derived from the selection-relative PDF and is defined as

$$\begin{aligned} \langle \kappa_{x|J} \rangle_{y,L} &= \langle \kappa_{x|J} | \mathbf{w}_J \in \Sigma_{y,L}^J \rangle \\ \langle K_{x,K}^J \rangle_{y,L} &= \langle K_{x,K}^J | \mathbf{w}_K \in \Sigma_{y,L}^K \rangle. \end{aligned} \quad (7)$$

If the values of $\kappa_{x|J}$ among different objects are independent of each other and the number of objects, then

$$\langle \kappa_{x|J} \rangle_{y,L} = \frac{1}{\langle N_{y,L}^J \rangle} \int_{W^J} \langle \kappa_{x|J} \rangle \Psi_{y,L}^J(\mathbf{w}_J | \mathbf{w}_L) d\mathbf{w}_J. \quad (8)$$

Selection-relative variances are defined using the selection-relative means: $\mathbb{V}[X]_{y,L} = \langle X^2 \rangle_{y,L} - \langle X \rangle_{y,L}^2$.

In this work, almost always the selection window is the same as the window in the variable. If we want to know the “average number of photons collected from a broadcast in an observation”, usually what we mean is the average number from a broadcast sampled by that observation – we do not care about all the broadcasts that happened a billion years ago that we measure no photons from. Hence, the selection-relative PDF, means, and variances “inherit” the variables they are averaging over: $\Psi[\kappa_{x|J}]_L = \Psi[\kappa_{x|J}]_{x,L}$, $\langle \kappa_{x|J} \rangle_L = \langle \kappa_{x|J} \rangle_{x,L}$,

$\mathbb{V}[\kappa_{x|J}]_L = \mathbb{V}[\kappa_{x|J}]_{x,L}$, and similarly for aggregate variables.

When Σ_K^J is Poissonian, and the individual $\kappa_{x|J}$ for each object in the population are identically distributed, mutually independent, and independent of $N_{x,K}^J$, $K_{x,K}^J$ has a compound Poisson distribution. This means it has a mean and variance of

$$\begin{aligned} \langle K_{x,K}^J \rangle &= \langle N_{x,K}^J \rangle \langle \kappa_{x|J} \rangle_K \\ \mathbb{V}[K_{x,K}^J] &= \langle N_{x,K}^J \rangle \langle \kappa_{x|J}^2 \rangle_K \end{aligned} \quad (9)$$

(Adelson 1966; Barbour & Chryssaphinou 2001; Bas 2019). We can use this to calculate the mean and variance of the aggregate emission of all broadcasts in a society and the aggregate emission of all societies in a galactic metasociety (see Paper I).

2.5. Working with surveys: regularization and multiwindow operations

A survey s typically consists of many observations \mathbf{o}_i , perhaps grouped into pointings at different locations in the sky. The set of observations that make up the survey is S_s . A lot of the questions we are interested in depend on the variations between observations in the survey: “What is the brightest broadcast fluence in an observation over the entire survey?”, for example, or “What is the variance of an observable we measure in a survey?”

The first tool invokes the finite reach of surveys. This becomes important when we consider probability distributions with very long tails. Broad fluence distributions naturally arise if there is a wide range in the intrinsic emission of individual broadcasts, their distances, or, for narrowband lines, drift rates, for example. Certain power laws can have infinite variances and means because of these heavy tails. In practice, however, we are interested in the means and variances of a typical sample. To do this, we can regularize random variables by truncating their distributions at values unlikely to be sampled:

$$\Psi[\kappa_{x|J}^{[y,K]}](\kappa) \equiv \frac{\Psi[\kappa_{x|J}](\kappa)}{P_{y,K}(\kappa^L \leq \kappa_{x|J} \leq \kappa^H)} \mathbb{I}[\kappa^L \leq \kappa \leq \kappa^H]. \quad (10)$$

The values of κ^H and κ^L are derived from the probability distributions of the maximum and minimum $\kappa_{x|J}$ in the sample $\Sigma_{y,K}^J$ using extreme value theory. The probability that the maximum $\kappa_{x|J}$, of all the $N_{y,K}^J$ values sampled, is above κ^H is a constant (1/4 in Paper I); the probability that the minimum $\kappa_{x|J}$ is below κ^L is also a constant (again, 1/4 in Paper I). Thus, $\mathbf{u}_{\mathbf{o}|B}^{[s,M]}$ is the fluence of a broadcast intercepted by the observation \mathbf{o} , regularized to only include broadcast fluence values likely to be measured in the survey as it covers the metasociety M .

The other issue is that sometimes we need to find a mean, variance, or maximum of some quantity over

a group of observations. The multiwindow mean and related observations generalize selection-relative operations. Selection-relative operations are defined for a single window, while multiwindow operations consider the range of values over many windows. The multiwindow mean is defined

$$\langle \kappa_{\mathbf{o}|J} \rangle_{\mathbf{s}} \equiv \langle \langle \kappa_{\mathbf{o}_i|J} \rangle | \mathbf{o}_i \in \mathbf{S}_{\mathbf{s}}^{\circ} \rangle. \quad (11)$$

The multiwindow mean can be combined with the selection-relative mean for a host,

$$\langle \kappa_{\mathbf{o}|J} \rangle_{\mathbf{s}|L} \equiv \langle \langle \kappa_{\mathbf{o}_i|J} \rangle_L | \mathbf{o}_i \in \mathbf{S}_{\mathbf{s}}^{\circ} \rangle. \quad (12)$$

The multiwindow variance follows from the definition of conditional variance:

$$\begin{aligned} \mathbb{V} [\kappa_{\mathbf{o}|J}]_{\mathbf{s}} &\equiv \langle \kappa_{\mathbf{o}|J}^2 \rangle_{\mathbf{s}} + \langle \kappa_{\mathbf{o}|J} \rangle_{\mathbf{s}}^2 \\ &= \langle \mathbb{V} [\kappa_{\mathbf{o}_i|J}] | \mathbf{o}_i \in \mathbf{S}_{\mathbf{s}}^{\circ} \rangle + \mathbb{V} [\langle \kappa_{\mathbf{o}_i|J} \rangle | \mathbf{o}_i \in \mathbf{S}_{\mathbf{s}}^{\circ}] \end{aligned} \quad (13)$$

This expression of the law of total variance says that the multiwindow variance results from both the average variation of the variable within each subwindow and the variation between them. Finally, we have multiwindow maxima, which are useful in defining maximum signal-to-noise ratio:

$$\begin{aligned} \max [\kappa_{\mathbf{o}|J}]_{\mathbf{s}} &\equiv \max [\kappa_{\mathbf{o}_i|J} | \mathbf{o}_i \in \mathbf{S}_{\mathbf{s}}^{\circ}] \\ \max [\kappa_{\mathbf{o}|J}]_{\mathbf{s}|L} &\equiv \max [\max [\kappa_{\mathbf{o}_i|J} | \mathbf{w}_J \in \Sigma_{\mathbf{o}_i,L}^J] | \mathbf{o}_i \in \mathbf{S}_{\mathbf{s}}^{\circ}] \end{aligned} \quad (14)$$

Of course, an aggregate variable can be used in place of the singleton variable in this equation as well.

2.6. The box and chord models

The box and chord models give us analytical results for the emission properties of broadcasts. In both models, the window \mathbf{x} is treated as a contiguous “box” covering the time range $\Theta_{\mathbf{x}} \leq t \leq \Theta_{\mathbf{x}} + \mathbf{T}_{\mathbf{x}}$, the frequency range $\Upsilon_{\mathbf{x}} - \mathbf{B}_{\mathbf{x}}/2 \leq \nu \leq \Upsilon_{\mathbf{x}} + \mathbf{B}_{\mathbf{x}}/2$, and $|\Pi_{\mathbf{x}}|$ independent polarizations (p) from the set $\Pi_{\mathbf{x}}$. Here $\mathbf{T}_{\mathbf{x}}$ is the duration of the window, $\mathbf{B}_{\mathbf{x}}$ is its bandwidth, $\Theta_{\mathbf{x}}$ is the starting time of the window, and $\Upsilon_{\mathbf{x}}$ is its central frequency.

Broadcasts may fall into one of four categories according to their duration $\tau_{\mathbf{B}}$ and (instantaneous) bandwidth $\beta_{\mathbf{t}|B}$, relative to that of the window. Lines are broadcasts that are narrowband and long-lived ($\tau_{\mathbf{B}} \gg \mathbf{T}_{\mathbf{x}}$; $\beta_{\mathbf{t}|B} \ll \mathbf{B}_{\mathbf{x}}$), while pulses are wideband and short-lived ($\tau_{\mathbf{B}} \ll \mathbf{T}_{\mathbf{x}}$; $\beta_{\mathbf{t}|B} \gg \mathbf{B}_{\mathbf{x}}$). Less commonly considered in SETI are the hisses, wideband and long-lived continuum sources ($\tau_{\mathbf{B}} \gg \mathbf{T}_{\mathbf{x}}$; $\beta_{\mathbf{t}|B} \gg \mathbf{B}_{\mathbf{x}}$), and the blips, narrowband transients ($\tau_{\mathbf{B}} \ll \mathbf{T}_{\mathbf{x}}$; $\beta_{\mathbf{t}|B} \ll \mathbf{B}_{\mathbf{x}}$). The box model is used for pulses, hisses, and blips, while the chord model allows for the treatment of lines with frequency drift.

2.6.1. The box model

The box model treats broadcasts as uniform “boxes” in time-frequency space as well, all with a single duration $\bar{\tau}$ and bandwidth $\bar{\beta}$. Each broadcast begins at time $\vartheta_{\mathbf{B}}$ and is centered at frequency $\nu_{\mathbf{B}}$. There is no skewness to the box, no drift or dispersion. The (effective isotropic) spectral luminosity per polarization of broadcast \mathbf{B} is unvarying within the box:

$$\begin{aligned} \dot{\ell}_{\nu,p;B}(t, \nu, p) &= \zeta_{p|B}(p) \frac{\dot{\epsilon}_{\mathbf{B}}}{\bar{\tau}\bar{\beta}} \\ &\cdot \mathbb{I}[0 \leq t - \vartheta_{\mathbf{B}} \leq \bar{\tau}] \cdot \mathbb{I}[|\nu - \nu_{\mathbf{B}}| \leq \bar{\beta}/2], \end{aligned} \quad (15)$$

where $\dot{\epsilon}_{\mathbf{B}}$ is the effective isotropic energy released during the broadcast, $\zeta_{p|B}(p)$ of which is into polarization p . A broadcast is selected by (\mathbf{x}, J) if its “box” overlaps the window’s “box” and it is part of J ’s broadcast population. The (effective isotropic) energy integrated over the overlap, $\dot{\epsilon}_{\mathbf{x}|B}$, is proportional to the time-frequency “area” of the overlapping region:

$$\dot{\epsilon}_{\mathbf{x}|B} = \frac{\dot{\epsilon}_{\mathbf{B}} \tau_{\mathbf{x}|B} \beta_{\mathbf{x}|B}}{\bar{\tau} \bar{\beta}} \sum_{p \in \Pi_{\mathbf{x}}} \zeta_{p|B}(p) = \frac{\dot{\epsilon}_{\mathbf{B}} \tau_{\mathbf{x}|B} \beta_{\mathbf{x}|B}}{\bar{\tau} \bar{\beta}} \zeta_{\mathbf{x}|B}, \quad (16)$$

where $\tau_{\mathbf{x}|B}$ is the length of time and $\beta_{\mathbf{x}|B}$ is the span of frequencies in which both the broadcast and the window are active. In the box model, the expected number of intercepted broadcasts in host J (regardless of detectability) is

$$\langle N_{\mathbf{x},J}^{\mathbf{B}} \rangle \approx \Lambda_J^{\mathbf{B}}(\Theta_{\mathbf{x}}, \Upsilon_{\mathbf{x}}) \cdot \langle N_{\mathbf{x},J}^{\star} \rangle (\mathbf{T}_{\mathbf{x}} + \bar{\tau}) (\mathbf{B}_{\mathbf{x}} + \bar{\beta}), \quad (17)$$

for a broadcast frequency rate per star of

$$\Lambda_J^{\mathbf{B}}(t, \nu) = \frac{1}{\langle N_{\mathbf{t},J}^{\star}(t) \rangle} \frac{d^2 \langle N_J^{\mathbf{B}} \rangle}{d\vartheta_{\mathbf{B}} d\nu_{\mathbf{B}}} (\vartheta_{\mathbf{B}} = t, \nu_{\mathbf{B}} = \nu), \quad (18)$$

where $N_{\mathbf{t},J}^{\star}(t)$ is the number of stars existing in the host J at time t and $N_{\mathbf{x},J}^{\star}$ is the number in J covered by the window \mathbf{x} .

2.6.2. The chord model

The chord model treats broadcasts as ultranarrowband lines that drift linearly in frequency. Thus, each broadcast acts like a “chord” cutting across the window “box.” Each broadcast’s drift rate $\delta_{\mathbf{B}}$ is constant, but the population of broadcasts has a whole distribution of drift rates. In this work, I adopt the uniform drift rate distribution,

$$\Psi[\delta_{\mathbf{B}}]_J = 1/(2\bar{\delta}_J) \cdot \mathbb{I}[|\delta_{\mathbf{B}} - \Delta_J^{\mathbf{B}}| \leq \bar{\delta}_J]. \quad (19)$$

Note this is the distribution unbiased by any window selection; narrowband windows are more likely to pick broadcasts with high drift rates. The chords have no intrinsic luminosity variability (but see Section 5.4).

Therefore, the total amount of emission from broadcast B intercepted during the window is directly proportional to the time it takes to cross the box, $\tau_{x|B}$. Each broadcast has an effective isotropic luminosity $\dot{\ell}_B$; it releases

$$\langle \dot{\epsilon}_{x|B} \rangle = \dot{\ell}_B \tau_{x|B} \sum_{p \in \Pi_x} \zeta_{p|B}(p) = \dot{\ell}_B \tau_{x|B} \zeta_{x|B} \quad (20)$$

as energy during the times, frequencies, and polarizations covered by the observation x . Selection by (x, J) happens when a broadcast has $\tau_{x|B} > 0$ and is part of J 's broadcast population.² From this criterion, the expected number of intercepted broadcasts is

$$\langle N_{x,J}^B \rangle \approx Z_J^B(\Theta_x, \Upsilon_x) \cdot \langle N_{x,J}^* \rangle (B_x + \langle |\delta_B| \rangle_J \Upsilon_x), \quad (21)$$

using the instantaneous broadcast frequency abundance per star

$$Z_J^B(t, \nu) = \frac{1}{\langle N_{t,J}^* \rangle} \frac{d^2 \langle N_{t,J}^B(t) \rangle}{dv_B} (v_B = \nu) \approx \Lambda_J^B \langle \tau_B \rangle_J, \quad (22)$$

with $N_{t,J}^B(t)$ equal to the number of active broadcasts in J at time t .

2.7. Assumptions Used in This Paper

A number of simplifying assumptions are used in this paper to make calculations tractable, summarized in Table 2.

In this paper, I consider constraints on broadcasts in individual galaxies, specifically their abundance and brightness. All intercepted broadcasts are assumed to arise from the one galaxy being targeted. This is important because observable quantities like energy received or photons counted cannot tell if the broadcasts are from within the galaxy or not.

There are several different ways of interpreting metasocieties described in Paper I, each reflecting different assumptions about the mutual influence and interstellar replication of societies. In this paper, I adopt the simplest scenario, the single metasociety assumption ($N_g^M = 1$). We cannot observationally distinguish a galaxy with a metasociety with sufficiently few technosignatures from one with no metasociety. Thus, for this paper, uninhabited galaxies have trivial metasocieties with no societies and no broadcasts. The practical effect is to ignore a term in the variance of observables related to the ‘‘clumping’’ of broadcasts into discrete metasocieties. The metasociety can be more or less identified with its host galaxy, but I consider astrophysical properties like number of stars to be fixed parameters

² As in Paper I, the broadcast’s parent society, metasociety, and galaxy must also be selected by the window, although that can be assumed for any broadcast falling within the window for this paper.

Table 2. Standard Assumptions Used in This Paper

Assumption	Description
Independence	Objects sharing the same ‘‘parent’’ have independent properties, conditionalized on the parent’s properties. The number of objects is independent of their properties.
Interchangeability	The broadcast distribution in one society at one epoch is identical to that in another society or epoch, except translated in space and time.
Interchangeable observations	Within a single metasociety, the statistical properties of broadcasts and societies are the same in every observation considered, regardless of frequency, time, or location.
Single metasociety	Each galaxy has one metasociety; one distribution characterizes all broadcasts and societies in it. Background and foreground galaxies are ignored.
Diffuse approximation	The number of sampled broadcasts per society is typically $\ll 1$. Their clumping into societies is ignored, as if the broadcasts themselves are scattered in a diffuse cloud throughout the galaxy according to a Poisson point process.
Distant galaxy	All objects within a galaxy are at the same distance and the same dilution (fluence-to-emission ratio).
Negligible extinction	No emission is absorbed or scattered en route to Earth ($\chi_{e;x B} = 1$).
Uniform beam	The instrumental response is uniform across the bandwidth and duration of an observation and across its footprint on the sky ($N_{o,M}^{B;n} = N_{o,M}^B$).

of the host galaxy. The metasociety M , on the other hand, contains the parameters describing the ETIs and their broadcasts; these are unknown variables, and the metasociety is considered to be random. SETI programs aimed at galaxies can be viewed as trying to constrain these unknown metasocietal parameters.

Societies in the metasociety are described by their position \mathbf{r}_C , and origin time ϑ_C . Furthermore, it is assumed that societies trace the stellar population, at least in bulk (see discussion in Paper I), with an abundance per star of Ξ_M^C . When the metasocietal properties are fixed, societies are described by a Poisson point process with distribution

$$\Psi_M^C(\mathbf{w}_C | \mathbf{w}_M) = \Xi_M^C(\mathbf{w}_M) \frac{d \langle N_{t,g}^*(\vartheta_C) \rangle}{d\mathbf{r}_*}(\mathbf{r}_C) \cdot \psi[\vartheta_C, \tau_C, \mathbf{w}'_C | \mathbf{w}_M]. \quad (23)$$

The \mathbf{w}'_C collects societal-level properties of the broadcast distribution, like a shared luminosity.

Each society can host broadcasts, which are characterized by their energy release $\dot{\epsilon}_B$, quantities relating to polarization of the broadcasts (ϖ_B), a position (\mathbf{r}_B)

identical to that of the transmitting society, and various parameters describing their time/frequency behavior. The distribution of broadcasts for each society is of the form

$$\begin{aligned} \Psi_{\mathbb{C}}^{\mathbb{B}}(\mathbf{w}_{\mathbb{B}}|\mathbf{w}_{\mathbb{C}}) &= \delta(\mathbf{r}_{\mathbb{B}} - \mathbf{r}_{\mathbb{C}}(\mathbf{w}_{\mathbb{C}}))\Psi[\hat{\epsilon}_{\mathbb{B}}]_{\mathbb{C}}\Psi[\varpi_{\mathbb{B}}]_{\mathbb{C}} \\ &\cdot \begin{cases} \check{A}_{\mathbb{C}}^{\mathbb{B}}(\mathbf{w}_{\mathbb{C}})\delta(\tau_{\mathbb{B}} - \bar{\tau})\delta(\beta_{\mathbb{t}|\mathbb{B}} - \bar{\beta})\delta(\delta_{\mathbb{B}}) & (\text{box}) \\ \check{Z}_{\mathbb{C}}^{\mathbb{B}}(\mathbf{w}_{\mathbb{C}})\delta(\vartheta_{\mathbb{B}})\delta(\tau_{\mathbb{B}} - \tau_{\infty})\delta(\beta_{\mathbb{t}|\mathbb{B}})\Psi[\delta_{\mathbb{B}}]_{\mathbb{C}} & (\text{chord}) \end{cases}. \end{aligned} \quad (24)$$

Each realized society's broadcasts also are described by a Poisson point process. I further adopt an interchangeability assumption: the statistical properties of the broadcasts of one society are equivalent to those of another, aside from translation in time and space. Hence, every society has the same broadcast energy release distribution $\Psi[\hat{\epsilon}_{\mathbb{B}}]_{\mathbb{M}}$ and the same polarization distribution $\Psi[\varpi_{\mathbb{B}}]_{\mathbb{M}}$, and all share the same frequency rate or abundance ($\check{A}_{\mathbb{C}}^{\mathbb{B}} = \langle \check{A}_{\mathbb{C}}^{\mathbb{B}} \rangle_{\mathbb{M}}$ in the box model; $\check{Z}_{\mathbb{C}}^{\mathbb{B}} = \langle \check{Z}_{\mathbb{C}}^{\mathbb{B}} \rangle_{\mathbb{M}}$ in the chord model). When I need to pick a $\hat{\epsilon}_{\mathbb{B}}$ distribution in this work, I assume that all broadcasts have the same effective isotropic energy, and, when relevant, luminosity (also known as effective isotropic radiated power or EIRP):

$$\Psi[\hat{\epsilon}_{\mathbb{B}}]_{\mathbb{C}} = \Psi[\hat{\epsilon}_{\mathbb{B}}]_{\mathbb{M}} = \delta(\hat{\epsilon}_{\mathbb{B}} - \bar{\epsilon}). \quad (25)$$

To simplify matters further, I often employ the diffuse approximation, which ignores the discreteness of societies. This is valid if there are many societies, dividing up a few broadcasts among them ($\langle N_{\mathbb{C}}^{\mathbb{B}} \rangle \ll 1$). In order for it to be false, the broadcasts of an individual society by itself must be confused in a single observation, not just the population in the entire galaxy. Failure requires extraordinary abundances for the fine observations of individualist surveys, but not so much for the coarse observations used in the collective bound. Combined with the single metasociety assumption, it means that $\Sigma_{\mathbb{M}}^{\mathbb{B}}$ itself is a Poisson point process with distribution

$$\begin{aligned} \Psi_{\mathbb{M}}^{\mathbb{B}}(\mathbf{w}_{\mathbb{B}}|\mathbf{w}_{\mathbb{M}}) &= \frac{d\langle N_{\mathbb{t},\mathbb{g}}^{\mathbb{B}}(\vartheta_{\mathbb{C}}) \rangle}{d\mathbf{r}_{\star}}(\mathbf{r}_{\mathbb{B}})\Psi[\hat{\epsilon}_{\mathbb{B}}]_{\mathbb{M}}\Psi[\varpi_{\mathbb{B}}]_{\mathbb{M}} \\ &\cdot \begin{cases} A_{\mathbb{M}}^{\mathbb{B}}(\mathbf{w}_{\mathbb{M}})\delta(\tau_{\mathbb{B}} - \bar{\tau})\delta(\beta_{\mathbb{t}|\mathbb{B}} - \bar{\beta})\delta(\delta_{\mathbb{B}}) & (\text{box}) \\ Z_{\mathbb{M}}^{\mathbb{B}}(\mathbf{w}_{\mathbb{M}})\delta(\vartheta_{\mathbb{B}})\delta(\tau_{\mathbb{B}} - \tau_{\infty})\delta(\beta_{\mathbb{t}|\mathbb{B}})\Psi[\delta_{\mathbb{B}}]_{\mathbb{M}} & (\text{chord}) \end{cases}. \end{aligned} \quad (26)$$

Finally, in addition to the other assumptions in Table 2, I assume that the host galaxy \mathbb{g} is distant, such that all broadcasts have the same distance $d_{\mathbb{g}}$ and redshift $z_{\mathbb{g}}$. I even apply this to wide-field surveys of the Milky Way to get order-of-magnitude constraints, as most stars in the Galaxy are of order ~ 10 kpc away.

3. MEASUREMENTS OF AGGREGATE EMISSION

Instruments collect some kind of emission, like energy or photons, and report an observable quantity. The most common kind of observable, one at the heart of most SETI analyses, is the integrated amount of collected emission from a target during a window \mathbb{x} . This quantity, $\mathfrak{M}_{\mathbb{x}}$ for a generic measurable ($\mathfrak{E}_{\mathbb{x}}$ for collected energy, and $\mathfrak{Q}_{\mathbb{x}}$ for number of collected photons) has two basic components. First is the aggregate emission from all the broadcasts covered by the observation, denoted $\mathfrak{M}_{\mathbb{x}}^{\mathbb{B}}$ with a superscript \mathbb{B} to indicate its origin in broadcasts. Second is the background $\mathfrak{m}_{\mathbb{x}|\mathbb{n}}$, from everything else – instrumental noise, natural background radiation from Earth, the target system, and things behind it.

The mean collected emission of a broadcast is directly proportional to the amount of effective isotropic emission it releases into the universe during the window \mathbb{x} , $\hat{\varrho}_{\mathbb{x}|\mathbb{B}}$. By the time it gets to Earth, propagating an emission distance $d_{\mathbb{e};\mathbb{B}}$, the emission is “diluted” by a factor $y_{\mathbb{e};\mathbb{B}} \equiv 1/(4\pi d_{\mathbb{e};\mathbb{B}}^2)$ from the inverse square law. I use the dilution factor in this work because it is more natural when calculating averages, with $\langle y_{\mathbb{e};\mathbb{B}} \rangle_{\mathbb{M}} \propto \langle d_{\mathbb{e};\mathbb{B}}^{-2} \rangle_{\mathbb{M}}$ occurring frequently.

Extinction can also suppress the observed flux. The surviving fraction of emission in \mathbb{x} after extinction is the transmittance $\chi_{\mathbb{e};\mathbb{x}|\mathbb{B}}$. Generally, it can be a function of frequency; the transmittance actually depends on the window chosen for wideband broadcasts (e.g., an optical pulse observed with a blue filter will be more subject to dust extinction than one observed with a red filter). Extinction is important for optical light broadcasts more than about a kiloparsec away (Howard et al. 2004); it could also be significant for more exotic bands at the far ends of the electromagnetic spectrum. Extinction is negligible in radio SETI bands ($\chi_{\mathbb{e};\mathbb{x}|\mathbb{B}} \approx 1$). It also includes extinction in the Earth's atmosphere, which would set $\chi_{\mathbb{e};\mathbb{x}|\mathbb{B}} \approx 0$ in much of the infrared spectrum.

The fluence of broadcast \mathbb{B} is the amount of emission received per unit area over the window:

$$\mathbf{u}_{\mathbb{x}|\mathbb{B}} = \frac{\hat{\varrho}_{\mathbb{x}|\mathbb{B}}\chi_{\mathbb{e};\mathbb{x}|\mathbb{B}}}{4\pi d_{\mathbb{e};\mathbb{B}}^2} = \hat{\varrho}_{\mathbb{x}|\mathbb{B}}\chi_{\mathbb{e};\mathbb{x}|\mathbb{B}}y_{\mathbb{e};\mathbb{B}}. \quad (27)$$

The emission is collected by an instrument with effective area \mathcal{A} and weighted by a nonconstant response function of frequency, time, polarization, and location on the sky. I assume that the response function is 0 outside the times, frequencies, and polarizations covered by \mathbb{x} , and otherwise only depends on sky location $\boldsymbol{\theta}$:

$$\begin{aligned} \mathcal{I}_{\mathfrak{M};\mathbb{x}}(t, \nu, p, \boldsymbol{\theta}) &= \mathcal{I}_{\mathfrak{M};\mathbb{x}}(\boldsymbol{\theta}) \cdot \mathbb{I}[0 \leq t - \Theta_{\mathbb{x}} \leq \Upsilon_{\mathbb{x}}] \\ &\cdot \mathbb{I}[|\nu - \Upsilon_{\mathbb{x}}| \leq \mathbb{B}_{\mathbb{x}}/2] \cdot \mathbb{I}[p \in \Pi_{\mathbb{x}}], \end{aligned} \quad (28)$$

where $\max \mathcal{I}_{\mathfrak{M};\mathbb{x}} = 1$. Given a fixed broadcast sample, the mean amount of emission measured by the instru-

ment is

$$\langle \mathfrak{M}_x | \Sigma_x^B, \Sigma_x^C \rangle = \langle \mathfrak{m}_{x|n} \rangle + \sum_{\mathbf{w}_B \in \Sigma_x^B} \langle \mathfrak{m}_{x|B} \rangle = \sum_{\mathbf{w}_B \in \Sigma_x^{B\ddagger}} \langle \mathfrak{m}_{x|B} \rangle. \quad (29)$$

On the right, the noise is regarded as a virtual “broadcast” \mathbf{n} , with a dummy broadcast tuple \mathbf{w}_n . Calculations are simplified by regarding the emission coming from an “adjoined sample” with this virtual broadcast, $\Sigma_x^{B\ddagger} = \Sigma_x^B \cup \{\mathbf{w}_n\}$.

Of course, we do not know what kinds of broadcasts are present in the sample, so we want to know the statistics of an observable over all possible samples. Under standard assumptions (section 2.7), the mean intercepted emission within window x is given by

$$\langle \mathfrak{M}_x \rangle = \langle \mathfrak{m}_{x|n} \rangle + \mathcal{A} \langle N_{x,M}^{B;1} \rangle \langle \mathbf{u}_{x|B} \rangle_M. \quad (30)$$

This also uses a weighted number of broadcasts,

$$N_{x,M}^{B;n} \equiv \sum_{\mathbf{w}_B \in \Sigma_{x,M}^B} \mathcal{I}_{\mathfrak{M};x}(\boldsymbol{\theta}_B)^n \quad (31)$$

with means

$$\langle N_{x,M}^{B;n} \rangle \equiv \Xi_M^C \langle N_{x,C}^B \rangle_M \int_{\boldsymbol{\theta} \in \Omega_x} \frac{d \langle N_{x,g}^* \rangle}{d \boldsymbol{\theta}} [\mathcal{I}_{\mathfrak{M};x}(\boldsymbol{\theta})]^n d \boldsymbol{\theta} \quad (32)$$

for different exponents n (Appendix A). In turn, Ξ_M^C is the mean instantaneous number of societies per star, $\langle N_{x,C}^B \rangle_M$ is the mean number of selected broadcasts per society, and $N_{x,g}^*$ is the number of stars in the window.

According to the law of total variance (Paper I; Wasserman 2004), the variance in the intercepted emission

$$\mathbb{V}[\mathfrak{M}_x] = \mathbb{V}[\langle \mathfrak{M}_x | \Sigma_x^B, \Sigma_x^C \rangle] + \langle \mathbb{V}[\mathfrak{M}_x | \Sigma_x^B, \Sigma_x^C] \rangle \quad (33)$$

splits into a sample variance term and a noise variance term, respectively. Here $\langle \mathfrak{M}_x | \Sigma_x^B, \Sigma_x^C \rangle$ and $\mathbb{V}[\mathfrak{M}_x | \Sigma_x^B, \Sigma_x^C]$ refer to the mean and variance, respectively, for a fixed sample from selection (x, M) ³, over all possible realizations of the measurement noise. The sample variance for observations of a distant metasociety is then

$$\mathbb{V}[\langle \mathfrak{M}_x | \Sigma_x^B, \Sigma_x^C \rangle] \approx \mathcal{A}^2 \langle N_{x,M}^{B;2} \rangle \left(\langle \mathbf{u}_{x|B}^2 \rangle_M + \langle N_{x,C}^B \rangle_M \langle \mathbf{u}_{x|B} \rangle_M^2 \right) \quad (34)$$

in single metasociety scenarios.

³ Actually, the selection associated with \mathfrak{M}_x , Σ_x^B , and Σ_x^C is (x, U) (see Paper I), but all broadcasts are assumed to arise from the single metasociety M in this paper.

4. INDIVIDUALIST CONSTRAINTS: SIGNAL-TO-NOISE RATIO AND CONFUSION

SETI surveys – and indeed most surveys for astrophysical objects – take an individualist approach, looking for single events that stand out from the background with high signal-to-noise ratio. Individualist constraints use the *extreme* values of an observable \mathfrak{M}_o , but they disregard the rest of its distribution. They can rule out even a single very bright broadcast, but say nothing about even a vast number of very faint broadcasts. In this section, I calculate effective signal-to-noise ratios using the statistics of energy and photon measurements. This lets me explore the effects of confusion with the framework.

4.1. The effective number of independent measurements

Surveys are groups of observations. An archetypal survey consists of N_s^π nonoverlapping pointings (π), each covering a fixed (possibly noncontiguous) field on the sky. While aimed at one location on the sky, the instrument can make independent observations in N_π^θ resolution elements (θ_i) on the sky. The sample of stars covered by these resolution elements is essentially fixed even at different times or frequencies. The number of stars covered in the survey is simply the sum over all resolution elements and pointings, and

$$\langle N_{s,g}^* \rangle \approx N_s^\pi N_\pi^\theta \langle N_{\theta_i,g}^* \rangle_s. \quad (35)$$

Unless a very bright source spills into multiple resolution elements, measurements made in different resolution elements and pointings are independent, taking samples of different societies.

In the box and chord models, a survey has $N_s^o = N_s^\pi N_\pi^\theta T_\theta B_\theta / (T_o B_o)$ observations, but their broadcast samples are not necessarily independent. If broadcasts are very wideband, the same ones will be present across many adjacent frequency channels; very long lived broadcasts will be present in many sequential snapshots. These measurements have high sample covariance, missing the sampling fluctuations between them. I estimate the effective number of independent measurements as $N_s^{o;\text{eff}} \equiv \langle N_s^B \rangle / \langle N_o^B \rangle$:

$$N_s^{o;\text{eff}} \approx \begin{cases} N_s^\pi N_\pi^\theta \frac{(T_\theta + \bar{\tau})(B_\theta + \bar{\beta})}{(T_o + \bar{\tau})(B_o + \bar{\beta})} & (\text{Box}) \\ N_s^\pi N_\pi^\theta \frac{B_\theta + T_\theta \langle |\delta_B| \rangle_M}{B_o + T_o \langle |\delta_B| \rangle_M} & (\text{Chord}). \end{cases} \quad (36)$$

4.2. Signal-to-noise ratio definitions

Most SETI surveys identify candidate “hits” with a differential measurement, looking for abnormally large fluctuations in measurements that are not expected statistically from noise. The signal-to-noise ratio is thus a key quantity in estimating the sensitivity reach of a SETI program. One can estimate the baseline value of

an observable and the usual size of the fluctuations empirically from a collection of related observations. The group of observations analyzed to yield these estimators is not necessarily the survey as a whole, or even all the observations of a particular pointing. Instead, the idea is generally that the observations within a group are comparable, with statistically interchangeable distributions of background (and presumably broadcasts). Hence, we generally want to compare only observations covering the same field at the same time; the noise can change at different times and at different points in the sky. Breakthrough Listen’s turboSETI estimates these quantities in narrowband line searches by comparison with other fine channels in a coarse channel, for instance (Enriquez et al. 2017). The estimation in other programs, particularly those searching for other types of signal, could use different groupings of observations; $\gamma(\mathbf{o})$ stands in for the actual group of observations used.

The signal-to-noise test statistic for each measurement is

$$\mathfrak{S}[\mathfrak{M}_{\mathbf{o}}] = \frac{\text{deviation from mean}}{\text{typical fluctuation}} = \frac{\mathfrak{M}_{\mathbf{o}} - \widehat{\langle \mathfrak{M}_{\mathbf{o}} \rangle}_{\gamma(\mathbf{o})}}{\widehat{\nabla^{1/2}} [\mathfrak{M}_{\mathbf{o}}]_{\gamma(\mathbf{o})}}, \quad (37)$$

where $\widehat{\langle \mathfrak{M}_{\mathbf{o}} \rangle}_{\gamma(\mathbf{o})}$ and $\widehat{\nabla^{1/2}} [\mathfrak{M}_{\mathbf{o}}]_{\gamma(\mathbf{o})}$ are estimators for the mean and standard deviation of $\mathfrak{M}_{\mathbf{o}}$ respectively. Although the sample mean and sample standard deviation of $\mathfrak{M}_{\mathbf{o}}$ within $\gamma(\mathbf{o})$ might be used to evaluate equation 37, this is not necessary: in Enriquez et al. (2017), for example, the trimmed sample mean and standard deviation are used to discard spectral features induced by the processing. The most extreme values of the sample are excluded (those outside the 5th–95th percentile range in Enriquez et al. 2017) before the sample mean and standard deviation are calculated (see Stigler 1973; Castillo et al. 2005). This makes them more robust to the outliers that are inevitable artifacts of data reduction.

A candidate detection is found for observation \mathbf{o} if $\mathfrak{S}[\mathfrak{M}_{\mathbf{o}}] > \bar{\mathfrak{S}}_s$, where the signal-to-noise threshold $\bar{\mathfrak{S}}_s$ is calculated to have a negligible false-alarm rate over the entire survey s . A null result happens when

$$\max [\mathfrak{S}[\mathfrak{M}_{\mathbf{o}}]]_s = \max \left[\frac{\mathfrak{M}_{\mathbf{o}} - \widehat{\langle \mathfrak{M}_{\mathbf{o}} \rangle}_{\gamma(\mathbf{o})}}{\widehat{\nabla^{1/2}} [\mathfrak{M}_{\mathbf{o}}]_{\gamma(\mathbf{o})}} \right]_s \leq \bar{\mathfrak{S}}_s. \quad (38)$$

We calculate the expected sensitivity of a survey by estimating the maximum $\mathfrak{S}[\mathfrak{M}_{\mathbf{o}}]$ expected from a population and comparing it to $\bar{\mathfrak{S}}_s$. If the latter is greater, then no detections are expected. Now, the actual value of $\mathfrak{S}[\mathfrak{M}_{\mathbf{o}}]$ is a nonlinear combination of several factors that is not easily tractable. If different observations have wildly different broadcast populations or noise properties, then the estimated variance itself can vary a lot; the signal-to-noise will be greater in those groups of observations where it is small. A full accounting of these effects may best be found through numerical simulation.

Our goal here is to understand the basic behavior of signal-to-noise ratio and survey sensitivity, how it rises and falls as the number of broadcasts increases. For that reason, I assume that all observations of a metasociety being considered are interchangeable: the $\mathfrak{M}_{\mathbf{o}_i}$ for each observation \mathbf{o}_i all have the same statistical properties, with a constant background noise level and similar broadcast populations sampled by each. I also posit that the background noise fluctuations in $\mathfrak{M}_{\mathbf{o}}$ are negligible compared to the contribution of a detectable broadcast. In other words, the large fluctuations that result in a detection happen because the observation covers more broadcasts or brighter broadcasts than typical. The maximum signal-to-noise ratio is then estimated:

$$\check{\mathfrak{S}}[\mathfrak{M}_{\mathbf{o}}] = \frac{\mathbb{M} \left[\max [\mathfrak{M}_{\mathbf{o},M}^B]_s \right] - \langle \mathfrak{M}_{\mathbf{o},M}^{B:[s,M]} \rangle}{\nabla^{1/2} [\mathfrak{M}_{\mathbf{o}}^{[s,M]}]}, \quad (39)$$

with \mathbf{o} understood to stand in for any representative observation of the galaxy, because the observations are assumed to be interchangeable.⁴ This estimate should be adequate as long as the variance between observations is not too great.

This lends itself to two simple approximations for different $\mathbf{u}_{\mathbf{o}|B}$ distributions, applying if the expected numbers of covered broadcasts and societies, $\langle N_{s,M}^B \rangle$ and $\langle N_{s,M}^C \rangle$, are $\gtrsim 1$. If the fluence distribution is narrow, then fluctuations in the brightness are due mainly to variability in the number of broadcasts intercepted by a broadcast:

$$\begin{aligned} & \mathbb{M} [\max [\mathfrak{M}_{\mathbf{o}}]_s] - \langle \mathfrak{M}_{\mathbf{o}}^{[s]} \rangle \\ & \approx \left(\mathbb{M} \left[\max [N_{\mathbf{o},M}^{B:1}] \right] - \langle N_{\mathbf{o},M}^{B:1} \rangle \right) \langle \mathbf{m}_{\mathbf{o}|B}^{[s,M]} \rangle. \end{aligned} \quad (40)$$

So the biggest signal is the greatest expected excess in the number of broadcasts times the expected emission from a single broadcast. Appendix D presents approximations for the median excess number of broadcasts, but when $\langle N_{\mathbf{o},M}^B \rangle \gtrsim 1$, it has a $\sim \langle N_{\mathbf{o},M}^B \rangle^{1/2}$ dependence up to a logarithmic factor. However, the variance grows at least as quickly, forcing the signal-to-noise ratio to remain below the threshold for detection.

In a broad fluence distribution, however, the fluctuations are determined by a single broadcast that dominates all the others, with $\max [\mathfrak{M}_{\mathbf{o},M}^B]_s \approx \max [\mathbf{m}_{\mathbf{o}|B}]_{s|M} + \langle \mathfrak{M}_{\mathbf{o},M}^B \rangle$:

$$\mathbb{M} [\max [\mathfrak{M}_{\mathbf{o}}]_s] - \langle \mathfrak{M}_{\mathbf{o}}^{[s,M]} \rangle \approx \mathbb{M} \left[\max [\mathbf{m}_{\mathbf{o}|B}]_{s|M} \right]. \quad (41)$$

Power-law distributions ($\psi [\mathbf{m}_{\mathbf{o}|B}]_M \propto \mathbf{m}_{\mathbf{o}|B}^{-\gamma}$) behave like broad distributions when $\gamma < 3$, as long as

⁴ The inverted hat is used here to mean a theoretical estimate, in contrast to an estimator derived from actual data.

$\mathbb{M} \left[\max [\mathbf{m}_{\text{o|B}}]_{s|M} \right]$ is much smaller than the maximum possible $\mathbf{m}_{\text{o|B}}$. Note, however, that any distribution with $\gamma \leq 1$ must have a maximum cutoff that is saturated quickly.

I define a single variable, an effective number of broadcasts, to encapsulate both approximations:

$$N_{\text{o},M}^{\text{B;eff}} \equiv \max \left[\left(\mathbb{M} \left[\max [N_{\text{o},M}^{\text{B};1}]_s \right] - \langle N_{\text{o},M}^{\text{B};1} \rangle \right), \frac{\mathbb{M} \left[\max [\mathbf{m}_{\text{o|B}}]_{s|M} \right]}{\langle \mathbf{m}_{\text{o|B}}^{[s,M]} \rangle} \right], \quad (42)$$

with

$$\check{\mathfrak{S}}[\mathfrak{M}_{\text{o}}] \approx \frac{N_{\text{o},M}^{\text{B;eff}} \langle \mathbf{m}_{\text{o|B}}^{[s,M]} \rangle}{\mathbb{V}^{1/2} [\mathfrak{M}_{\text{o}}^s]}. \quad (43)$$

Ideally, we would like a very large number of *independent* measurements to both accurately estimate the mean and observe rare maxima in \mathfrak{M}_{o} . As noted, wide-band and long-duration broadcasts reduce the number of effective independent measurements to $N_{\text{s}}^{\text{B;eff}}$ (equation 36).

4.3. The sparse limit

The common assumption in SETI is that broadcasts are very rare, with $\langle N_{\text{o},M}^{\text{B}} \rangle \ll 1$. In the sparse limit, if any broadcasts are intercepted at all, all observations have at most one ($\max [N_{\text{o},M}^{\text{B}}]_s = 1$) and the maximum signal-to-noise occurs for the observation containing the brightest broadcast ($\max [\mathfrak{M}_{\text{o},M}^{\text{B}}]_s = \max [\mathbf{m}_{\text{o|B}}]_{s|M}$). Then, a null result implies either

$$\frac{\max [\mathbf{m}_{\text{o|B}}]_{s|M}}{\mathbb{V}^{1/2} [\mathfrak{M}_{\text{o}}]} \lesssim \bar{\mathfrak{S}}_s \text{ or } N_{\text{s},M}^{\text{B}} = 0 : \quad (44)$$

they are either too faint or too rare to observe. The two conditions in fact correspond to the luminosity and rate limits that are so commonly quoted in SETI (e.g., Enriquez et al. 2017 and references therein, as shown in that work’s Figure 7).

Usually, the broadcasts are assumed to be sparse enough that the background noise is expected to dominate the variance, with $\mathbb{V} [\mathbf{m}_{\text{o|n}}]$ used to estimate total variance. Sufficiently powerful broadcasts can dominate the variance, however, long before $\langle N_{\text{o},M}^{\text{B}} \rangle$ increases past 1, just because they are contributing so much energy. Trimmed means and standard deviations help address this problem by discarding a certain percentage of the observations with the highest values of \mathfrak{M}_{o} , but once $\langle N_{\text{o},M}^{\text{B}} \rangle$ rises past that fraction, the effect of broadcasts on the noise must be taken into account.

4.4. The confusion limit

As $\langle N_{\text{o},M}^{\text{B}} \rangle$ increases past 1, however, $\mathfrak{M}_{\text{o},M}^{\text{B}}$ nearly converges to a stable distribution by the central limit

theorem under certain general conditions (Embree et al. 2013).⁵ If $\langle \mathbf{m}_{\text{o|B}} \rangle_M$ exists, then once there are enough broadcasts to sample the emission distribution well in each observation ($\langle \mathbf{m}_{\text{o|B}} \rangle_M \approx \langle \mathbf{m}_{\text{o|B}}^{[s,M]} \rangle_M$), $\mathfrak{M}_{\text{o},M}^{\text{B}}$ should approach $\langle N_{\text{o},M}^{\text{B}} \rangle \langle \mathbf{m}_{\text{o|B}} \rangle_M$ by the law of large numbers. This is a quantity that continues growing with $\langle N_{\text{o},M}^{\text{B}} \rangle$. The mean emission from all the broadcasts intercepted by an observation eventually becomes much greater than the brightest single broadcast. In this confusion limit, the broadcasts effectively blend together into another noise background and the individualist approach of equation 38 fails. This leads to a new problem in SETI: we might fail to detect ETIs not because they are too rare but because they are too common!

To be clear, confusion only sets in when there are too many broadcasts per observation – generally a separate epoch, channel, and beam in radio. The number of broadcasts covered in a survey, or even a single pointing, can be far greater, while still leaving “empty” observations that contrast with the occupied observations. The more fine-grained the survey, the less of an issue confusion should be. Modern surveys may cover billions of observations and could detect many millions of broadcasts before confusion sets in.

The convergence happens even in the absence of noise and is an effect of the underlying distribution of samples. Confusion is implicit in the sample variance $\mathbb{V} [\langle \mathfrak{M}_{\text{o}} | \Sigma_{\text{o}}^{\text{B}}, \Sigma_{\text{o}}^{\text{C}} \rangle]$. Because the variance is necessarily larger than the sample variance alone, equation 34 gives a hard upper bound on the estimated signal-to-noise ratio:

$$\check{\mathfrak{S}}[\mathfrak{M}_{\text{o}}] \lesssim N_{\text{o},M}^{\text{B;eff}} \left[\langle N_{\text{o},M}^{\text{B};2} \rangle \frac{\langle \mathbf{u}_{\text{o|B}}^{[s,M]2} \rangle_M}{\langle \mathbf{u}_{\text{o|B}}^{[s,M]} \rangle_M^2} \right]^{-1/2} \quad (45)$$

for distant galaxies with one metasociety under the diffuse approximation. Confusion resulting from the sample variance alone is dubbed here “sample confusion”, to contrast with the (rarer) “noise confusion” from noise variance. Sample confusion can be said to set in when the right-hand side falls below the detection threshold $\bar{\mathfrak{S}}_s$.

Assuming that the fluence distribution is narrow and the diffuse approximation applies, this converges to

$$\check{\mathfrak{S}}[\mathfrak{M}_{\text{o}}] \lesssim \left(\mathbb{M} \left[\max [N_{\text{o},M}^{\text{B};1}]_s \right] - \langle N_{\text{o},M}^{\text{B};1} \rangle \right) / \sqrt{\langle N_{\text{o},M}^{\text{B};2} \rangle}. \quad (46)$$

⁵ These conditions do not precisely hold because $N_{\text{o},M}^{\text{B}}$ is itself a random variable; the limiting distribution is a mixture of stable distributions. Nonetheless, in the diffuse approximation for Poissonian broadcasts, $N_{\text{o},M}^{\text{B}}$ itself converges to a narrow Gaussian, so the effects of the spread are weak.

The sample variance is driven by a kind of shot noise – not in photons or electrons, but in the broadcasts themselves, akin to the “graininess” of good optical images of galaxies arising from variations in the number of discrete bright stars (Tonry & Schneider 1988). But the numerator falls and rises as $\mathbb{M}[\max[N_{\circ,M}^B]_s] / \langle N_{\circ,M}^B \rangle$; this ratio is large only if most observations have no broadcasts so we can compare unoccupied and occupied observations. Thus, the estimated maximum signal-to-noise ratio decreases at least as $\langle N_{\circ,M}^B \rangle^{1/2}$, until $\langle N_{\circ,M}^B \rangle \gtrsim 1/\bar{\mathfrak{S}}_s^2$ by which point it is too small to pass the stringent cuts used to eliminate false positives.

Broad $u_{\circ|B}$ distributions may be essentially immune to confusion even when $\langle N_{\circ,M}^B \rangle \gg 1$, because increasing $\langle N_{\circ,M}^B \rangle$ also results in much brighter broadcasts being intercepted. The maximum fluence broadcast rises above the background of confused broadcasts present in all observations for a broad enough distribution. Often, however, there is a maximum fluence, limited by the maximum available power, the nearest star, or zero drift rate. These brightest broadcasts must be submerged in the aggregate background in order for confusion to set in. Define a window ζ that samples from \circ but only passes broadcasts from this end of the distribution:

$$\Sigma_{\zeta,J}^B = \{\mathbf{w}_B | \mathbf{w}_B \in \Sigma_{\circ,J}^B \text{ and } u_{\circ|B} \approx \max u_{\circ|B}\}. \quad (47)$$

This effectively *induces* a narrow fluence distribution in the remaining sample; if there’s already a narrow fluence distribution, the ζ window is equivalent to the observation window. Now, if the bright subset of broadcasts picked by ζ are confused on their own, then the entire sample is confused – there are no even brighter broadcasts to stick out of the blended emission, and the faint broadcasts only add to the “noise.” Thus, a very conservative constraint for confusion is that it sets in when

$$\langle N_{\zeta,M}^B \rangle \gtrsim 1/\bar{\mathfrak{S}}_s^2, \quad (48)$$

an approximate result for equation 46 applied to a population of only these brightest broadcasts, with the signal-to-noise required to be above $\bar{\mathfrak{S}}_s$.

4.5. The rise and fall of signal-to-noise ratio

Consider the behavior of $\check{\mathfrak{S}}[\mathfrak{E}_\circ]$ when $u_{\circ|B}$ has a narrow distribution. As $\langle N_{\circ,M}^B \rangle$ increases, we can discern six regimes:

- In a null regime, $\max[N_{\circ,M}^B]_s = 0$. Derived signal-to-noise ratios have values of order unity, resulting entirely from fluctuations in the background.
- When considering possible hits, most SETI analyses work in a strongly sparse regime, where the broadcasts are rare enough to have no effect on the estimated background. Furthermore,

$\max[N_{\circ,M}^B]_s = 1$ because there are too few observations for multiple broadcasts to ever “touch” the same observation window. Thus, $\check{\mathfrak{S}}[\mathfrak{E}_\circ]$ remains constant at a value that can be $\gg 1$.

- In a moderately sparse regime, the background noise continues to dominate the variance. Although the typical observation still has no broadcasts, some have at least one, and $\max[N_{\circ,M}^B]_s > 1$. $\check{\mathfrak{S}}[\mathfrak{E}_\circ]$ is rising in this regime because $\max[N_{\circ,M}^B]_s$ is growing while $\langle N_{\circ,M}^B \rangle$ remains below one. The onset of this regime occurs at $\langle N_{\circ,M}^B \rangle \sim (N_s^{\circ:\text{eff}})^{-1/2}$.
- In a transition regime, the broadcasts themselves dominate the variance of \mathfrak{E}_\circ . The slow rise of $\max[N_{\circ,M}^B]_s$ is overcome by the rising variance. $\check{\mathfrak{S}}[\mathfrak{E}_\circ]$ falls as $\langle N_{\circ,M}^B \rangle^{-1/2}$ to $\langle N_{\circ,M}^B \rangle^{-1}$ in this regime, although it may be still high enough to claim a detection. Using the trimmed means and standard deviations effectively delays the onset of the transition regime so that it has no dependence on $N_s^{\circ:\text{eff}}$.
- In the confusion regime, the typical observation has at least one broadcast. $\check{\mathfrak{S}}[\mathfrak{E}_\circ]$ continues to decline due to the sample variance, as according to equation 45. The rate of the decline slows down because $\max[N_{\circ,M}^B]_s - \langle N_{\circ,M}^B \rangle$ starts growing as $\langle N_{\circ,M}^B \rangle_s^{1/2}$. At this point $\check{\mathfrak{S}}[\mathfrak{E}_\circ]$ is a factor of order unity, too small to make any individualist detections.
- Finally, radio broadcasts experience a mutual interference regime, where the broadcasts are so numerous that the noise variance from their wave noise dominates over the sample variance. $\check{\mathfrak{S}}[\mathfrak{E}_\circ]$ becomes indistinguishable from the null case. Equation 39 no longer describes the numerator of $\check{\mathfrak{S}}[\mathfrak{E}_\circ]$ – the wave noise fluctuations from the interference between the broadcasts, not the Poisson fluctuations, dominate variations in \mathfrak{E}_\circ .

In short, the signal-to-noise ratio at first rises as broadcasts start being sampled and then falls as they overlap with each other. The borders between these regimes depend on the number of independent observations, the construction of observations, and the luminosities of the broadcasts. Not all of these regimes occur for all parameters or all types of broadcasts. In broad distributions, $\check{\mathfrak{S}}[\mathfrak{E}_\circ]$ is governed by the broadcasts with the greatest fluence. The strong sparse regime can split into two stages: signal-to-noise ratio increases at first, as signals with increasing energy per observation are intercepted, followed by a regime of flat signal-to-noise ratio, where all observations have 0 or 1 broadcast with near-maximal fluence.

5. INDIVIDUALIST CONSTRAINTS: RADIO BROADCASTS

5.1. Wave noise, modes, and amplitudes

Natural electromagnetic radiation can be regarded as the sum of many microscopic emitters with different locations, frequencies, and phases. The mutual interference between all these sources results in the amplitude of the detected radiation fluctuating chaotically instead of maintaining a constant magnitude. In quantum terms, chaotic light displays photon bunching (e.g., Foellmi 2009; Tan et al. 2014; Zmuidzinas 2015). These wave noise fluctuations greatly dominate over photon shot noise at radio wavelengths because the photon occupation number in each field mode (cell in phase space) is much greater than one (Radhakrishnan 1999). Thermal noise in the receiver usually overwhelms over the wave noise from sources, with a greater noise temperature, but it too is the chaotic sum of many microscopic fluctuations. Artificial broadcasts may be coherent (Hippke 2021; see also Appendix B of Cordes et al. 1997), but wave noise is still present in the background and in the mutual interference of many broadcasts.

Although we generally measure energy in radio SETI, the statistics of the intercepted energy follow from the underlying wave amplitudes of the electric field, commonly measured as voltages (Wilson et al. 2009). Each amplitude is measured for an individual mode μ of the electromagnetic field. A mode is an independent oscillator of the electromagnetic field. A photon can be localized to a single mode, but no further. In terms of temporal properties, a mode includes only one polarization and has a bandwidth-duration product $T_\mu B_\mu = 1$ (Yamamoto & Haus 1986; Nityananda 1994; Caves & Drummond 1994; Hippke 2021). Amplitudes add linearly: the amplitude measured in mode μ is

$$\mathfrak{A}_\mu = \mathfrak{a}_{\mu|n} + \sum_{\mathbf{w}_B \in \Sigma_\mu^B} \mathfrak{a}_{\mu|B}. \quad (49)$$

The background amplitude $\mathfrak{a}_{\mu|n}$ is an independent random variable with a zero-mean complex Gaussian distribution (e.g., Wilson et al. 2009). The same is true for the amplitudes of broadcasts that are incoherent, although each has its own amplitude variance.

Square-law detectors derive the energy in the mode by taking the square of its complex modulus, $\mathfrak{E}_\mu = \mathfrak{A}_\mu \mathfrak{A}_\mu^*$.⁶ As a thermal noise, the background energy $\mathfrak{e}_{\mu|n} = |\mathfrak{a}_{\mu|n}|^2$ per mode has a mean value $k_B \mathcal{T}_n$, which is the background temperature (including system noise and natural background radio flux in the field) multiplied by

⁶ This is the power if voltage is being directly squared, up to a constant factor; I adopt a convention that $|\mathfrak{A}_\mu| = \sqrt{\mathfrak{E}_\mu}$.

Boltzmann's constant (Radhakrishnan 1999).⁷ The energy intercepted from a broadcast, $\mathfrak{e}_{\mu|B}$, is the product of fluence, collecting area, and instrumental response.⁸ Thus,

$$\langle \mathfrak{E}_\mu | \Sigma_\mu^B, \Sigma_\mu^C \rangle = k_B \mathcal{T}_n + \sum_{\mathbf{w}_B \in \Sigma_\mu^B} \mathcal{A} \mathcal{I}_{\mathfrak{E};\mu}(\theta_B) \mathfrak{h}_{\mu|B}, \quad (50)$$

and, for distant metasocieties,

$$\langle \mathfrak{E}_\mu \rangle \approx k_B \mathcal{T}_n + \langle N_{\mu,M}^{B;1} \rangle \mathcal{A} \langle \mathfrak{h}_{\mu|B} \rangle_M. \quad (51)$$

The variance depends on the number and type of broadcasts.

5.2. Energy measured in an observation

Where complications arise is that usually the analysis does not work directly with these mode energies either. The energy in N_\circ^μ modes per observation – covering different times, frequencies, or polarizations – is summed together to yield an observed energy \mathfrak{E}_\circ :

$$\mathfrak{E}_\circ = \sum_{\mu \in S_\circ^\mu} \mathfrak{E}_\mu, \quad (52)$$

where S_\circ^μ is the set of modes that are summed for the observation \circ . It can be assumed that the modes are interchangeable, with statistically equivalent populations of broadcasts, because observations are so fine-grained. The mean energy in the observation follows simply enough from equation 51 and the linearity of expectation:

$$\langle \mathfrak{E}_\circ \rangle \approx N_\circ^\mu \left[k_B \mathcal{T}_n + \langle N_{\mu,M}^{B;1} \rangle \mathcal{A} \langle \mathfrak{h}_{\mu|B} \rangle_M \right], \quad (53)$$

assuming that the target galaxy is distant.

The sample variance for a distant galaxy with a single metasociety is

$$\mathbb{V} [\langle \mathfrak{E}_\circ | \Sigma_\circ^B, \Sigma_\circ^C \rangle] \approx \mathcal{A}^2 \left\langle N_{\circ,M}^{B;2} \right\rangle \left[\langle \mathfrak{h}_{\circ|B}^2 \rangle_M + \langle N_{\circ,C}^{B;1} \rangle_M \langle \mathfrak{h}_{\circ|B} \rangle_M^2 \right]. \quad (54)$$

$\langle N_{\circ,C}^{B;1} \rangle_M$ is the mean number of broadcasts per society, representing a clumping effect.

⁷ This also follows from the Rayleigh-Jeans law, with one mode covering a solid angle equal to the wavelength squared divided by collecting area (Zmuidzinas 2003).

⁸ Note that $\mathcal{I}_{\mathfrak{E};\mu}$ is the *energy* (power) beam pattern of the instrument, not the amplitude (voltage) response $\mathcal{I}_{\mathfrak{A};\mu} = \sqrt{\mathcal{I}_{\mathfrak{E};\mu}}$.

In Appendix B.1, I show that the noise variance for distant metasocieties is

$$\begin{aligned} \langle \mathbb{V}[\mathfrak{E}_o | \Sigma_o^B, \Sigma_o^C] \rangle &\approx \sum_{\mathbf{w}_B \in \Sigma_o^B} \sum_{\mu_1, \mu_2 \in \mathcal{S}_o^\mu} \text{Cov}[\mathfrak{e}_{\mu_1|B}, \mathfrak{e}_{\mu_2|B}] \\ &+ N_o^\mu \left[\left(k_B \mathcal{T}_n + \mathcal{A} \langle N_{\mu,M}^{B;1} \rangle \langle \mathfrak{h}_{\mu|B} \rangle_M \right)^2 \right. \\ &\quad \left. + \mathcal{A}^2 \langle N_{\mu,M}^{B;2} \rangle \langle \mathfrak{h}_{\mu|B}^2 \rangle_M \right]. \end{aligned} \quad (55)$$

by working with the amplitudes. The covariance $\text{Cov}[\mathfrak{e}_{\mu_1|B}, \mathfrak{e}_{\mu_2|B}]$ for broadcast B equals $\langle \mathfrak{e}_{\mu_1|B} \mathfrak{e}_{\mu_2|B} \rangle - \langle \mathfrak{e}_{\mu_1|B} \rangle \langle \mathfrak{e}_{\mu_2|B} \rangle$ and is related to the coherence properties of the broadcast.

The noise variance includes the mutual interference of the background and numerous broadcasts, resulting in a quasi-thermal background even if the broadcasts are coherent. This interference puts an additional upper limit to the signal-of-noise ratio of

$$\check{\mathfrak{S}}[\mathfrak{E}_o] \lesssim \frac{N_{o,M}^{B;\text{eff}}}{\sqrt{N_o^\mu} \langle N_{\mu,M}^{B;1} \rangle}. \quad (56)$$

This can lead to a “noise confusion”, which in some cases can set in before the previously derived sample confusion (equation 46).

5.3. Incoherent radio broadcasts

The incoherent case applies to all known natural phenomena, including astrophysical masers where radio amplitude statistics have been measured (Evans et al. 1972). It may also apply to artificial broadcasts if they are sufficiently broadband, as expected if they are rich in information (see Caves & Drummond 1994; Messerschmitt 2015). We can model a broadcast as a burst of white noise with a (possibly frequency drifting) band-pass filter applied to it, as in the box model; if the instantaneous bandwidth $\beta_{t|B}$ is wider than τ_μ^{-1} , the broadcast is incoherent. Furthermore, when many coherent broadcasts are confused, the aggregate emission also behaves like an incoherent source.

The noise variance calculation is presented in Appendix B.1, but essentially it may be calculated from the fact that the noise is independent between modes. We find for distant galaxies under the diffuse approximation

$$\begin{aligned} \mathbb{V}[\mathfrak{E}_o] &\approx N_o^\mu \left(k_B \mathcal{T}_n + \mathcal{A} \langle N_{\mu,M}^{B;1} \rangle \langle \mathfrak{h}_{\mu|B} \rangle_M \right)^2 \\ &+ \mathcal{A}^2 \left[N_o^\mu \langle N_{\mu,M}^{B;2} \rangle \langle \mathfrak{h}_{\mu|B}^2 \rangle_M + \langle N_{o,M}^{B;2} \rangle \langle \mathfrak{h}_{o|B}^2 \rangle_M \right] \end{aligned} \quad (57)$$

(see Appendix B.2 for the full expression).

5.3.1. Confusion and searching for continuum sources in the box model

In the box model, hisses are flat-spectrum continuum sources ($\bar{\tau} \gg \tau_o$, $\bar{\beta} \gg \beta_o$). When observing a distant galaxy in both polarizations,

$$\begin{aligned} \check{\mathfrak{S}}[\mathfrak{E}_o] &\approx N_{o,M}^{B;\text{eff}} \check{\mathfrak{S}}[\mathfrak{e}_{o|B}] \left[\left(1 + \frac{\check{\mathfrak{S}}[\mathfrak{e}_{o|B}] \langle N_{o,M}^{B;1} \rangle}{\sqrt{N_o^\mu}} \right)^2 \right. \\ &\quad \left. + \check{\mathfrak{S}}[\mathfrak{e}_{o|B}]^2 \langle N_{o,M}^{B;2} \rangle \frac{\langle \langle \ell_{\nu;B}^{[s,M]} \rangle^2 \rangle_M}{\langle \ell_{\nu;B}^{[s,M]} \rangle_M^2} \left(\frac{1}{N_o^\mu} + 1 \right) \right]^{-1/2} \end{aligned} \quad (58)$$

where I have applied the diffuse approximation, and

$$\check{\mathfrak{S}}[\mathfrak{e}_{o|B}] \equiv \frac{\mathcal{A} \langle \mathfrak{h}_{o|B}^{[s,M]} \rangle_M}{\sqrt{N_o^\mu} k_B \mathcal{T}_n} \approx \frac{\mathcal{A} \langle \ell_{\nu;B}^{[s,M]} \rangle_M \langle y_{\epsilon;B} \chi_{\epsilon;B} \rangle_M \sqrt{N_o^\mu}}{2k_B \mathcal{T}_n} \quad (59)$$

is the expected signal-to-noise ratio for a single broadcast at $\mathcal{I}_{\mathfrak{e},o} = 1$ in the presence of background noise only. If individual broadcasts in isolation are detectable ($\check{\mathfrak{S}}[\mathfrak{e}_{o|B}] \gtrsim 1$), the threshold of the transition region (section 4.5) is passed when $\langle N_{o,M}^B \rangle \gtrsim 1/\check{\mathfrak{S}}[\mathfrak{e}_{o|B}]^2$. The confusion regime occurs around when $\langle N_{o,M}^B \rangle \gtrsim 1/\bar{\mathfrak{S}}_s^2$, which translates to

$$\Xi_M^B \gtrsim \left[\bar{\mathfrak{S}}_s^2 \langle N_{o,g}^* \rangle \right]^{-1} \quad (60)$$

for hisses. Broadcast mutual interference becomes the dominant noise source for $\langle N_{o,M}^B \rangle \gtrsim N_o^\mu$. Figure 2 shows how $\check{\mathfrak{S}}[\mathfrak{E}_o]$ varies with $\langle N_{o,M}^B \rangle$ under standard assumptions – in particular, how the transition regime is absent for $\check{\mathfrak{S}}[\mathfrak{e}_{o|B}] = 1$, while the moderate sparse regime vanishes for high $\check{\mathfrak{S}}[\mathfrak{e}_{o|B}]$.

5.4. Fully and partially coherent radio broadcasts

Unlike known natural sources, artificial radio broadcasts can be coherent. Although a perfect coherent carrier contains negligible information, it conveys one important fact very well – the existence of technology at that location – perhaps “advertising” dimmer information-rich broadcasts in the vicinity.

Perfectly coherent broadcasts are characterized as perfect chirps, with a constant luminosity and a well-defined phase φ_B at any time: $\mathfrak{a}_B(t, p) = |\mathfrak{a}_B(p)| \exp(i\varphi_B(t, p))$. The measured amplitudes can vary from mode to mode as the broadcast drifts across channels, but there is zero noise variance, ignoring the miniscule Poissonian photon shot noise – ϵ_B is exactly proportional to \mathfrak{h}_B – and thus all covariance terms are zero.

The partially coherent case is an important one for actual ultranarrowband broadcasts. Any modulation of a perfect chirp will broaden the instantaneous bandwidth. This leads to fluctuations that are correlated on long timescales. In fact, even if the broadcast itself is perfectly coherent, scintillation in the interstellar medium introduces observed variability (Cordes

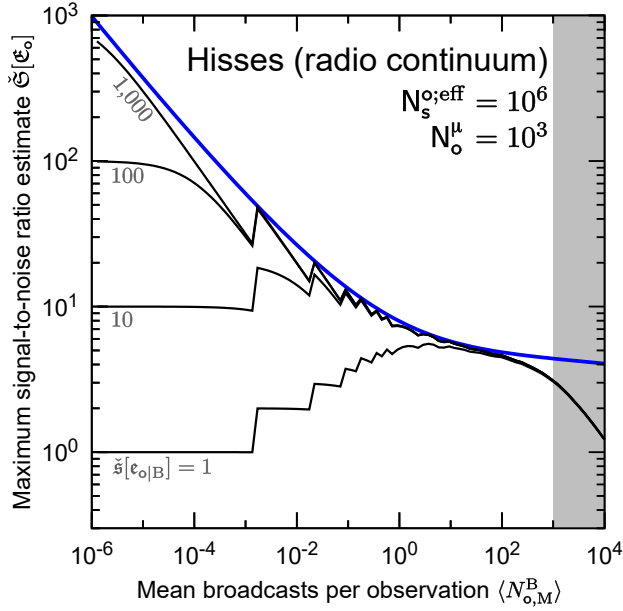


Figure 2. Growth and fall of total signal-to-noise ratio $\check{S}[\epsilon_o]$ as the number of broadcasts per observation increases and confusion sets in, as depicted for for radio continuum sources, in the hiss regime of the box model. I adopt the standard assumptions of Table 2. All broadcasts have the same luminosity. Each individual source, in the absence of other sources, would have a signal-to-noise ratio of $\check{s}[\epsilon_{o|B}]$ ranging from 1 to 1000. The blue line indicates the bound from sample variance. The mutual interference regime, where the approximation for $\check{S}[\epsilon_o]$ breaks down, is shaded in grey. The survey contains 10^6 independent observations, where each observation is summed from 10^3 electromagnetic modes.

et al. 1997; Brzycki et al. 2023). In the partially coherent case, the coherence timescale $\tau_{c;B} \approx \beta_{t|B}^{-1}$ is greater than T_μ . Modes of the same polarization and separated by less than $\tau_{c;B}$ in time then have $\text{Cov}[\epsilon_{\mu_1|B}, \epsilon_{\mu_2|B}] \sim \langle \epsilon_{\mu_1|B} \rangle \langle \epsilon_{\mu_2|B} \rangle$. The fall-off of the covariance can be described by the well-known $g_{p;B}^{(2)}(\Delta t)$ function (e.g., Foellmi 2009; see Appendix B.3).

Both the fully coherent and partially coherent cases can be covered in a single formula with the use of a factor describing the self-interference:

$$\begin{aligned} \mathbb{V}[\epsilon_o] \approx N_o^\mu & \left(k_B \mathcal{T}_n + \mathcal{A} \langle N_{\mu,M}^{B;1} \rangle \langle h_{\mu|B} \rangle_M \right)^2 \\ & + \mathcal{A}^2 \langle N_{o,M}^{B;2} \rangle \langle h_{o|B}^2 \rangle_M (1 + \langle \xi_{c;o|B} \rangle_M) \end{aligned} \quad (61)$$

in the diffuse approximation for a distant galaxy. The coherence term $\xi_{c;o|B}$ ranges from 0 for fully coherent broadcasts to 1 for polarized, partially coherent broadcasts with slow ($\tau_{c;B} \gg T_o$), high-amplitude fluctuations (see Appendix B.1).

Although the variance is missing a term related to self-interference, it is greatly increased by strong, long-

timescale fluctuations, with $\langle \xi_{c;o|B} \rangle_M \approx 1$ essentially doubling the sample variance. It may seem odd that a perfectly coherent broadcast with $\beta_{t|B} = 0$ has less noise variance than expected from Gaussian statistics, while a partially coherent broadcast with $\tau_{c;B} \gg T_o$ can have more, despite being indistinguishable – especially since this is the regime of actual coherent broadcasts from space modulated by strong scattering. The discrepancy basically amounts to whether we treat the fluctuations as noise variance or sample variance.

Suppose we took a snapshot of a large population of partially coherent broadcasts, all with infinite life spans and fully polarized, all with the same $\tau_{c;B} \gg T_o$, and all with the same *time-averaged* luminosity. Because they are only partially coherent, the *measured* brightness of the different broadcasts will vary – in fact, we might generally expect them to have an exponential distribution just as if they are incoherent (compare with Cordes et al. 1997).⁹ The partial coherence approach treats the variations as the result of microscopic fluctuations on an underlying constant luminosity. Thus, the variations are included in the noise variance.

But since the fluctuations are much too slow to observe, from an empirical point of view, we could conclude that the broadcasts are perfectly coherent but that *the luminosities themselves differ*. That is, the exponential distribution in fluence reflects an exponential distribution in luminosity, and thus we regard the fluctuations as sample variance, resulting from a $\langle \hat{\ell}_B^2 \rangle_M = 2 \langle \hat{\ell}_B \rangle_M^2$ term. Either approach is consistent as long as we choose one convention and stick with it, to avoid double-counting the fluctuations.

If we take many snapshots of the population separated by $\gg \tau_{c;B}$, we will observe the partially coherent broadcasts varying in luminosity. The sample variance approach would interpret this as intrinsic variability in the broadcast luminosities themselves; the instantaneous distribution of $\hat{\ell}_B$ in the population would reflect the temporal distribution of $\hat{\ell}_B$ for each individual broadcast. Since the box and chord models assume a nonvarying luminosity, I proceed with the noise interpretation for partially coherent broadcasts (degenerate $\hat{\ell}_B$, $\langle \xi_{c;o|B} \rangle_M = 1$). Despite this, I group the corresponding variance term with the sample variance because it behaves in exactly the same way, considering this noise term to contribute to sample confusion instead of noise confusion.

⁹ The wave noise of an unpolarized broadcast does not have an exponential distribution – the power received in *each* polarization has an exponential distribution, but the polarizations can vary independently of each other. As a result, the total power in both polarizations has a χ_4^2 distribution. An exponential distribution still applies if the modulation in both polarizations is identical, as might apply for interstellar scintillation.

5.4.1. *Confusion and lines in the chord model*

Ultrabroadband line searches look for lines with different drift rates, essentially seeking concentrations of energy when summing along skewed lines in spectrograms (for example, by applying a frequency shift to each time step, as in [Siemion et al. 2013](#)). The dedrifting is performed on data that sample time and frequency (\mathbf{d} -type windows). With coherent dedispersion, each data point corresponds to one mode. More often, dedrifting is performed on a spectrogram where each data point is the sum of the energy in several modes, summed sequentially in time (as in [Lebofsky et al. 2019](#)). After dedrifting, a detected line appears on a spectrogram like a broadened line with no drift. An observation is constructed by summing several sequential data points together into an observation. Each observation has an associated (de)drift rate Δ_o applied to it. A dedrifted line B has

$$\langle \mathbf{e}_{o|B}(\text{dedrifted}) \rangle \approx \frac{\mathcal{I}_{\mathbf{e};o}(\boldsymbol{\theta}_B) \mathcal{A}_{\mathcal{L}_B}^{\circ} y_{\epsilon;B} \chi_{\epsilon;B} \zeta_{o|B} T_o}{\max(1, |\delta_B| T_d / B_o)}. \quad (62)$$

The second term in the denominator accounts for smearing resulting from the line crossing in and out of each datum point within T_d ([Sheikh et al. 2019](#); [Margot et al. 2021](#)). Any remaining lines continue to have a range of drift rates.

In order to understand how a wider spread in drift rate affects detectability, I express the signal-to-noise of an observation in terms of the counterfactual expected number of broadcasts and individual broadcast signal-to-noise ratio if the drift rate for all broadcasts were forced to zero. The former quantity is

$$\langle N_{0;o,M}^B \rangle = \langle N_{o,g}^* \rangle Z_M^B B_o \quad (63)$$

(equation 21), and is the expected number of broadcasts per observation channel at any one instant. It is a direct proxy for the abundance of transmitters. The latter is

$$\begin{aligned} \check{s}_0[\mathbf{e}_{o|B}] &\equiv \check{s}[\mathbf{e}_{o|B} | \delta_B = \Delta_o = 0] \\ &= \frac{\mathcal{A} \langle \ell_B^{[s,M]} \rangle_M \langle y_{\epsilon;B} \chi_{\epsilon;B} \rangle_M |\Pi_o| T_o}{2\sqrt{N_o^u} k_B \mathcal{T}_n}. \end{aligned} \quad (64)$$

There are fewer broadcasts in the absence of drift, but they individually would have higher signal-to-noise ratios, and the product is invariant ($\check{s}_0[\mathbf{e}_{o|B}] \langle N_{0;o,M}^B \rangle = \check{s}[\mathbf{e}_{o|B}] \langle N_{o,M}^B \rangle$; see [Appendix B.3](#)).

For a randomly chosen trial drift rate Δ_o , there may be lines that serendipitously are dedrifted, but a SETI analysis seeks for drift rates that yield the highest signal-to-noise ratio. Hence, sensitivity is generally better evaluated by supposing that the analysis has found one of these lines and chosen $\Delta_o = \delta_B$ for that line. We specify whether or not we have found a line with $I_{o,M}^B$: it is 1 when we consider only an observation that definitely has

a dedrifted line in it, and 0 if we have a typical observation with a typical sample of serendipitous lines. For observations in both polarizations of a distant galaxy with transmitters of identical luminosity, the diffuse approximation gives us

$$\begin{aligned} \check{\mathfrak{S}}[\mathfrak{E}_o] &\approx \check{s}_0[\mathbf{e}_{o|B}] \left[\frac{I_{o,M}^B}{\max(1, |\Delta_o| T_d / B_o)} + \Delta N_{o,M}^{\text{B;eff}} \right] \\ &\cdot \left[\left(1 + \frac{\check{s}_0[\mathbf{e}_{o|B}] \langle N_{0;o,M}^{\text{B};1} \rangle}{\sqrt{N_o^u}} \right)^2 \right. \\ &\left. + \check{s}_0[\mathbf{e}_{o|B}]^2 \langle N_{0;o,M}^{\text{B};2} \rangle \xi_{\delta;o,M}^B (1 + \langle \xi_{c;o|B} \rangle_M) \right]^{-1/2}, \end{aligned} \quad (65)$$

where $\xi_{\delta;o,M}^B \equiv \langle \tau_{o|B}^2 \rangle_M / (T_o \langle \tau_{o|B} \rangle_M)$ and $\Delta N_{o,M}^{\text{B;eff}}$ is a quantity describing the contribution of serendipitous lines (see [Appendix B.3.4](#) for details). The value of $\xi_{\delta;o,M}^B$ is difficult to calculate when a dedrifting algorithm is applied, because of the way it ‘‘slices’’ lines, complicating the analysis ([Appendix B.3](#)). I present results for the case when no dedrifting is applied in [Figure 3](#), in which case there is no smearing. Basically, however, the signal-to-noise ratio for high intrinsic drift rate lines is expected to be suppressed, but it may be more resistant to confusion.

Dedrifting serves to accumulate the energy in $\max[1, |\Delta_o| T_d / B_o]$ channels when we do find a line ($I_{o,M}^B = 1$). Sample variance is generally suppressed; when $\Delta_o = 0$, $\xi_{\delta;o,M}^B \propto \bar{\delta}_M^{-1} \ln \bar{\delta}_M$ – the mean collected fluence is the same, but it is divided among a larger number of quickly transiting broadcasts. In the sparse regime, the smearing within each time point decreases the signal-to-noise ratio of individual broadcasts (as noted in [Sheikh et al. 2019](#); [Margot et al. 2021](#)). The reduction of sample variance can be expected to delay sample confusion, however, compared to the low drift rate case.

We can evaluate when sample confusion sets in by again using the sample variance as a minimum variance and finding when $\check{\mathfrak{S}}[\mathfrak{E}_o] \lesssim \bar{\mathfrak{S}}_s$. The sample variance is increased by a factor $(1 + \langle \xi_{c;o|B} \rangle_M)$ because the slow wave noise fluctuations effectively spread out the intrinsic luminosity distribution ([section 5.4](#)). As discussed in [Appendix B.3.5](#), confusion is evaluated for $\Delta_o = 0$, because some lines will have nearly zero drift rate by chance, and these, with minimal leakage into other channels, will be the last to be confused as $\langle N_{o,M}^B \rangle$ increases. Using the numerator from [equation 65](#) to define the expected maximum signal, detection fails when

$$\bar{\mathfrak{S}}_s \gtrsim \frac{I_{o,M}^B + \Delta N_{o,M}^{\text{B;eff}}}{\sqrt{\langle N_{0;o,M}^{\text{B};2} \rangle \xi_{\delta;o,M}^B (1 + \langle \xi_{c;o|B} \rangle_M)}}, \quad (66)$$

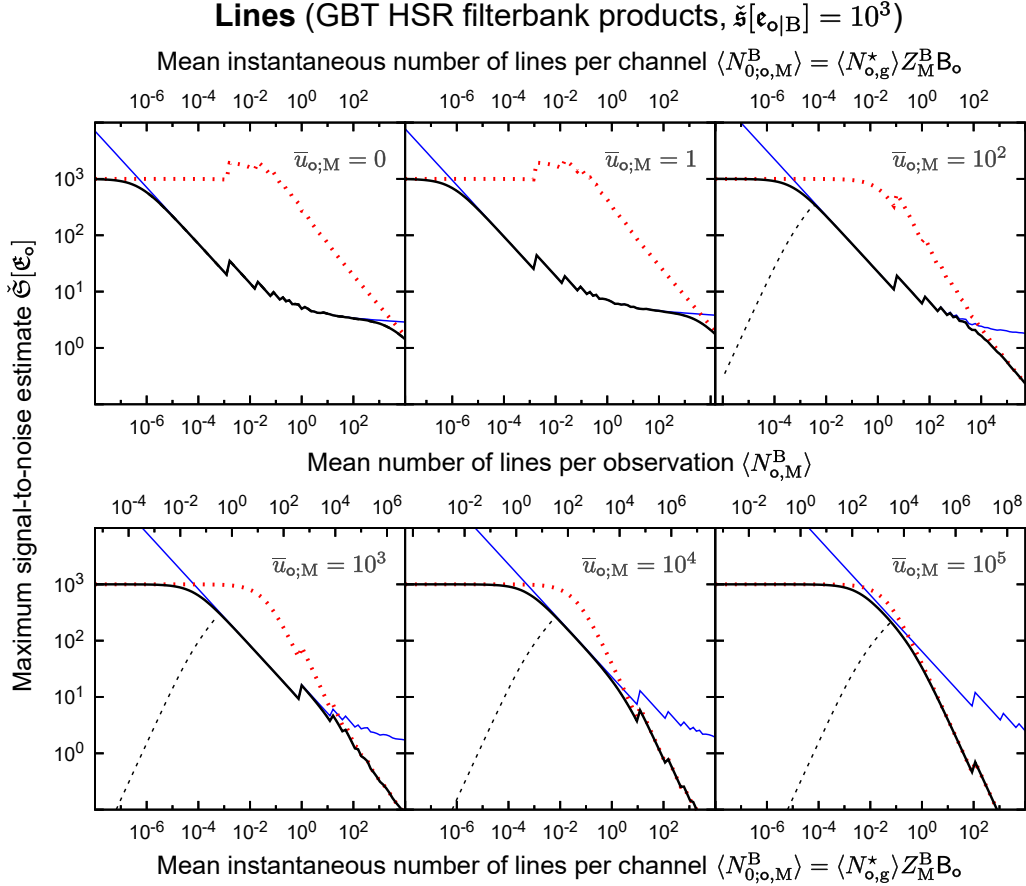


Figure 3. The impact of confusion on $\check{\mathfrak{S}}[\mathfrak{E}_o]$, the estimated maximum signal-to-noise ratio found in the survey, when observing a population of narrowband lines, as compared for different drift rate distributions. I adopt the standard assumptions of Table 2. The lines all have the same luminosity; individually they would have signal-to-noise 1000 if they were not drifting ($\bar{s}_0[\epsilon_{o|B}] = 1000$). Their drift rate distribution has a spread of $\bar{\delta}_M = \bar{u}_{o;M} B_o / T_o$, centered on $\delta_B = 0$. No dedrifting has been applied ($\Delta_o = 0$). The blue lines show the limits from sample variance alone, and determines when sample confusion occurs. The red dotted lines show limits from the quasi-thermal noise variance caused by the mutual interference and self-noise of all the broadcasts and background, and determines when noise confusion occurs. Wider spreads in drift rates delay the onset of sample confusion, but not noise confusion. Different line styles indicate whether or not we conditionalize on having found a line: solid for $I_{o,M}^B = 1$ (a line has definitely been found), and dashed for $I_{o,M}^B = 0$ (only serendipitous lines are included). The observations here are modeled according to the high spectral resolution filterbank products used in Breakthrough Listen for the Green Bank Telescope, for a single coarse channel (two polarizations, $T_d = 51 T_\mu$, $T_o = 16 T_d$, $B_s = 2^{20} B_o$).

with the standard assumptions and when all broadcasts have the same luminosity. Let us focus on the signal from a single detected nondrifting line ($I_{o,M}^B = 1$, $\Delta N_{o,M}^{B;\text{eff}} = 0$). By solving for $N_{0;o,M}^{B;2} \approx \langle N_{0;o,M}^B \rangle = Z_M^B \langle N_{o,g}^* \rangle B_o$, I find that sample confusion results in a null detection when

$$Z_M^B \gtrsim \left[\bar{\mathfrak{S}}_s^2 \langle N_{o,g}^* \rangle B_o \xi_{\delta;o,M}^B (1 + \langle \xi_{c;o|B} \rangle_M) \right]^{-1} \quad (67)$$

When the drift rate spread becomes big enough, most lines are spread over many observations, and sample variance is so low that noise confusion becomes the impediment to detection when there are many broadcasts. This is seen in Figure 3 for the highest $\bar{u}_{o;M} (\bar{\delta}_M T_o / B_o)$ cases. Using the quasi-thermal noise term in the vari-

ance, and again evaluating when no dedrifting is applied with standard assumptions, detection fails when

$$\bar{\mathfrak{S}}_s \lesssim \sqrt{N_o^u} \frac{I_{o,M}^B + \Delta N_{o,M}^{B;\text{eff}}}{\langle N_{0;o,M}^{B;1} \rangle}. \quad (68)$$

I again solve for $N_{0;o,M}^{B;1} \approx \langle N_{0;o,M}^B \rangle$, finding that noise confusion prevents a detection for

$$Z_M^B \gtrsim \sqrt{N_o^u} \left[\bar{\mathfrak{S}}_s \langle N_{o,g}^* \rangle B_o \right]^{-1}. \quad (69)$$

Since most radio SETI observations use filterbank products that integrate many modes together, noise confusion is only a concern when the drift rate spread is quite high. For a zero-centered drift rate distribution, noise confusion happens first if $\bar{\delta}_M / \ln(\bar{\delta}_M T_o / B_o) \gtrsim$

$\sqrt{N_{\text{o}}^{\text{u}} \overline{\mathcal{G}}_{\text{s}} (1 + \langle \xi_{\text{c};\text{o}|\text{B}} \rangle_{\text{M}})} \text{B}_{\text{o}}/\text{T}_{\text{o}}$, which I estimate to be $\bar{\delta}_{\text{M}} \gtrsim 14 \text{ Hz s}^{-1}$ for line searches with the Green Bank Telescope.

5.5. Special considerations for radio interferometers

Interferometric arrays are playing an increasing role in radio SETI (e.g., Rampadarath et al. 2012; Harp et al. 2016; Tremblay & Tingay 2020). Nominally, they provide increased angular resolution, which should decrease $\langle N_{\text{o};\text{g}}^{\text{*}} \rangle$, $\langle N_{\text{o};\text{M}}^{\text{B}} \rangle$, and thus confusion. But the situation is complicated by the presence of strong sidelobes in the synthesized “dirty” beam that span the primary (antenna) beam.

Signals from the \mathcal{N}_{A} antennas in an array are combined either coherently or incoherently. Incoherent summing simply adds together the voltages from all the antennas. The summed beam pattern is the same as the primary beam pattern, an advantage when searching for bright signals over a wide field. Sensitivity increases as $\mathcal{N}_{\text{A}}^{1/2}$ if detector noise dominates the variance in \mathfrak{E}_{u} , but celestial radio noise hampers sensitivity if it dominates the variance (Kudale & Chengalur 2017), analogous to the self-noise limit for single-dish observations (Radhakrishnan 1999). Sample confusion occurs when there is one broadcast on average in the time-frequency window of the observation anywhere within the primary beam.

Coherent beamforming processes the voltages to synthesize narrow beams with complex sidelobes. The “thinned array curse” implies that, given a fixed collection of antennas, the maximum gain is invariant with respect to how those antennas are arranged (Forward 1984).¹⁰ Increasing the spacing of the antennas merely shrinks the size of the main lobe. It can be shown then that the mean response over the primary beam is $1/\mathcal{N}_{\text{A}}$, and for a sparse array with filling factor $\ll 1$, almost all of this response comes from the sidelobes.

There are two basic strategies for beamforming that are used. Coherent summing synthesizes tied-array beams by applying phase corrections to each antenna before adding the voltages. It requires no time-averaging and is used for observations of transients and pulsars (Stappers et al. 2011). It also is the basis of Breakthrough Listen’s million-star survey with MeerKAT (Czech et al. 2021). However, computational limits currently allow only a few dozen beams to be formed in the primary beam, sampling only a small part of it. Aperture synthesis, the more well-known technique, performs a Fourier transform on the visibilities formed by multiplying the voltages of two antennas together and time-averaging. This approach generates a map of the entire primary beam but is not suited for detection of rapid transients because of the averaging and computational

cost. In addition, only baselines between distinct antennas are included, so there is no sensitivity to diffuse backgrounds that cover the entire primary beam: these observations only detect spatial *fluctuations* in broadcasts and could fail to detect a heavily populated galaxy covering a large enough sky area.

In both approaches, the dirty beam sidelobes have an amplitude $1/\mathcal{N}_{\text{A}}$.¹¹ The relatively strong sidelobes lead to much greater confusion than would normally be expected, hampering deconvolution of the dirty map. Under most circumstances relevant to radio astronomy, the sky can be regarded as basically empty, with only a few sources covering a small fraction of the primary beam, so this is not an issue (Högbom 1974). If there are more sources in the primary beam than independent measurements, however, it becomes impossible to disentangle them. Coherent summing yields only one independent measurement per antenna per observation, \mathcal{N}_{A} in total; aperture synthesis provides only one per baseline, \mathcal{N}_{B} in total (Högbom 1974; Schwarz 1978). Thus, confusion necessarily sets in when

$$\langle N_{\text{o};\text{A},\text{M}}^{\text{B}} \rangle \gtrsim \begin{cases} \mathcal{N}_{\text{A}} & \text{(coherent summing)} \\ \mathcal{N}_{\text{B}} & \text{(aperture synthesis)} \end{cases}. \quad (70)$$

The minimum number of baselines is $\mathcal{N}_{\text{A}}(\mathcal{N}_{\text{A}} - 1)/2$ from a single snapshot. Rotational synthesis using multiple snapshots to increase \mathcal{N}_{B} is limited to long-lasting broadcasts.

6. INDIVIDUALIST CONSTRAINTS: OPTICAL BROADCASTS

6.1. Noise variance in optical photon counting

At frequencies beyond radio, the mean number of photons arriving in an electromagnetic field mode (the photon occupation number) is much less than 1. When that happens, the photon shot noise completely overwhelms the photon bunching effect of wave noise (Radhakrishnan 1999).¹²

Instruments at these higher frequencies nowadays count photons, with the measured quantity being the number of photons collected during an observation, \mathfrak{Q}_{o} . The number of photons from the background, $\mathfrak{q}_{\text{o}|\text{n}}$, can be regarded as a pure Poisson random variable. In the absence of modulation, the number of photons from each broadcast B, $\mathfrak{q}_{\text{o}|\text{B}}$, is also Poissonian. This greatly simplifies analysis compared to the radio case, because the

¹⁰ Originally derived for energy transmitters, it also applies to receivers by reciprocity.

¹¹ In aperture synthesis, the lack of zero-spacing data shifts the beam pattern to have zero mean overall with negative responses over much of the sidelobes (Kogan 1999).

¹² Under certain circumstances, photon counts can have *sub-Poissonian* statistics, with the Fock states having no number fluctuations at all (e.g., Foellmi 2009). This is a purely quantum phenomenon, requiring photon detectors to measure, and is not expected from natural astrophysical sources, but it could be a technosignature (Hippke 2021).

sum of a fixed number of independent Poisson random variables is another Poisson random variable (Kingman 1993). I assume the broadcasts have constant intrinsic luminosity, as in the box model, with no significant modulation on timescales $\gtrsim \tau_o$. Let $\mathbf{q}_{o|B}$ be the photon fluence from each broadcast B within the observation o. For a distant metasociety, the mean is

$$\langle \mathfrak{Q}_o \rangle \approx \langle \mathbf{q}_{o|n} \rangle + \mathcal{A} \langle N_{o,M}^{B;1} \rangle \langle \dot{\mathbf{q}}_{o|B} \rangle_M \langle y_{q;B} \chi_{q;o|B} \rangle_M. \quad (71)$$

In the absence of attenuation, it can also be shown (Appendix C) that the variance under the diffuse approximation is

$$\begin{aligned} \mathbb{V}[\mathfrak{Q}_o] \approx & \langle \mathbf{q}_{o|n} \rangle + \mathcal{A} \langle \dot{\mathbf{q}}_{o|B} \rangle_M \langle y_{q;B} \chi_{q;B} \rangle_M \langle N_{o,M}^{B;1} \rangle \\ & + \mathcal{A}^2 \langle (\dot{\mathbf{q}}_{o|B})^2 \rangle_M \langle y_{q;B}^2 \chi_{q;B}^2 \rangle_M \langle N_{o,M}^{B;2} \rangle, \end{aligned} \quad (72)$$

which includes the mean number $\langle \mathbf{q}_{o|n} \rangle$ of noise photons from the sky background, dark current, and readout noise. Slow modulation increases the variance, which can be modeled either as an intrinsic spread in the photon fluence of the broadcasts or by an additional self-noise term (much like as in Section 5.4).

6.2. The behavior of signal-to-noise ratio for Poissonian photon counts

It is straightforward to estimate the signal-to-noise ratio with photon counting instruments at high frequencies using equation 72. The expected signal-to-noise ratio of an isolated broadcast at $\mathcal{I}_{\mathfrak{Q};o} = 1$,

$$\check{\mathfrak{s}}[\mathbf{q}_{o|B}] \equiv \frac{\mathcal{A} \langle \mathbf{g}_{o|B}^{[s,M]} \rangle_M}{\sqrt{\langle \mathbf{q}_{o|n} \rangle}} = \frac{\mathcal{A} \langle \dot{\mathbf{q}}_{o|B}^{[s,M]} \rangle_M \langle y_{q;B} \chi_{q;o|B} \rangle_M}{\sqrt{\langle \mathbf{q}_{o|n} \rangle}}, \quad (73)$$

provides another convenient scaling variable. Then, for distant galaxies and using the diffuse approximation,

$$\begin{aligned} \check{\mathfrak{S}}[\mathfrak{Q}_o] = & N_{o,M}^{B;\text{eff}} \check{\mathfrak{s}}[\mathbf{q}_{o|B}] \cdot \left(1 + \check{\mathfrak{s}}[\mathbf{q}_{o|B}] \frac{\langle N_{o,M}^{B;1} \rangle}{\sqrt{\langle \mathbf{q}_{o|n} \rangle}} \right. \\ & \left. + \check{\mathfrak{s}}[\mathbf{q}_{o|B}]^2 \langle N_{o,M}^{B;2} \rangle \frac{\langle (\dot{\mathbf{q}}_{o|B}^{[s,M]})^2 \rangle_M}{\langle \dot{\mathbf{q}}_{o|B}^{[s,M]} \rangle_M^2} \right)^{-1/2}. \end{aligned} \quad (74)$$

Sample variance exceeds background noise when

$$\langle N_{o,M}^{B;2} \rangle > \left(\check{\mathfrak{s}}[\mathbf{q}_{o|B}]^2 \frac{\langle (\dot{\mathbf{q}}_{o|B}^{[s,M]})^2 \rangle_M}{\langle \dot{\mathbf{q}}_{o|B}^{[s,M]} \rangle_M^2} \right)^{-1}, \quad (75)$$

similar to the radio case. Moreover, sample variance dominates the photon shot noise from the broadcasts

when

$$\langle \mathbf{q}_{o|B} \rangle_M > \left[\frac{\langle N_{o,M}^{B;1} \rangle}{\langle N_{o,M}^{B;2} \rangle} \left(1 + \frac{\mathbb{V}[\dot{\mathbf{q}}_{o|B}^{[s,M]}]_M}{\langle \dot{\mathbf{q}}_{o|B}^{[s,M]} \rangle_M^2} \right) \right]^{-1}. \quad (76)$$

Under normal circumstances, this second inequality holds as long as at least ~ 1 photon is expected to be detected per broadcast.

This means that there is no mutual interference regime for optical broadcasts – $\check{\mathfrak{S}}[\mathfrak{Q}_o]$ remains at a factor of a few from sample variance alone. Noise confusion by itself never prevents detection. Because each broadcast is contributing many photons, the photons can be thought of as coming in groups, one for each broadcast. This introduces an intrinsic “graininess” to the photon count statistics, reminiscent of the surface brightness fluctuations observed in distant galaxies from discrete bright stars (Tonry & Schneider 1988; Raimondo et al. 2005). Now, there still is a (sample) confusion regime, so this cannot be exploited to make an individual detection and does not intrinsically favor optical over radio. Perhaps the graininess might be discerned in the photon count statistics when in the confusion regime, and the lack of interference can extend the range of that kind of technique in optical. In any case, the confusion regime already implies extremely high abundances of broadcasts, so these considerations only apply to an arguably contrived region of parameter space.

7. THE COLLECTIVE BOUND: THE TOTAL EMISSION OF THE GALAXY

The collective bound, by contrast, is based on the total emission received from all the broadcasts in the target galaxy. The concept is very simple: the broadcast from ETIs cannot outshine the galaxy as a whole (including the broadcasts) when we’re looking at it. To be clear, this is an entirely empirical constraint, applying the observed emission rather than how much emission we expect from natural processes. It is possible that ETIs might vastly increase the apparent luminosity of a galaxy by harnessing its central black hole or invoking unknown physics – or, more practically, by beaming emission in our direction – but the observed emission necessarily includes this increased luminosity, along with any additional natural emission. We already know that there are no trillion L_\odot radio beacons in M31, for instance, because the radio luminosity of M31 is a lot lower than a trillion Suns, even though such beacons could hypothetically be constructed.

It is impossible to make a detection using the collective approach alone, since any emission we detect could be natural, but an estimated fluence $\widehat{\mathfrak{U}}_o$ derived from measurement does let us conclude that most likely $\mathfrak{U}_{o,M}^B \lesssim \widehat{\mathfrak{U}}_o$. Statistical analysis lets us constrain a combination of the abundance and brightness distribution.

Observations in the literature effectively report fluences, generally cast as a flux. Now, the variance in $\mathfrak{U}_{\circ,M}^B$ includes sample variance and noise variance. Noise variance is included in the reported errors $\Delta\widehat{\mathfrak{U}}_{\circ}$ on the reported fluence. Given a cumulative fluence distribution $F[\mathfrak{U}_{\circ,M}^B]$, a confidence interval only allows those models for which

$$\bar{P} \leq F[\mathfrak{U}_{\circ,M}^B](\widehat{\mathfrak{U}}_{\circ} + C_{\circ}\Delta\widehat{\mathfrak{U}}_{\circ}), \quad (77)$$

where C_{\circ} is some predefined constant and $\bar{P} \approx 0$ is a conservative probability threshold. That is, we want to include all models where there is any significant chance that the broadcast population is fainter than the observed luminosity. When only an upper limit on the emission is known, it can be substituted for $\widehat{\mathfrak{U}}_{\circ} + C_{\circ}\Delta\widehat{\mathfrak{U}}_{\circ}$. Taking the inverse CDF of both sides, we find

$$F^{-1}[\mathfrak{U}_{\circ,M}^B](\bar{P}) \leq \widehat{\mathfrak{U}}_{\circ} + C_{\circ}\Delta\widehat{\mathfrak{U}}_{\circ}. \quad (78)$$

If the broadcast fluence has a narrow distribution with a well-defined variance, we can approximate the left-hand side as

$$F^{-1}[\mathfrak{U}_{\circ,M}^B](\bar{P}) \approx \langle \mathfrak{U}_{\circ,M}^B \rangle - C_M \mathbb{V}^{1/2} [\mathfrak{U}_{\circ,M}^B] \quad (79)$$

for some suitable constant C_M that absorbs the dependence on \bar{P} .¹³

Now, say that *all* of the observed fluence from from broadcasts, with no natural background. We could estimate the number of broadcasts that are contributing to the observed emission simply as

$$\hat{N}_{\circ,M}^B = \frac{\widehat{\mathfrak{U}}_{\circ} + C_{\circ}\Delta\widehat{\mathfrak{U}}_{\circ}}{\langle \mathfrak{u}_{\circ|B} \rangle_M} = \frac{B_{\circ}(\widehat{L}_{\nu} + C_{\circ}\Delta\widehat{L}_{\nu})}{\langle \ell_B \rangle_M}, \quad (80)$$

the number of typical broadcasts that can “fit” into the emission (in terms of fluence and spectral luminosity, respectively). This naive estimate is in fact central to the collective bound. Under our usual assumptions of a single galactic metasociety, with interchangeable broadcasts and societies and Poissonian $N_{\circ,C}^B(\mathbf{w}_C)$ and $N_{\circ,M}^C(\mathbf{w}_M)$

$$\langle \mathfrak{U}_{\circ,M}^B \rangle \approx \langle N_{\circ,M}^B \rangle \langle \mathfrak{u}_{\circ|B} \rangle_M \quad (81)$$

and

$$\mathbb{V} [\mathfrak{U}_{\circ,M}^B] \approx \langle N_{\circ,M}^B \rangle \left(\langle \mathfrak{u}_{\circ|B}^2 \rangle_M + \langle N_{\circ,C}^B \rangle_M \langle \mathfrak{u}_{\circ|B} \rangle_M^2 \right) \quad (82)$$

Plugging these into the left-hand side of equation 79 by use of equation 78, we find the expression for the

collective bound:

$$\langle N_{\circ,M}^B \rangle \lesssim \hat{N}_{\circ,M}^B + \frac{C'^2}{2} \left(1 + \sqrt{1 + \frac{4}{C'^2} \hat{N}_{\circ,M}^B} \right), \quad (83)$$

where

$$C' \equiv C_M \sqrt{\frac{\langle \mathfrak{u}_{\circ|B}^2 \rangle_M}{\langle \mathfrak{u}_{\circ|B} \rangle_M^2} + \langle N_{\circ,C}^B \rangle_M}. \quad (84)$$

The meaning of equation 83 depends on the average brightness of a broadcast. When $\langle \mathfrak{u}_{\circ|B} \rangle_M$ is very small, many broadcasts can “fit” into the observed emission, and equation 83 reduces to $\langle N_{\circ,M}^B \rangle \leq \hat{N}_{\circ,M}^B + C' \sqrt{\hat{N}_{\circ,M}^B}$, the maximum number that are allowed before the aggregate population outshines the actual emission (with allowances for Poissonian fluctuations).

When $\langle \mathfrak{u}_{\circ|B} \rangle_M$ is very bright, even one broadcast would produce more emission than is observed, and is thus ruled out by how faint the galaxy actually is. In this limit, when the broadcast fluence distribution is narrow, $\hat{N}_{\circ,M}^B \rightarrow 0$ and equation 83 reduces to $\langle N_{\circ,M}^B \rangle \lesssim C'^2$. When $\langle N_{\circ,C}^B \rangle_M \lesssim 1$, $C' \approx C_M$, so the bound says that broadcasts are just too rare to have been caught in the observation: $\langle N_{\circ,M}^B \rangle \lesssim C_M^2$. If $\langle N_{\circ,C}^B \rangle_M \gtrsim 1$, broadcasts outnumber societies and $C' \approx C_M \langle N_{\circ,C}^B \rangle_M$; equation 83 simplifies to $\langle N_{\circ,M}^C \rangle \lesssim C_M^2$. Equation 83 thus contains the discreteness bound (Paper I) – it cannot rule out a model that predicts a good chance of there being no societies or broadcasts covered by an observation, because no artificial emission is expected then.

In the box model, equations 83 and 17 give us the constraint that either $\langle N_{\circ,M}^C \rangle \approx 0$ or

$$A_M^B \lesssim \frac{\hat{N}_{\circ,M}^B + (C'^2/2) \left[1 + \sqrt{1 + 4\hat{N}_{\circ,M}^B/C'^2} \right]}{\langle N_{\circ,g}^* \rangle (\mathbb{T}_{\circ} + \bar{\tau})(B_{\circ} + \bar{\beta})}. \quad (85)$$

Applying the collective bound instead to the chord model using equation 21, the bound is

$$Z_M^B \lesssim \frac{\hat{N}_{\circ,M}^B + (C'^2/2) \left[1 + \sqrt{1 + 4\hat{N}_{\circ,M}^B/C'^2} \right]}{\langle N_{\circ,g}^* \rangle B_{\circ} (1 + \langle |\delta_B| \rangle_M \mathbb{T}_{\circ}/B_{\circ})} \quad (86)$$

unless $\langle N_{\circ,M}^C \rangle \approx 0$. Observations of continuum galactic luminosity use wideband observations, so $(1 + \langle |\delta_B| \rangle_M \mathbb{T}_{\circ}/B_{\circ}) \approx 1$ in practice.

The collective bound is sensitive to the full brightness distribution instead of only the most extreme values, and thus explores a different range of parameter space than individualist searches. Observations used to derive galactic luminosities are usually relatively wideband by SETI standards; they also have long integration times compared to the time resolution of pulse searches.

¹³ If the aggregate fluence has a power-law tail, the distribution is likely to be highly asymmetrical and this approximation will fail, even using the regularized mean and variance.

This increases the fluence collected from noise and background emission, burying the brightest individual signals, but the mean total fluence in ETI broadcasts also increases proportionally. Collective bounds apply to arbitrarily faint broadcasts as long as they are numerous enough, even when they fail to limit rare but very bright single broadcasts. The collective approach therefore has the distinct capability of setting constraints on pervasive Kardashev Type I–II transmitters in very distant galaxies, far below the detection threshold of typical SETI surveys.

The other advantage of this seemingly trivial limit is that it is unaffected by confusion. In fact, it demands we are near or in the confusion limit for the observation we are applying – the longer, wideband observations used to evaluate \widehat{L}_ν reach this limit much sooner than typical SETI measurements. This mostly closes the gap in parameter space opened by the confusion limit in individualist approaches (section 8).

8. CONSTRAINTS ON ARTIFICIAL RADIO TRANSMISSIONS IN NEARBY GALAXIES

A comparison of the collective bound with individualist constraints using extant or planned SETI observations illustrates their relative merits, with the latter becoming weaker at greater distance. I present these comparisons for narrowband line searches in L-band, near 1.4 GHz. This region of the spectrum has historically been favored in radio SETI: background noise from synchrotron emission is quiet in this regime, and it contains the “water hole”, a band between radio lines presumed to be well-known to alien astrophysicists wanting to make contact (Cocconi & Morrison 1959; Oliver & Billingham 1971). The need to know which frequency to “meet at” was important when back ends covered at best only a few megahertz at a time, but modern instrumentation largely sidesteps the problem. Although there have been narrowband radio SETI surveys at much lower and higher frequencies, L-band is used here because it has the most results to compare with (see Tarter 1985; Enriquez et al. 2017), including extragalactic results (Horowitz & Sagan 1993; Shostak et al. 1996; Gray & Mooley 2017). But it is also commonly used to study galaxies’ radio continuum emission (e.g., Yun et al. 2001 among many others). Thus, it is a natural choice for collective bounds derived from the literature. The basic ideas should apply for other types of broadcasts, however.

The broadcasts are assumed to all have the same luminosity $\bar{\ell}$ and an instantaneous abundance per unit frequency Z_M^B . The power of individualist searches to detect lines is estimated using the chord model, assuming a single line ($I_{\circ,M}^B = 1$; equation 65) and no dedrifting ($\Delta_\circ = 0$). The diffuse approximation is also applied. Sample confusion is evaluated according to equations 67

and 70; noise confusion is also considered (equation 69) as a robust limit against background broadcasts.

The range of mean broadcast luminosities considers spans many orders of magnitude. As a rough guide, I compare the results for different Kardashev scale levels. As in Kardashev (1964), the levels measure the *broadcast* effective isotropic power, with Type I representing a “planetary”-scale beacon ($\sim 10^{-10} L_\odot$), Type II a “stellar”-scale beacon ($\sim 1 L_\odot$), and Type III a “galactic”-scale beacon ($\sim 10^{10} L_\odot$). When considered quantitatively, I adopt a Sagan-like normalization of $1 L_\odot$ for Type II, with a ratio of 10^{10} between each class (see Ćirković 2015).

8.1. Milky Way

The great majority of targeted SETI programs have observed things within our own Galaxy, focusing on nearby stars. At distances of parsecs instead of megaparsecs, we are able to detect far weaker transmissions – comparable to our planetary radars, although still well above any permanent broadcast we maintain (Enriquez et al. 2017). There is, however, a great diversity of surveys, ranging from observations of one or two very nearby stars to large-scale surveys of millions of stars in the Galactic Center (Table 3).

The regions of 1.4 GHz luminosity–abundance parameter space constrained by SETI literature are sketched as the colored shaded regions in Figure 4. The bounds of these regions should be understood as order-of-magnitude estimates, as they assume a single characteristic distance for all stars in the sample and only include targeted stars. Broadcasts from background stars are detectable if bright enough (Włodarczyk-Sroka et al. 2020), increasing the mean number of sampled broadcasts at larger distances. Thus, the lower boundaries of the shaded regions excluded by individualist programs should actually bow downward at high $\bar{\ell}$.

Unlike when we observe a single, distant metasociety, background societies within the Milky Way can have a wide range of distances. This spread in distances widens the fluence distribution to $\Psi[h_{\circ|B}]_M \propto h_{\circ|B}^{-5/2}$, broad enough to prevent confusion (Section 4.2). Confusion thus only sets in if the broadcasts from *each* society are confused, regardless of whether we consider the targeted stars or the background stars. Seeing as each society is located at a single location, one star, I evaluate confusion as if $\langle N_{\circ,g}^* \rangle = 1$ in equations 67 and 69, representing the host of this nearest society. Confusion also depends on the drift rate spread. It is most severe when all lines have zero drift (solid regions); the maximum abundances allowed, when only noise confusion is an issue, are $\sim 10^2$ – $10^{4.5}$ times higher (hatched regions).

Also shown is a collective bound that would arise if the Milky Way lies on the far-infrared–radio correlation (FRC; see section 9.1) for star-forming galaxies (SFGs). I employ a bandwidth of 64 MHz, which is the band-

Table 3. Summary of individualist Milky Way searches for lines covering 1.4 GHz

Survey	Instrument	B_o	B_π	T_d	T_o	T_π	$\bar{\mathcal{E}}_s$	N_s^π	$\langle N_{o,g}^* \rangle$	$\langle N_{s,g}^* \rangle$	$\bar{\ell}_B$	N_s^{eff}
		Hz	GHz	s	s	min					W	
R12 ^a	LBA	1950	0.314	2400	2400	480	5	1	1	1	1.4×10^9	7.2×10^4
H16 ^b	ATA	0.7	8	1.5	93	180	6.5	65	1	65	8.8×10^{16}	5.5×10^9
		0.7	2.04	1.5	93	45	6.5	1959	1	1959	5.5×10^{16}	4.3×10^{10}
		0.7	0.337	1.5	93	7.5	6.5	2822	1	2822	3.8×10^{14}	1.0×10^{10}
		0.7	0.268	1.5	93	5.9	6.5	7459	1	7459	1.1×10^{15}	2.1×10^{10}
BL (P20)	GBT (L)	2.79	0.660	18.25	300	15	10	882	1	882	2.1×10^{12}	1.9×10^9
BL (G21)	Parkes (UWL)	3	3.328	18	600	120 ^c	20	7	8.6×10^6 ^d	6×10^7	4×10^{18}	3.9×10^7

NOTE—Abbreviations: ATA – Allen Telescope Array; BL – Breakthrough Listen; GBT (L) – Green Bank Telescope, L-band receiver; LBA – Long Baseline Array; and UWL – Ultra Wideband Low receiver.

^aR12 used very long baseline interferometry to observe Gl 581. I only consider broadcasts from that star, including when deriving the confusion limit. Thus, confusion for lines is determined by frequency resolution only, regardless of the increased angular resolution.

^bBoth T_o and $\bar{\mathcal{E}}_s$ were lowered during the program, from 192 to 93 s and from 9 to 6.5, respectively. In H16, the ATA only had an instantaneous bandwidth of $B_v = 70$ MHz. Thus, many “tunings” at different frequencies were necessary to cover the entire survey bandwidth, with T_π calculated here as $T_v(B_\pi/B_v)$. The B_π are averages, based on the total “star-MHz” accumulated in each series of observations.

^cActual observation times varied from 1 to 3 hr.

^dWhen evaluating confusion, $\langle N_{o,g}^* \rangle = 1$ is used, representing the nearest society’s host star, as discussed in the text.

References—R12 – Rampadarath et al. (2012); H16 – Harp et al. (2016); P20 – Price et al. (2020); G21 – Gajjar et al. (2021); M04 – Meyer et al. (2004); N11 – Norris et al. (2011)

width covered by CHIPASS, a recent 1.4 GHz southern sky survey used to estimate the Milky Way’s radio emission (Calabretta et al. 2014; see also Zheng et al. 2017). We cannot directly measure the radio luminosity of the Milky Way since we live inside it, but the assumption is validated by models of the Galaxy’s synchrotron emission (Strong et al. 2010). The collective bound becomes more stringent for brighter broadcasts, of course, because fewer are needed to outshine the amount of radio emission that we actually expect from the Milky Way. Nonetheless, these models are fit to observations of the Milky Way that only cover parts of the radio spectrum, leaving open the possibility that some radio transmitters could be hiding in the “gaps” (consider the literature data in Table 1 of Zheng et al. 2017). The fact that we need to sample at least one broadcast to detect any artificial emission sets a Z_M^B threshold, below which the collective bounds fail to be constraining.¹⁴ Future work can set collective bounds along individual sight lines by comparing the sky density of stars with the Galactic radio background.

¹⁴ Values of $\Upsilon_s Z_M^B = d^2 \langle N_{t,M}^B \rangle / [d\vartheta_B d \ln v_B]$ much lower than one per Galaxy are meaningful because broadcasts turn on and off over time. The Galaxy could have 10^{-3} active transmitters on average, for example, if only one turns on per millennium and transmits for just a year.

It is clear from Figure 4 that the conventional individualist search strategy is highly effective in the Milky Way. Collective bounds set some weak limits on very low luminosity broadcasts ($\bar{\ell} \lesssim 10^{10}$ W), and rule out the possibility that extreme confusion is preventing detection of bright broadcasts, but the Z_M^B values involved are far-fetched: more than one broadcast per star per kilohertz for $\bar{\ell}$ up to 10^{13} W, the EIRP of our brightest transmitters, the planetary radars on facilities like Arecibo. Kardashev Type I radio transmitters are limited to about 200 per star per gigahertz through the collective bound, compared with the individualist limits of $\sim 10^{-3}$ per star per gigahertz from Harp et al. (2016). As we progress to higher broadcast EIRPs, surveys probing more distant regions of the Galaxy, like Gajjar et al. (2021), continue to be more restrictive than the collective bound because they cannot find even one to have a null result. For Kardashev Type II radio transmitters, the collective bound sets a limit of one per 50 million stars per gigahertz, while Gajjar et al. (2021) set a limit about one order of magnitude stronger.

Surprisingly, though, the collective bound is the tightest of those in Figure 4 for the rarest, very bright transmitters – reaching about one per five billion stars per gigahertz. The plotted individualist SETI programs are targeted, covering only a small fraction of the Galaxy’s stars. There are also historical all-sky SETI surveys, and even continuum and HI radio surveys that could be brought to bear. The problem is that these all have lim-

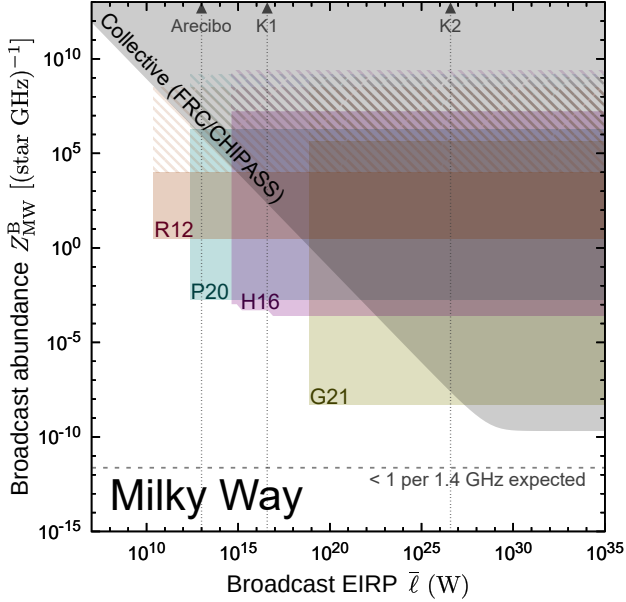


Figure 4. Order-of-magnitude constraints on ETI radio line broadcast luminosity and abundance in the Milky Way, assuming all broadcasts have the same luminosity. The collective bound from the assumption that the Galaxy lies on the FRC (grey) is shown against approximate individualist results from recent SETI surveys: R12 (red), P20 (green), H16 (violet), and G21 (gold). For the SETI surveys, solid shading is used for the constraints when all drift rates are zero; if only noise confusion is present, the hatched regions are constrained as well. These constraints assume that $\bar{\tau}$ is longer than the observational programs. The approximate EIRPs for the Arecibo planetary radar and Kardashev Type I (K1) and II (K2) broadcasts are marked.

ited frequency ranges: if there is only one transmitter in the Galaxy somewhere in the frequency band 0–10 GHz, it almost certainly falls outside the 0.4–0.5 MHz covered by Big Ear or META (Dixon 1985; Horowitz & Sagan 1993), or the 40–60 MHz bandwidth of NVSS, HIPASS, or CHIPASS (Condon et al. 1998; Meyer et al. 2004; Calabretta et al. 2014). Breakthrough Listen is surveying the bulk of the Galactic Plane over hundreds of megahertz (Isaacson et al. 2017), partly closing this window.

8.2. M31

M31 is the nearest large spiral galaxy to our own, the only one besides the Milky Way and the lower-mass M33 with a completed SETI survey since the turn of the century until very recently (Table 4). Gray & Mooley (2017) carried out a search for narrowband radio transmitters on the Jansky Very Large Array (JVLA). The Five-hundred-meter Aperture Spherical Radio Telescope (FAST) also will observe M31 in partnership with Breakthrough Listen (Li et al. 2020). Null results from these surveys are plotted with the collective bound from

single-dish Effelsberg observations of total 1.4 GHz radio emission (Beck et al. 1998; Table 5) in Figure 5.

Gray & Mooley (2017) and future FAST limits especially can already rule out a wide chunk of $\bar{\ell}$ – Z_M^B parameter space, but they are much more limited than Milky Way observations. At the bright end, the JVLA line search and the Effelsberg-derived collective bound only probe $Z_M^B \gtrsim 100$ – $1,000 \text{ GHz}^{-1} \text{ M31}^{-1}$ because they have limited bandwidth, the same problem encountered with the Milky Way. Because M31 covers a smaller region of the sky, it is a relatively simple matter for FAST to scan all of M31 with its wide bandwidth and close this window. The collective bound is the only constraint on line broadcasts with $\bar{\ell} \lesssim 10^{19} \text{ W}$. Since M31 is much fainter than the Milky Way is presumed to be in L-band despite having more stars, the collective bound is about 10 times stronger than for our Galaxy. With the collective bound, we can rule out the existence of hundreds of Kardashev Type I transmitters per gigahertz around each star in M31, for example, a population easily built by an advanced galactic metasociety. Additionally, confusion sets in much sooner for M31 than in the Milky Way, when there is ~ 0.01 – 10 line broadcast per star per gigahertz.

Overall, the basic pattern is the same as for the Milky Way limits, but the collective bound is needed to rule out a much greater region of parameter space.

8.3. Virgo cluster ellipticals

Of the galaxies in the Breakthrough Listen nearby galaxies survey (Isaacson et al. 2017), the early-type Virgo Cluster galaxies are among the most massive and the most distant, which favor collective bounds. On the other hand, they also include radio galaxies, which are radio-bright, and thus their collective bounds are weakened, allowing a more luminous broadcast population. Three of these galaxies are chosen here as representatives: M87, one of the brightest radio sources on the sky; M49, the largest and a much quieter radio galaxy; and M59, an elliptical with no detected 1.4 GHz radio emission at all (Table 5). All three have been observed with the Green Bank Telescope (GBT) during Breakthrough Listen’s survey (Isaacson et al. 2017; Table 4). The L-band beam width is much larger than the effective radii of these galaxies, so a single pointing will cover almost all of the stellar population.¹⁵

The line broadcast constraints in Figure 5 show how collective bounds become progressively stronger as the galaxy’s observed radio flux goes down. In fact, collective bounds already rule out a substantial chunk of M59’s EIRP-abundance parameter space being probed by the GBT. This follows from how faint it is in the radio, less than $\sim 40 L_\odot \text{ GHz}^{-1}$. GBT’s advantages in

¹⁵ The effective radii are comparable to the beam width of FAST at 1.4 GHz, or GBT at ~ 10 GHz, however.

Table 4. Summary of past and proposed individualist searches for lines covering 1.4 GHz in M31 or Virgo Cluster ellipticals

Quantity	Unit	M31			Virgo Ellipticals
		G17 (HI)	G17 (LSR)	FAST (HSR)	GBT (HSR)
Instrument	...	JVLA	JVLA	FAST	GBT
Type	...	Line	Line	Line	Line
Completed?	...	✓	✓		
Reference	...	G17	G17	L20	I17
Υ_{\circ}	GHz	1.420	1.421–1.423	1.4	1.4
θ_{FWHM} (primary)	arcmin	31.7	31.7	1.5	9
θ_{FWHM} (synthesized)	arcsec	4.3–14	4.3–14
\mathcal{N}_A	...	27	27	1	1
\mathcal{N}_s^{π}	...	5	5	84	1
$\mathcal{N}_{\pi}^{\theta}$...	$\sim 2 \times 10^5$	$\sim 2 \times 10^5$	19	1
T_d	s	1200	300	0.25^a	18
T_{\circ}	s	1200	300	600	300
B_{\circ}	Hz	122	15	4	3
T_{θ}	s	1200	300	600	900
B_{θ}	MHz	1	0.125	500	660
$\langle N_{\theta,g}^* \rangle$...	5.3×10^8 ^b	5.3×10^8 ^b	7.8×10^7 ^b	$(0.6\text{--}2.1) \times 10^{12}$ ^c
$\overline{\mathcal{C}}_s$...	7	7	10	10
$\bar{\ell}$ limit	W	2.2×10^{21}	1.5×10^{21}	2.3×10^{19}	$(2.9\text{--}3.3) \times 10^{23}$

NOTE—Abbreviations: LSR –local standard of rest; HSR – high spectral resolution.

^a Minimum possible time; used for observations of GJ 273 reported in Li et al. (2020).

^b The projected sky density $d\langle M_{s,g}^* \rangle / d\Omega$ of M31’s stars is roughly $2,700 M_{\odot} \text{ arcsec}^{-2}$ in the center of the M31N3 and M31S3 pointings (Tamm et al. 2012). The effective number of stars in the beam for confusion noise is calculated using this density instead of the higher densities closer to the center, since a detection was not found in any pointing.

^c Stellar mass of M87, M49, and M59 unresolved by GBT; total number of stars in galaxy is used.

References—G17 – Gray & Mooley (2017); L20 – Li et al. (2020); I17 – Isaacson et al. (2017)

M59 are for a “corner” of rare, sub-Kardashev II transmitters ($10^{24}\text{--}10^{27}$ W), and ultrarare bright transmitters, where the need to detect at least one broadcast limits the collective bound because of the relatively narrow bandwidth of VLSS (42 MHz; Condon et al. 1998). Even the advantage for ultrarare lines could be eliminated by measuring M59’s diffuse emission across a few gigahertz of bandwidth. Of course, the issue is not just that the collective bounds are strong for the radio-silent M59, but that the individualist bounds are weak because of the great distances and insensitivity to faint broadcasts. An isotropic narrowband transmitter in the Virgo Cluster would have to be about as luminous as Proxima Centauri to be detected by GBT.

Individualist bounds are more important for M49 and especially M87, since more abundant and/or brighter transmitters would be needed to match their radio luminosities. In all three galaxies, however, confusion sets in no later than when there is about one line broadcast per thousand stars per gigahertz, and one per million stars per gigahertz for lines with zero drift. Thus, con-

fusion is a legitimate concern, as these abundances are plausible in a fully populated galaxy.

9. GENERAL EXPECTATIONS FOR THE COLLECTIVE BOUND

9.1. The Far-infrared–Radio correlation and collective bounds

With the exception of some active galactic nuclei, galaxies are radio quiet. This makes the radio band well suited to collective bounds, because it would not take much power for ETIs to overwhelm the natural radio emission of a galaxy. Low radio background in fact motivated radio transmitters as possible technosignatures (Cocconi & Morrison 1959). In the range below ~ 10 GHz, the radio emission of most galaxies, if present, is dominated by synchrotron emission from cosmic-ray electrons and positrons, with $\mathfrak{F}_{\nu;g} \propto \nu^{-\alpha}$ where $\alpha \sim 0.7\text{--}0.8$ for most normal SFGs (Condon 1992). These are accelerated by phenomena associated with young massive stars and thus trace star-formation rate. In fact, most SFGs lie on the FRC, with a ratio

Table 5. Summary of galaxy properties and observations used for collective bounds

Quantity	Units	MW	M31	M87	M49	M59
d	Mpc	...	0.783	16.65	16.40	15.45
$\langle M_{s,g}^* \rangle$	M_\odot	$10^{10.78}$	$10^{11.00}$	$10^{11.53}$	$10^{11.62}$	$10^{11.08}$
$\langle N_{s,g}^* \rangle^a$...	3.0×10^{11}	4.5×10^{11}	1.7×10^{12}	2.1×10^{12}	6.0×10^{11}
Instrument	...	(FRC)	Effelsberg	VLA	VLA	VLA
Radio reference	...	C14	B98	C98	C98	C98, B11
\mathcal{T}_o	GHz	1.3945^b	1.465	1.4	1.4	1.4
$\widehat{\mathfrak{F}}_{\nu;o,g}^c$	Jy	...	4.6 ± 0.4	138 ± 5^d	0.220 ± 0.008	-0.0004 ± 0.00045
\widehat{L}_ν^e	W Hz $^{-1}$	2.6×10^{21f}	4.0×10^{20}	4.9×10^{24}	7.6×10^{21}	1.4×10^{19}
$\widehat{L}_\nu / \langle N_{t,g}^* \rangle$	W GHz $^{-1}$ star $^{-1}$	8.7×10^{18}	8.8×10^{17}	2.9×10^{21}	3.6×10^{18}	2.4×10^{16}
θ_{FWHM} (primary)	arcmin	...	9.35^g	31	31	31
N_s^g	68^h	1	1	1
N_π^g (primary)	1	1	1	1
\mathcal{T}_o	s	...	0.67^i	23.3	23.3	23.3
B_o	MHz	64^b	20	42	42	42

^a Assumes mean stellar mass of $0.2 M_\odot$ (Chabrier 2003).

^b Values for the CHIPASS southern sky continuum radio survey.

^c Reported spectral flux; $\widehat{\mathfrak{F}}_{\nu;o,g} = \widehat{\mathfrak{F}}_{\nu;o,g} / (\mathcal{T}_o B_o)$.

^d By including single-dish data, Brown et al. (2011) find a larger M87 radio flux of 210 Jy. M87's radio emission includes significant contributions from large-scale lobes and jets that are outside of the bulk of the stellar mass; if ETIs trace stellar mass, artificial radio emission would be more compact. I thus use the VLSS measurement.

^e Uses 2σ flux upper bound on flux.

^f Value derived from the FRC (equation 87), using a star-formation rate of $1.65 M_\odot \text{yr}^{-1}$ (Licquia & Newman 2015).

^g Angular resolution of B98 map.

^h Effective number of pointings for M31 calculated as $4 \langle M_{o,g}^* \rangle / (\pi \theta_{\text{FWHM}}^2 d \langle M_{s,g}^* \rangle / d\Omega)$, where $d \langle M_{s,g}^* \rangle / d\Omega = 6,000 M_\odot \text{arcsec}^{-2}$ is average over half-light isophote (Tamm et al. 2012).

ⁱ Calculated as $\mathcal{T}_o = [2k_B \mathcal{T}_n / (\mathcal{A} \mathbb{V}^{1/2} [\widehat{\mathfrak{F}}_{\nu;g}])]^2 / B_o$, from given rms noise of $\mathbb{V}^{1/2} [\widehat{\mathfrak{F}}_{\nu;g}] = 5 \text{ mJy beam}^{-1}$, system temperature 26 K, and notional effective area of $0.5(\pi/4)(100 \text{ m})^2$ for 100-meter aperture Effelsberg dish.

References—Distances: McConnachie (2012) (M31), Kashibadze et al. (2020) (M87, M49, M59); stellar masses: Licquia & Newman (2015) (MW), Tamm et al. (2012) (M31), Jarrett et al. (2019) (M87, M49, M59); radio data: B98 (Beck et al. 1998), C98 (Condon et al. 1998), B11 (Brown et al. 2011), C14 (Calabretta et al. 2014)

of far-infrared to 1.4 GHz radio luminosity ratio that is constant within a factor of about two at $z \sim 0$ (Yun et al. 2001). For a Kroupa initial mass function, Murphy et al. (2011) relate the mass star formation rate \dot{M}_g^* and radio brightness:

$$\left(\frac{\dot{L}_{\nu;g}(1.4 \text{ GHz})}{\text{W Hz}^{-1}} \right) = 1.57 \times 10^{-21} \left(\frac{\dot{M}_g^*}{M_\odot \text{yr}^{-1}} \right), \quad (87)$$

although dwarf galaxies have previously been found to be radio-quieter (Bell 2003). SFGs also become somewhat brighter in radio synchrotron emission at high redshift (Delhaize et al. 2017).

Additionally, the majority of SFGs at a given redshift and SFR have similar stellar masses $\langle M_{t,g}^* \rangle$, a relation sometimes called the “main sequence” of SFGs. Speagle et al. (2014) find a best-fit relation that can be expressed

as

$$\left(\frac{\dot{M}_g^*}{M_\odot \text{yr}^{-1}} \right) = 10^{-0.13} \left(\frac{\langle M_{t,g}^* \rangle}{10^{10} M_\odot} \right)^{0.49}, \quad (88)$$

at $z = 0$, in terms of the Kroupa initial mass function. The main sequence and FRC can be combined to estimate the radio emission of most SFGs at $z = 0$:

$$\left(\frac{\dot{L}_{\nu;g}(1.4 \text{ GHz})}{\text{W Hz}^{-1}} \right) = 1.17 \times 10^{21} \left(\frac{\langle M_{t,g}^* \rangle}{10^{10} M_\odot} \right)^{0.49}. \quad (89)$$

In turn, this radio luminosity can be plugged into equations 80, 85, and 86 to yield a collective bound. The population of artificial narrowband radio transmitters in nonactive $z = 0$ galaxies is limited by the FRC

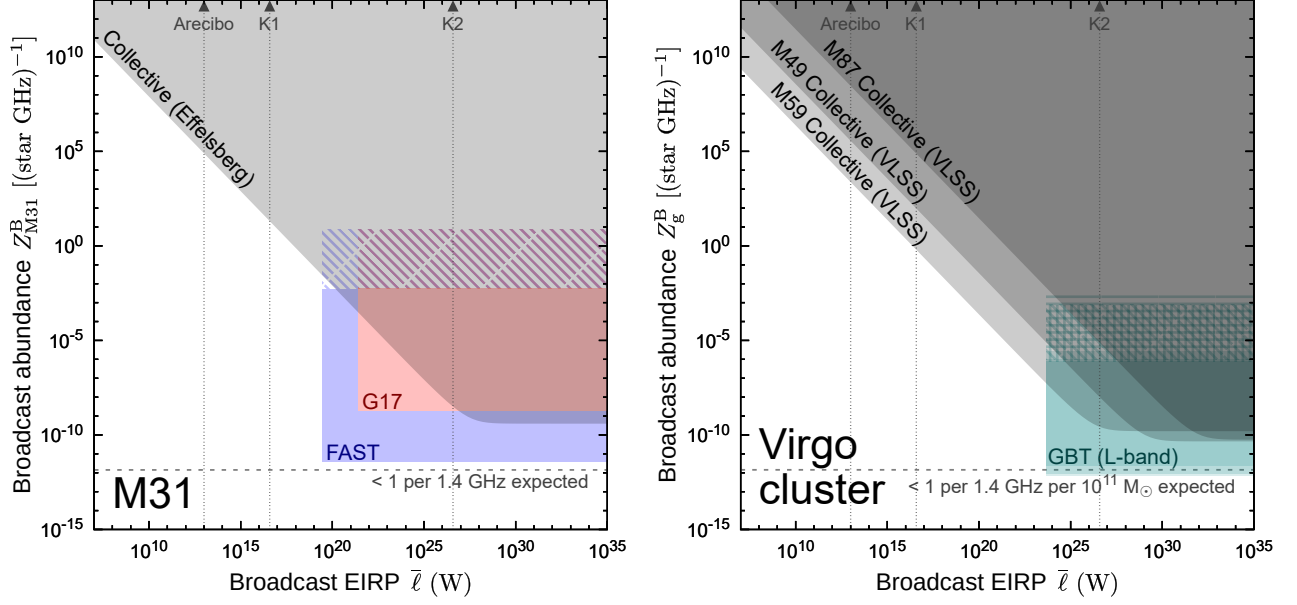


Figure 5. Current and forthcoming constraints on radio line broadcasts in M31 (left) and three example Virgo cluster ellipticals (right), assuming that all broadcasts in each galaxy have the same EIRP \bar{l} . The G17 observations of M31 exclude the red shaded region, while example future observations with FAST and GBT are in blue and green, respectively. Solid shading applies to individualist constraints when $\bar{\delta}_M = 0$, and hatched shading is for the noise confusion limit at high $\bar{\delta}_M$ (vertical for M49, diagonal for M31 and M87, horizontal for M59).

to:

$$Z_M^B(\nu) \lesssim 0.23 \text{ GHz}^{-1} \text{ star}^{-1} \left(\frac{\langle M_{t,g}^* \rangle}{10^{10} M_\odot} \right)^{0.49} \cdot \left(\frac{\langle \dot{\ell}_B \rangle_M}{10^{20} \text{ W}} \right) \left(\frac{\nu}{1.4 \text{ GHz}} \right)^{-\alpha} \left(\frac{\langle m_* \rangle_g}{0.2 M_\odot} \right), \quad (90)$$

within a factor of a few, as long as the broadcasts are individually much fainter than $\sim B_o \dot{\ell}_{\nu,g}(1.4 \text{ GHz})$. For comparison, present SETI surveys of nearby galaxies are expected to be sensitive to broadcasts with $\dot{\ell}_B \gtrsim 10^{19}\text{--}10^{20} \text{ W}$ (Isaacson et al. 2017). The FRC automatically implies that, in the vast majority of SFGs, most stars do not have a transmitter that bright in the examined frequency ranges.

A large fraction of stellar mass at low redshift is found in red early-type galaxies (Moffett et al. 2016). Although these galaxies can contain residual star formation and its attendant radio emission, by and large, most of them are radio quiet (Nyland et al. 2017). Thus, collective bounds on radio emission can be even more powerful than for SFGs (section 8.3). Large early-type galaxies typically do have radio emission, however (Sabater et al. 2019).

9.2. Prospects for the collective bound for broadcasts at higher energies and other messengers

The collective bound only lets us say that the ETI broadcast population is fainter than the galaxy as a whole. It thus favors wavebands where the galaxy’s luminosity is known to be a small fraction of the bolometric luminosity.

Infrared—SFGs are bright in infrared because of the presence of thermal dust emission, with some residual contribution of stellar emission at short wavelengths (e.g., Silva et al. 1998). Waste heat technosignature searches effectively use the collective bound (Griffith et al. 2015; Garrett 2015), and they have focused on the mid-infrared because the classical Dyson sphere is “habitable” (Dyson 1960). SFGs are fortuitously fainter in mid-infrared, but nonetheless about $\sim 10\text{--}20\%$ of the emission is released at $5\text{--}20 \mu\text{m}$ (though in the form of narrow bands from small dust grains; e.g., Dale et al. 2001), limiting these types of searches (Wright et al. 2014a). Quiescent galaxies, however, including most ellipticals and lenticulars, are deficient in dust and infrared emission, though not entirely bereft of it (Temi et al. 2007; Smith et al. 2012), allowing more stringent collective bounds (Wright et al. 2014a).

Optical—Although optical transmissions are a long-sought technosignature, collective bounds are of dubious value for constraining them. Starlight is peaked in near-infrared, optical, and ultraviolet, so in order for broadcasts to contribute meaningfully to a galaxy’s optical luminosity, they must practically outshine all the

stars in the galaxy! Optical SETI’s technosignatures are viable because we are not looking at the mean emission of a target galaxy, but for individualist rare fluctuations – ultranarrowband lines or ultrashort pulses that stick out from the normal emission (Schwartz & Townes 1961; Howard et al. 2004; Abeyssekara et al. 2016). Optical megastructure searches instead seek abnormal extinction of the starlight by the putative structures (Annis 1999; Zackrisson et al. 2015).

Conceivably, the collective emission could be detectable if it was beamed, probably resulting in a smooth spectral component not found in nearby galaxies. Alternatively, broadcasts clustering around a “magic frequency” aggregate into an unnatural emission line in the galaxy’s spectrum, which may stand out as being at an unusual wavelength or by apparently dominating the galaxy’s luminosity if beamed without the usual signs of intense star formation or an active nucleus. Finally, the discreteness of extremely bright optical transmitters with $\dot{\ell}_B \gg 1 L_\odot$ might be detectable from galactic surface brightness fluctuations.

High energy radiation—Collective bounds should be moderately useful for constraining broadcasts of high-energy radiation. X-ray SETI has been considered theoretically a few times in the literature, although observational results are scant (Corbet 1997; Hippke & Forgan 2017; Lacki 2020). The same is true for neutrino SETI (Subotowicz 1979; Learned et al. 1994, 2012; Lacki 2015b), and gamma-ray SETI is even more underdeveloped (for a rare exception, see Harris 1986, 2002). The collective bound serves as a default upper limit.

Most galaxies are X-ray emitters, as low-mass X-ray binaries alone contribute a minimum luminosity tracing stellar mass, about $\sim 10^{-4.5} L_\odot/M_\odot$ at $z = 0$ and roughly 10 times higher at $z \sim 2-3$ (Lehmer et al. 2010, 2016). Star-forming galaxies also have soft X-ray emission from their interstellar medium and hard X-rays from high-mass X-ray binaries tracing star-formation rate (Lehmer et al. 2010; Mineo et al. 2012). X-ray telescopes are powerful enough to detect the comparatively low X-ray luminosities of normal galaxies out to cosmological distances, so the collective bound can be applied for a large number of galaxies (Lehmer et al. 2012). Although not as stringent as the radio collective bounds, X-ray collective bounds are likely to be useful, especially given how underdeveloped high-energy SETI is.

In principle, gamma-ray and neutrino emission from galaxies is faint enough that the collective bound should be very useful. Observations of nearby SFGs indicate that typically $\sim 10^{-5}$ to 10^{-4} of the bolometric power is released as GeV gamma rays (Ackermann et al. 2012). Quiescent galaxies may be even fainter in gamma rays (for theoretical discussion, see Lien & Fields 2012). Our sensitivity to gamma rays is comparatively weak, however: about a dozen star-forming galaxies beyond the

Milky Way have been detected, only four of them (the Magellanic Clouds, M31, and M33) not intense starburst galaxies (Abdollahi et al. 2020; Ajello et al. 2020). We thus cannot rule out that many galaxies are abnormally gamma-ray bright from broadcasts. Abdollahi et al. (2020) report a current flux detection limit of $\sim 2 \times 10^{-12} \text{ erg cm}^{-2} \text{ s}^{-1}$ from *Fermi-LAT* for GeV gamma-ray sources with an $\dot{\epsilon}_{\nu;B} \propto \nu^{-1}$ spectrum. The collective bound applied to narrowband sources suggests a maximum abundance of

$$\nu Z_M^B \sim 6 \times 10^{-5} \text{ star}^{-1} \left[\frac{\langle \dot{\ell}_B \rangle_M}{1 L_\odot} \frac{\langle N_{o,g}^* \rangle}{10^{11}} \left(\frac{d_\epsilon}{10 \text{ Mpc}} \right)^2 \right]^{-1}. \quad (91)$$

Neutrino limits are also quite poor. IceCube reports the ability to detect point sources in the northern TeV-PeV neutrino sky with fluxes below $\sim 3 \times 10^{-12} \text{ erg cm}^{-2} \text{ s}^{-1}$, assuming 1:1:1 flavor ratios and an E^{-2} spectrum (Aartsen et al. 2017). The resulting limit is similar:

$$\nu Z_M^B \sim 9 \times 10^{-5} \text{ star}^{-1} \left[\frac{\langle \dot{\ell}_B \rangle_M}{1 L_\odot} \frac{\langle N_{o,g}^* \rangle}{10^{11}} \left(\frac{d_\epsilon}{10 \text{ Mpc}} \right)^2 \right]^{-1}. \quad (92)$$

Still, given that we have essentially no gamma-ray or neutrino SETI constraints, even weak collective bounds from upper limits can serve as a starting point. These limits are already sufficient to eliminate the possibility that most big nearby galaxies like M81 are home to ETIs that convert $\gtrsim 0.01\%$ of available starlight into GeV gamma rays or TeV neutrinos.

Gravitational waves—Gravitational waves have occasionally been suggested as a messenger for ETI broadcasts (Hippke 2018). The difficulty of gravitational-wave SETI is the sheer weakness of gravity. LIGO and other gravitational wave observatories can detect black hole mergers from hundreds of megaparsecs away simply because they are the most powerful known events in the Universe (Abbott et al. 2019). Still, LIGO and Virgo have been able to set limits on point sources of gravitational waves with flat spectra at around 25 Hz. The most recent limits are of order 10^{-10} to $10^{-9} \text{ erg cm}^{-2} \text{ s}^{-1} \text{ Hz}^{-1}$, depending on location on the sky (Abbott et al. 2021). For a population of persistent narrowband transmitters, the collective bound gives an abundance limit of

$$\nu Z_M^B \lesssim 0.1-0.9 \text{ star}^{-1} \left[\frac{\langle \dot{\ell}_B \rangle_M}{1 L_\odot} \frac{\langle N_{o,g}^* \rangle}{10^{11}} \left(\frac{d_\epsilon}{10 \text{ Mpc}} \right)^2 \right]^{-1}. \quad (93)$$

We can therefore reject the existence of Kardashev Type III metasocieties broadcasting all of their power in ~ 25 Hz gravitational waves in the nearest large galaxies. This still leaves the rest of the gravitational-wave

spectrum unexplored, however, and allows the existence of less powerful broadcasts of gravitational waves even in the nearest galaxies.

10. CONCLUSION

I consider two general types of constraints derived from the collection of measurements we make in a SETI survey, the individualist signal-to-noise constraint and the collective bound. Both types of limits are subject to a discreteness criterion: they cannot constrain models where broadcasts, or the transmitting societies, are sufficiently rare.

The individualist approach searches for single anomalous measurements that are incompatible with a natural background, a spike rising above the background past some signal-to-noise threshold. Most SETI results employ the individualist strategy. Only a single, sufficiently bright broadcast in the sample is necessary for a detection, which makes it useful if ETIs are rare. But if there are too many broadcasts per observation, with too narrow a fluence distribution, the signal-to-noise ratio falls because they start to overlap, ultimately resulting in the confusion limit where no detection is possible. The sample variance sets an upper limit of

$$\bar{\mathfrak{S}}[\mathfrak{M}_o] \lesssim \left(\mathbb{M} \left[\max \left[N_{o,M}^{B;1} \right] \right] - \langle N_{o,M}^{B;1} \rangle \right) / \sqrt{\langle N_{o,M}^{B;2} \rangle}$$

to the signal-to-noise ratio when the broadcasts are all about equally bright. Sample confusion occurs when this ratio falls below a threshold $\bar{\mathfrak{S}}_s$ for detection; in some cases, the noise of the mutually interfering broadcasts can produce a noise confusion effect. I present calculations about this degradation, including estimates for when confusion sets in for continuum sources,

$$\Xi_M^B \gtrsim \left[\bar{\mathfrak{S}}_s^2 \langle N_{o,g}^* \rangle \right]^{-1}$$

and narrowband radio lines,

$$Z_M^B \gtrsim \left[\bar{\mathfrak{S}}_s^2 \langle N_{o,g}^* \rangle B_o \xi_{\delta;o,M}^B (1 + \langle \xi_{c;o|B} \rangle_M) \right]^{-1}$$

$$Z_M^B \gtrsim \sqrt{N_o^u} \left[\bar{\mathfrak{S}}_s \langle N_{o,g}^* \rangle B_o \right]^{-1}$$

under standard assumptions (Table 2) with broadcasts of equal brightness. Confusion only happens for dense populations – about one per channel per resolution element for narrowband observations – but *a priori* we cannot rule those out. As near as the Virgo Cluster, billions of stars and all their broadcasts can be blended into one radio beam, preventing detection if ~ 1 in 1000 stars has a gigahertz radio “beacon.” As we approach the confusion limit, more abundant broadcasts actually *worsen* the prospects for detection.

The collective bound,

$$\langle N_{o,M}^B \rangle \lesssim \hat{N}_{o,M}^B + \frac{C'^2}{2} \left(1 + \sqrt{1 + \frac{4}{C'^2} \hat{N}_{o,M}^B} \right),$$

follows from the aggregate emission, and is the simple observation that ETI broadcasts cannot outshine the galaxy’s observed emission itself. It is unable to make a detection but is robust to confusion and uncertainty about the form of the broadcasts. Generally speaking, the collective bound is more suitable for distant galaxies, because it only needs a measurement of the luminosity and because confusion is more severe at larger distances. The collective bound closes the window opened by confusion: we are not in fact missing vast populations of ETIs because their broadcasts are overlapping with each other. Collective bounds are most useful in wavebands where galaxies are faint and our instruments are sensitive, especially radio but also possibly X-rays. Radio collective bounds of similar strength apply to all galaxies on the FRC, out to cosmological distances, and are even more constraining for radio-quiet quiescent galaxies. They set a limit of a few hundred Kardashev Type I radio transmitters per gigahertz in galaxies like the Milky Way and about a few hundred thousand Kardashev Type II GeV gamma-ray or TeV neutrino transmitters in nearby galaxies, and they constrain Local Group Kardashev Type III gravitational wave transmitters in the band observed by LIGO.

Only the simplest properties of the aggregate emission of ETI populations have been considered. More powerful constraints could be found by exploiting the detailed statistical properties of this emission using the broadcast distributions. The underlying discrete nature of broadcasts affects the flux statistics (Cordes et al. 1997), with an implied presence of Poisson fluctuations and spatial and temporal correlations. An example of this kind of approach can be found in the $P(D)$ method of constraining faint cosmic radio sources by examining fluctuations of the radio background (Scheuer 1957; Condon 1974; Condon et al. 2012; Vernstrom et al. 2014) and extended to X-rays and gamma-rays (Scheuer 1974; Malyshev & Hogg 2011). Likewise, measuring stellar Poisson fluctuations serves as a means of probing the stellar content and distance of other galaxies (as in Tonry & Schneider 1988; Raimondo et al. 2005). Statistical methods allow us to glimpse deeper into the ETI luminosity function than we can hope with near-future targeted searches, sweeping another layer off the “cosmic haystack” (c.f., Wright et al. 2018).

ACKNOWLEDGMENTS

As with Paper I, I thank the referee, whose dedicated efforts resulted in detailed and helpful comments on this paper. I also thank the Breakthrough Listen program for their support. Funding for *Breakthrough Listen* research is sponsored by the Breakthrough Prize Foundation (<https://breakthroughprize.org/>). In addition, I acknowledge the use of NASA’s Astrophysics Data System and arXiv for this research.

APPENDIX

A. DERIVATIONS FOR THE MEAN AND SAMPLE VARIANCE OF THE AGGREGATE EMISSION

As before, we assume that all the broadcasts come from a single metasociety in a single galaxy (possibly the Milky Way). Suppose the mean aggregate emission is the sum of the mean individual signals.¹⁶ Suppose the collected emission adds linearly. The sample-conditionalized mean tells us the mean emission that is collected during an observation from a fixed collection of societies and broadcasts:

$$\langle \mathfrak{M}_{\circ}^{\text{B}} | \Sigma_{\circ}^{\text{B}}, \Sigma_{\circ}^{\text{C}} \rangle = \langle \mathfrak{m}_{\circ|\text{n}} \rangle + \sum_{\mathbf{w}_{\text{C}} \in \Sigma_{\circ, \text{M}}^{\text{C}}} \sum_{\mathbf{w}_{\text{B}} \in \Sigma_{\circ, \text{C}}^{\text{B}}} \langle \mathfrak{m}_{\circ|\text{B}} \rangle = \langle \mathfrak{m}_{\circ|\text{n}} \rangle + \sum_{\mathbf{w}_{\text{C}} \in \Sigma_{\circ, \text{M}}^{\text{C}}} \sum_{\mathbf{w}_{\text{B}} \in \Sigma_{\circ, \text{C}}^{\text{B}}} \mathcal{A} \mathcal{I}_{\mathfrak{M}; \circ}(\boldsymbol{\theta}_{\text{B}}) \hat{\varrho}_{\circ|\text{B}} \chi_{\varrho; \circ|\text{B}} y_{\varrho; \text{B}}. \quad (\text{A1})$$

In order to calculate the mean over all samples, we start by calculating the emission from a single society. Because a society is localized, all the broadcasts have the same dilution (distance). If the instrumental response has no dependence on frequency or time within the window \circ (equation 28), all the $\mathcal{I}_{\mathfrak{M}; \circ}$ terms will be the same as well, depending only on the sky position of the society $\boldsymbol{\theta}_{\text{C}}$. Now, this is not precisely true: actual observations do not have perfectly sharp bandpasses, and beam size falls with frequency, for example, but this assumption should still suffice for typical SETI observations, which involve fine channels. Then, given the society's parameter tuple \mathbf{w}_{C} , we have

$$\langle \mathfrak{M}_{\circ, \text{C}}^{\text{B}} | \mathbf{w}_{\text{C}} \rangle = \mathcal{A} \mathcal{I}_{\mathfrak{M}; \circ}(\boldsymbol{\theta}_{\text{C}}) \chi_{\varrho; \text{B}} y_{\varrho; \text{B}} \left\langle \sum_{\mathbf{w}_{\text{B}} \in \Sigma_{\circ, \text{C}}^{\text{B}}} \chi_{\varrho; \circ|\text{B}} \hat{\varrho}_{\circ|\text{B}} \right\rangle = \mathcal{A} \mathcal{I}_{\mathfrak{M}; \circ}(\boldsymbol{\theta}_{\text{C}}) y_{\varrho; \text{B}} \langle N_{\circ, \text{C}}^{\text{B}} \rangle \langle \hat{\varrho}_{\circ|\text{B}} \rangle_{\text{C}} \langle \chi_{\varrho; \circ|\text{B}} \rangle_{\text{C}}, \quad (\text{A2})$$

where the second equality follows from Campbell's formula.

Now this quantity can be interpreted as a random variable describing the society. We can therefore calculate the total mean with another application of Campbell's formula:

$$\langle \mathfrak{M}_{\circ, \text{M}}^{\text{B}} \rangle = \left\langle \sum_{\mathbf{w}_{\text{C}} \in \Sigma_{\circ, \text{M}}^{\text{C}}} \langle \mathfrak{M}_{\circ, \text{C}}^{\text{B}} | \mathbf{w}_{\text{C}} \rangle \right\rangle = \int_{W_{\text{C}}} \langle \mathfrak{M}_{\circ, \text{C}}^{\text{B}} | \mathbf{w}_{\text{C}} \rangle \Psi_{\circ, \text{M}}^{\text{C}}(\mathbf{w}_{\text{C}} | \mathbf{w}_{\text{M}}) d\mathbf{w}_{\text{C}}. \quad (\text{A3})$$

Plugging in the societal distribution from equation 23, we get

$$\langle \mathfrak{M}_{\circ, \text{M}}^{\text{B}} \rangle = \Xi_{\text{M}}^{\text{C}} \mathcal{A} \langle \hat{\varrho}_{\circ|\text{B}} \rangle_{\text{M}} \langle N_{\circ, \text{C}}^{\text{B}} \rangle_{\text{M}} \int_{V_{\circ}} \mathcal{I}_{\mathfrak{M}; \circ}(\mathbf{r}_{\star}) y_{\varrho; \text{B}}(\mathbf{r}_{\star}) \langle \chi_{\varrho; \circ|\text{B}} | \mathbf{r}_{\star} \rangle_{\text{M}} \frac{d \langle N_{\circ, \text{g}}^{\star} \rangle}{d\mathbf{r}_{\star}} d\mathbf{r}_{\star}. \quad (\text{A4})$$

This assumes that $\langle \hat{\varrho}_{\circ|\text{B}} \rangle_{\text{C}} = \langle \hat{\varrho}_{\circ|\text{B}} \rangle_{\text{M}}$, $\langle \chi_{\varrho; \circ|\text{B}} \rangle_{\text{C}} = \langle \chi_{\varrho; \circ|\text{B}} | \mathbf{r}_{\star} \rangle_{\text{M}}$ and $\langle N_{\circ, \text{C}}^{\text{B}} \rangle = \langle N_{\circ, \text{C}}^{\text{B}} \rangle_{\text{M}}$.

The sample variance is slightly trickier, because of the double sum over the broadcast and societal samples. To start, we note that the societies are a Poisson point process for a metasociety of given \mathbf{w}_{M} , and so Campbell's second formula applies:

$$\mathbb{V} [\langle \mathfrak{M}_{\circ, \text{M}}^{\text{B}} \rangle | \Sigma_{\circ}^{\text{B}}, \Sigma_{\circ}^{\text{C}}] = \mathbb{V} \left[\sum_{\mathbf{w}_{\text{C}} \in \Sigma_{\circ, \text{M}}^{\text{C}}} \left\langle \sum_{\mathbf{w}_{\text{B}} \in \Sigma_{\circ, \text{C}}^{\text{B}}} \langle \mathfrak{m}_{\circ|\text{B}} \rangle \right\rangle \right] = \int_{W_{\text{C}}} \left\langle \left(\sum_{\mathbf{w}_{\text{B}} \in \Sigma_{\circ, \text{C}}^{\text{B}}} \langle \mathfrak{m}_{\circ|\text{B}} \rangle \right)^2 \middle| \mathbf{w}_{\text{C}} \right\rangle \Psi_{\circ, \text{M}}^{\text{C}}(\mathbf{w}_{\text{C}} | \mathbf{w}_{\text{M}}) d\mathbf{w}_{\text{C}} \quad (\text{A5})$$

While the background has variance, the mean background is a constant and does not contribute to sample variance (the background is always "sampled"). By the definition of variance,

$$\mathbb{V} [\langle \mathfrak{M}_{\circ, \text{M}}^{\text{B}} \rangle | \Sigma_{\circ}^{\text{B}}, \Sigma_{\circ}^{\text{C}}] = \int_{W_{\text{C}}} \left[\mathbb{V} \left[\sum_{\mathbf{w}_{\text{B}} \in \Sigma_{\circ, \text{C}}^{\text{B}}} \langle \mathfrak{m}_{\circ|\text{B}} \rangle \middle| \mathbf{w}_{\text{C}} \right] + \left\langle \sum_{\mathbf{w}_{\text{B}} \in \Sigma_{\circ, \text{C}}^{\text{B}}} \langle \mathfrak{m}_{\circ|\text{B}} \rangle \middle| \mathbf{w}_{\text{C}} \right\rangle^2 \right] \Psi_{\circ, \text{M}}^{\text{C}}(\mathbf{w}_{\text{C}} | \mathbf{w}_{\text{M}}) d\mathbf{w}_{\text{C}}. \quad (\text{A6})$$

¹⁶ The total energy collected in radio observations is not generally the sum of the energies of each broadcast and the background, because they interfere with each other. But it can be shown that the mean energies do add linearly, so the condition still applies.

For the variance term in the integral, we again note that broadcasts are a Poisson point process for a society with given \mathbf{w}_C , and so

$$\mathbb{V} \left[\sum_{\mathbf{w}_B \in \Sigma_{\circ,C}^B} \langle \mathbf{m}_{\circ|B} \rangle \middle| \mathbf{w}_C \right] = \langle N_{\circ,C}^B | \mathbf{w}_C \rangle \langle \langle \mathbf{m}_{\circ|B}^2 \rangle_C | \mathbf{w}_C \rangle = \langle N_{\circ,C}^B \rangle \mathcal{A}^2 \mathcal{I}_{\mathfrak{M};\circ}(\boldsymbol{\theta}_C)^2 y_{\ell;C}^2 \langle \hat{\varrho}_{\circ|B}^2 \rangle_C \langle \chi_{\ell; \circ|B}^2 \rangle_C. \quad (\text{A7})$$

A difficulty arises if the transmittance is not a simple function of position: the first term in equation A6 uses $\langle \chi_{\ell; \circ|B}^2 \rangle_C$, while the second uses $\langle \chi_{\ell; \circ|B} \rangle_C^2$, and unlike the amount of emission, it is not independent of position. If the transmittance is solely a function of position, and not time or frequency, then it has a single value for each society and the two quantities are equal. This, of course, cannot be entirely accurate, but if we are dealing with observations of moderate bandwidths in the absence of absorption lines, we can approximate the extinction as constant over that bandwidth, and $\chi_{\ell; \times|B} = \chi_{\ell; B}$. Again assuming that $\langle \hat{\varrho}_{\circ|B} \rangle_C = \langle \hat{\varrho}_{\circ|B} \rangle_M$ and $\langle N_{\circ,C}^B \rangle = \langle N_{\circ,C}^B \rangle_M$,

$$\mathbb{V} [\langle \mathfrak{M}_{\circ,M}^B | \Sigma_{\circ}^B, \Sigma_{\circ}^C \rangle] = \mathcal{A}^2 \Xi_M^C \langle N_{\circ,C}^B \rangle_M \left[\langle \hat{\varrho}_{\circ|B}^2 \rangle_M + \langle N_{\circ,C}^B \rangle_M \langle \hat{\varrho}_{\circ|B} \rangle_M^2 \right] \int_{V_{\circ}} [\mathcal{I}_{\mathfrak{M};\circ}(\mathbf{r}_{\star}) y_{\ell;B}(\mathbf{r}_{\star}) \chi_{\ell;B}(\mathbf{r}_{\star})]^2 \frac{d\langle N_{\circ,g}^{\star} \rangle}{d\mathbf{r}_{\star}} d\mathbf{r}_{\star}. \quad (\text{A8})$$

We can define the variable

$$Y_{x,M}^{B;n} = \sum_{\mathbf{w}_B \in \Sigma_{x,M}^B} [\mathcal{I}_{\mathfrak{M};x}(\boldsymbol{\theta}_B) y_{\ell;B} \chi_{\ell;B}]^n, \quad (\text{A9})$$

for all n , in which case our assumptions give us

$$\langle Y_{x,M}^{B;n} \rangle = \Xi_M^C \langle N_{\circ,C}^B \rangle_M \int_{V_x} [\mathcal{I}_{\mathfrak{M};\circ}(\mathbf{r}_{\star}) y_{\ell;B}(\mathbf{r}_{\star}) \chi_{\ell;B}(\mathbf{r}_{\star})]^n \frac{d\langle N_{\circ,g}^{\star} \rangle}{d\mathbf{r}_{\star}} d\mathbf{r}_{\star}, \quad (\text{A10})$$

Equation A4 reduces to

$$\langle \mathfrak{M}_{\circ,M}^B \rangle = \mathcal{A} \langle \hat{\varrho}_{\circ|B} \rangle_M \langle Y_{x,M}^{B;1} \rangle, \quad (\text{A11})$$

while equation A8 can be written as

$$\mathbb{V} [\langle \mathfrak{M}_{\circ,M}^B | \Sigma_{\circ}^B, \Sigma_{\circ}^C \rangle] = \mathcal{A}^2 \left[\langle \hat{\varrho}_{\circ|B}^2 \rangle_M + \langle N_{\circ,C}^B \rangle_M \langle \hat{\varrho}_{\circ|B} \rangle_M^2 \right] \langle Y_{\circ,M}^{B;2} \rangle. \quad (\text{A12})$$

When the broadcasts are all part of a single distant galaxy and extinction is negligible or constant (e.g., from a smooth foreground screen like Earth's atmosphere), the dilution factor of each broadcast can be assumed to be the same, allowing the substitution

$$\langle \hat{\varrho}_{x|B}^n \rangle_M \langle Y_{x,J}^{B;n} \rangle \approx \langle \hat{\varrho}_{x|B}^n \rangle_M \langle \chi_{\ell;B}^n y_{\ell;B}^n \rangle_{x|M} \langle N_{x,M}^{B;n} \rangle \approx \langle \mathbf{u}_{x|B}^n \rangle_M \langle N_{x,M}^{B;n} \rangle. \quad (\text{A13})$$

It uses an a weighted number of broadcasts,

$$N_{x,M}^{B;n} = \sum_{\mathbf{w}_B \in \Sigma_{x,M}^B} [\mathcal{I}_{\mathfrak{M};x}(\boldsymbol{\theta}_B)]^n, \quad (\text{A14})$$

with a mean value of

$$\langle N_{x,M}^{B;n} \rangle = \Xi_M^C \langle N_{x,C}^B \rangle_M \int_{V_x} [\mathcal{I}_{\mathfrak{M};x}(\boldsymbol{\theta}_B)]^n \frac{d\langle N_{\circ,g}^{\star} \rangle}{d\mathbf{r}_{\star}} d\mathbf{r}_{\star}. \quad (\text{A15})$$

B. FURTHER DETAILS ON CALCULATION OF RADIO ENERGY STATISTICS

B.1. Noise variance in radio detection

This appendix provides a summary of the mean noise variance calculation for radio broadcasts, $\langle \mathbb{V} [\mathfrak{E}_{\circ} | \Sigma_{\circ}^B, \Sigma_{\circ}^C] \rangle$. We start by describing the raw amplitudes with a complex phasor, $\mathbf{a}_{\mu|B} = |\mathbf{a}_{\mu|B}| \exp(i\varphi_{\mu|B})$ (with $i = \sqrt{-1}$). As in section 5.1, I adopt a convention that $\mathfrak{e}_{\mu|B} = |\mathbf{a}_{\mu|B}|^2$. The $\mathfrak{e}_{\mu|B}$ may be fully randomized for incoherent signals, be constant for coherent signals, or display correlations for partially coherent signals. The measured energy can be

regarded as the sum of an unvarying mean component that is a measure of the mean energy output of the broadcast and a fluctuation component with zero mean (section 5.1):

$$\epsilon_{\mu|B} = \langle \epsilon_{\mu|B} \rangle + \Delta \epsilon_{\mu|B} = \mathcal{A} \mathcal{I}_{\epsilon;\mu}(\boldsymbol{\theta}_B) \mathfrak{h}_{\mu|B} + \Delta \epsilon_{\mu|B} = \mathcal{A} \mathcal{I}_{\epsilon;\mu}(\boldsymbol{\theta}_B) y_{\epsilon;B} \chi_{\epsilon;\mu|B} \mathring{\epsilon}_{\mu|B} + \Delta \epsilon_{\mu|B}. \quad (\text{B16})$$

Likewise, the phases may be linked by a relation, but individually they have a uniform distribution over $[-\pi, \pi)$ and I generally consider them independent between broadcasts and modes. These are summed together with a background of noise with $\mathbf{a}_{\mu|n} = |\mathbf{a}_{\mu|n}| \exp(i\varphi_{\mu|n})$. The background amplitude has a complex Gaussian distribution, with $\langle \epsilon_{\mu|n} \rangle = \langle |\mathbf{a}_{\mu|n}|^2 \rangle = k_B \mathcal{T}_n$. Furthermore, the background energy has an exponential (χ_2^2) distribution, with $\mathbb{V}[\epsilon_{\mu|n}] = \langle \epsilon_{\mu|n} \rangle^2$. Thus, the measured amplitude for mode μ is

$$\mathfrak{A}_{\mu} = |\mathbf{a}_{\mu|n}| \exp(i\varphi_{\mu|n}) + \sum_{\mathbf{w}_B \in \Sigma_o^B} |\mathbf{a}_{\mu|B}| \exp(i\varphi_{\mu|B}) = \sum_{\mathbf{w}_B \in \Sigma_o^{B\ddagger}} |\mathbf{a}_{\mu|B}| \exp(i\varphi_{\mu|B}). \quad (\text{B17})$$

The adjoined sample $\Sigma_{x,j}^{B\ddagger} = \Sigma_{x,j}^B \cup \{\mathbf{w}_n\}$ includes the background noise with amplitude $\mathbf{a}_{\mu|n}$, which is, for the purposes of these calculations, a special broadcast that is always present.

Square-law detectors measure the total energy as $\mathfrak{E}_{\mu} = \mathfrak{A}_{\mu} \mathfrak{A}_{\mu}^*$:

$$\mathfrak{E}_{\mu} = \sum_{\mathbf{w}_B \in \Sigma_{\mu}^{B\ddagger}} \epsilon_{\mu|B} + \sum_{\substack{\mathbf{w}_{B_1}, \mathbf{w}_{B_2} \in \Sigma_{\mu}^{B\ddagger} \\ \mathbf{w}_{B_1} \neq \mathbf{w}_{B_2}}} |\mathbf{a}_{\mu|B_1}| |\mathbf{a}_{\mu|B_2}| \cos(\varphi_{\mu|B_1} - \varphi_{\mu|B_2}). \quad (\text{B18})$$

Then, the energy from several modes can be added together to yield the energy measured by the observation. Let $\epsilon_{o|B} = \sum_{\mu \in S_o^{\mu}} \epsilon_{\mu|B}$:

$$\mathfrak{E}_o = \sum_{\mathbf{w}_B \in \Sigma_o^{B\ddagger}} \epsilon_{o|B} + \sum_{\mu \in S_o^{\mu}} \sum_{\substack{\mathbf{w}_{B_1}, \mathbf{w}_{B_2} \in \Sigma_o^{B\ddagger} \\ \mathbf{w}_{B_1} \neq \mathbf{w}_{B_2}}} |\mathbf{a}_{\mu|B_1}| |\mathbf{a}_{\mu|B_2}| \cos(\varphi_{\mu|B_1} - \varphi_{\mu|B_2}). \quad (\text{B19})$$

The broadcasts in a sample have independent phases, giving us $\langle \cos(\varphi_{\mu|B_1} - \varphi_{\mu|B_2}) | \Sigma_o^B, \Sigma_o^C \rangle = 0$ if $B_1 \neq B_2$. Since $\langle \epsilon_{o|n} | \Sigma_o^B, \Sigma_o^C \rangle = \langle \epsilon_{o|n} \rangle = N_o^{\mu} k_B \mathcal{T}_n$, $\langle \epsilon_{o|B} | \Sigma_o^B, \Sigma_o^C \rangle = \langle \epsilon_{o|B} \rangle = \mathcal{A} \mathcal{I}_{\epsilon;o}(\boldsymbol{\theta}_B) y_{\epsilon;B} \chi_{\epsilon;o|B} \mathring{\epsilon}_{o|B}$, and the broadcasts have independent phases,

$$\langle \mathfrak{E}_o | \Sigma_o^B, \Sigma_o^C \rangle = \langle \epsilon_{o|n} | \Sigma_o^B, \Sigma_o^C \rangle + \sum_{\mathbf{w}_B \in \Sigma_o^B} \langle \epsilon_{o|B} | \Sigma_o^B, \Sigma_o^C \rangle = N_o^{\mu} k_B \mathcal{T}_n + \sum_{\mathbf{w}_B \in \Sigma_o^B} \mathcal{A} \mathcal{I}_{\epsilon;o}(\boldsymbol{\theta}_B) y_{\epsilon;B} \chi_{\epsilon;o|B} \mathring{\epsilon}_{o|B}, \quad (\text{B20})$$

just as in equation 53. It can then be shown that

$$\langle \mathfrak{E}_o \rangle = N_o^{\mu} k_B \mathcal{T}_n + \mathcal{A} \langle \mathring{\epsilon}_{o|B} \rangle_M \langle Y_{o,M}^{B;1} \rangle, \quad (\text{B21})$$

when transmittance depends only on position, just as for additive emission (equation A11).

For the noise variance, we must calculate $\mathbb{V}[\mathfrak{E}_o | \Sigma_o^B, \Sigma_o^C] = \langle \mathfrak{E}_o^2 | \Sigma_o^B, \Sigma_o^C \rangle - \langle \mathfrak{E}_o | \Sigma_o^B, \Sigma_o^C \rangle^2$. To start,

$$\begin{aligned} \mathfrak{E}_o^2 &= \left(\sum_{\mathbf{w}_B \in \Sigma_o^{B\ddagger}} \epsilon_{o|B} \right)^2 + 2 \sum_{\mathbf{w}_{B_1} \in \Sigma_o^{B\ddagger}} \epsilon_{o|B_1} \sum_{\substack{\mu \in S_o^{\mu} \\ \mathbf{w}_{B_{2,1}}, \mathbf{w}_{B_{2,2}} \in \Sigma_o^{B\ddagger} \\ \mathbf{w}_{B_{2,1}} \neq \mathbf{w}_{B_{2,2}}} } |\mathbf{a}_{\mu|B_{2,1}}| |\mathbf{a}_{\mu|B_{2,2}}| \cos(\varphi_{\mu|B_{2,1}} - \varphi_{\mu|B_{2,2}}) \\ &+ \sum_{\substack{\mu_1, \mu_2 \in S_o^{\mu} \\ \mathbf{w}_{B_{1,1}}, \mathbf{w}_{B_{1,2}} \in \Sigma_o^{B\ddagger} \\ \mathbf{w}_{B_{1,1}} \neq \mathbf{w}_{B_{1,2}}} } \sum_{\substack{\mathbf{w}_{B_{2,1}}, \mathbf{w}_{B_{2,2}} \in \Sigma_o^{B\ddagger} \\ \mathbf{w}_{B_{2,1}} \neq \mathbf{w}_{B_{2,2}}} } |\mathbf{a}_{\mu_1|B_{1,1}}| |\mathbf{a}_{\mu_1|B_{1,2}}| |\mathbf{a}_{\mu_2|B_{2,1}}| |\mathbf{a}_{\mu_2|B_{2,2}}| \cos(\varphi_{\mu_1|B_{1,1}} - \varphi_{\mu_1|B_{1,2}}) \cos(\varphi_{\mu_2|B_{2,1}} - \varphi_{\mu_2|B_{2,2}}). \end{aligned} \quad (\text{B22})$$

Note that the final term includes in the summation the cases when $\mu_1 = \mu_2$. After averaging, the middle term vanishes. The final sum has nonzero terms when $B_{1,1} = B_{2,1}$ and $B_{1,2} = B_{2,2}$, or when $B_{1,1} = B_{2,2}$ and $B_{1,2} = B_{2,1}$, generally when $\mu_1 = \mu_2$. The other terms are taken to average to zero, under the assumption that the phases of the broadcasts are independent. If two different pairs of broadcasts are chosen for μ_1 and μ_2 , then the phase differences

between each pair should also be independent. If the same pair of broadcasts is chosen for μ_1 and μ_2 , conceivably $\cos(\varphi_{\mu_1|B_1} - \varphi_{\mu_1|B_2}) = \cos(\varphi_{\mu_2|B_1} - \varphi_{\mu_2|B_2})$ if B_1 and B_2 are coherent and always at the same exact frequency, but otherwise the phase differences should be scrambled by different frequencies and drift rates, so those cases are assumed to average to zero too.

After proceeding through the algebra, we find

$$\mathbb{V}[\mathfrak{e}_o|\Sigma_o^B, \Sigma_o^C] = \sum_{\mu \in \mathbb{S}_o^\mu} \sum_{\substack{\mathbf{w}_{B_1}, \mathbf{w}_{B_2} \in \Sigma_o^{B\dagger} \\ \mathbf{w}_{B_1} \neq \mathbf{w}_{B_2}}} \langle \mathfrak{e}_{\mu|B_1} \rangle \langle \mathfrak{e}_{\mu|B_2} \rangle + \sum_{\mathbf{w}_B \in \Sigma_o^{B\dagger}} \sum_{\mu_1, \mu_2 \in \mathbb{S}_o^\mu} \text{Cov}[\mathfrak{e}_{\mu_1|B}, \mathfrak{e}_{\mu_2|B}]. \quad (\text{B23})$$

The covariance term contains all the information about the coherence of the signal. It is given by

$$\text{Cov}[\mathfrak{e}_{\mu_1|B}, \mathfrak{e}_{\mu_2|B}] = \langle \Delta \mathfrak{e}_{\mu_1|B} \Delta \mathfrak{e}_{\mu_2|B} \rangle - \langle \Delta \mathfrak{e}_{\mu_1|B} \rangle \langle \Delta \mathfrak{e}_{\mu_2|B} \rangle. \quad (\text{B24})$$

This property of the fluctuations is described by the $g_B^{(2)}$ function (Appendix B.3).

The noise variance is the average of this quantity over all possible samples. Under the assumption that the properties of the broadcast population and noise do not vary with mode,

$$\langle \mathbb{V}[\mathfrak{e}_o|\Sigma_o^B, \Sigma_o^C] \rangle = \mathbb{N}_o^\mu \left[\left(k_B \mathcal{T}_n + \mathcal{A} \langle Y_{\mu,M}^{B;1} \rangle \langle \dot{\mathfrak{e}}_{\mu|B} \rangle_M \right)^2 + \mathcal{A}^2 \langle N_{\mu,C}^B \rangle_M \langle Y_{\mu,M}^{B;2} \rangle \langle \dot{\mathfrak{e}}_{\mu|B} \rangle_M^2 \right] + \left\langle \sum_{\mathbf{w}_B \in \Sigma_o^B} \sum_{\mu_1, \mu_2 \in \mathbb{S}_o^\mu} \text{Cov}[\mathfrak{e}_{\mu_1|B}, \mathfrak{e}_{\mu_2|B}] \right\rangle_M \quad (\text{B25})$$

for extinction that depends only on position. The average over covariances does *not* include the background noise (i.e., the sample is not adjoined), which has already been accounted for under the assumption that it is incoherent.

B.2. Incoherent radio broadcasts

Incoherent sources have complex Gaussian amplitudes, and their sum is also a complex Gaussian. Thus, we generally expect the energy to be exponentially distributed, with $\mathbb{V}[\mathfrak{e}_\mu|\Sigma_o^B, \Sigma_o^C] = \langle \mathfrak{e}_\mu|\Sigma_o^B, \Sigma_o^C \rangle^2$. Furthermore, the noise should be independent between modes, so that $\mathbb{V}[\mathfrak{e}_o|\Sigma_o^B, \Sigma_o^C] = \mathbb{N}_o^\mu \mathbb{V}[\mathfrak{e}_\mu|\Sigma_o^B, \Sigma_o^C]$. These conclusions are borne out from equation B23, if we adopt¹⁷

$$\text{Cov}[\mathfrak{e}_{\mu_1|B}, \mathfrak{e}_{\mu_2|B}] = \begin{cases} \langle \mathfrak{e}_{\mu|B} \rangle^2 & \text{if } \mu = \mu_1 = \mu_2 \\ 0 & \text{if } \mu = \mu_1 \neq \mu_2 \end{cases}. \quad (\text{B26})$$

According to equation B26, the only nonzero covariance terms are the variance terms, so the noise variance is

$$\langle \mathbb{V}[\mathfrak{e}_o|\Sigma_o^B, \Sigma_o^C] \rangle = \mathbb{N}_o^\mu \left[\left(k_B \mathcal{T}_n + \mathcal{A} \langle Y_{\mu,M}^{B;1} \rangle \langle \dot{\mathfrak{e}}_{\mu|B} \rangle_M \right)^2 + \mathcal{A}^2 \langle Y_{\mu,M}^{B;2} \rangle \left(\langle \dot{\mathfrak{e}}_{\mu|B}^2 \rangle_M + \langle N_{\mu,C}^B \rangle_M \langle \dot{\mathfrak{e}}_{\mu|B} \rangle_M^2 \right) \right]. \quad (\text{B27})$$

When expanded, there are five terms in the noise variance: (1) a constant term from system noise and natural background emission; (2) a term linear in $\langle Y_{\mu,M}^{B;1} \rangle \langle \dot{\mathfrak{e}}_{\mu|B} \rangle_M$, describing interference between the noise and the broadcasts; (3) a $\langle Y_{\mu,M}^{B;1} \rangle^2 \langle \dot{\mathfrak{e}}_{\mu|B} \rangle_M^2$ term describing the interference between the broadcasts among all societies; (4) a $\langle Y_{\mu,M}^{B;2} \rangle \langle N_{\mu,C}^B \rangle_M \langle \dot{\mathfrak{e}}_{\mu|B} \rangle_M^2$ term for the interference between different broadcasts from the same society; and (5) a $\langle Y_{\mu,M}^{B;2} \rangle \langle \dot{\mathfrak{e}}_{\mu|B}^2 \rangle_M$ term describing the wave noise from self-interference. The last term is the mean self-noise of an individual broadcast (e.g., Kulkarni 1989), a noise that is intrinsic to the source even in the absence of all other noise. Terms three and four might also be included as “self-noise” of the broadcast population as a whole.

The noise variance depends on how each broadcast’s energy is apportioned into modes. If the energy is clumped into a small fraction of the modes summed in an observation, the noise variance of incoherent broadcasts is increased: the $\mathbb{V}[\mathfrak{e}_{\mu|B}]_M$ for occupied cells is $\propto (\mathbb{N}_o^\mu)^{-2}$, while the number of occupied cells is only proportional to \mathbb{N}_o^μ (Figure 6).

¹⁷ Strictly speaking, $g_{p;B}^{(2)}(|\Theta_{\mu_1} - \Theta_{\mu_2}|) - 1$ is not exactly zero for nonzero time delays – its form is related to the Fourier transform of the (channel) bandpass-filtered signal (Tan & Kurtziefer 2017). Polyphase filterbanks use samples from several coarsely channelized spectra separated in time to suppress sidebands (Price 2021), so we do expect nonzero covariance. However, the covariance should be small, decreasing rapidly as the delay grows past T_μ .

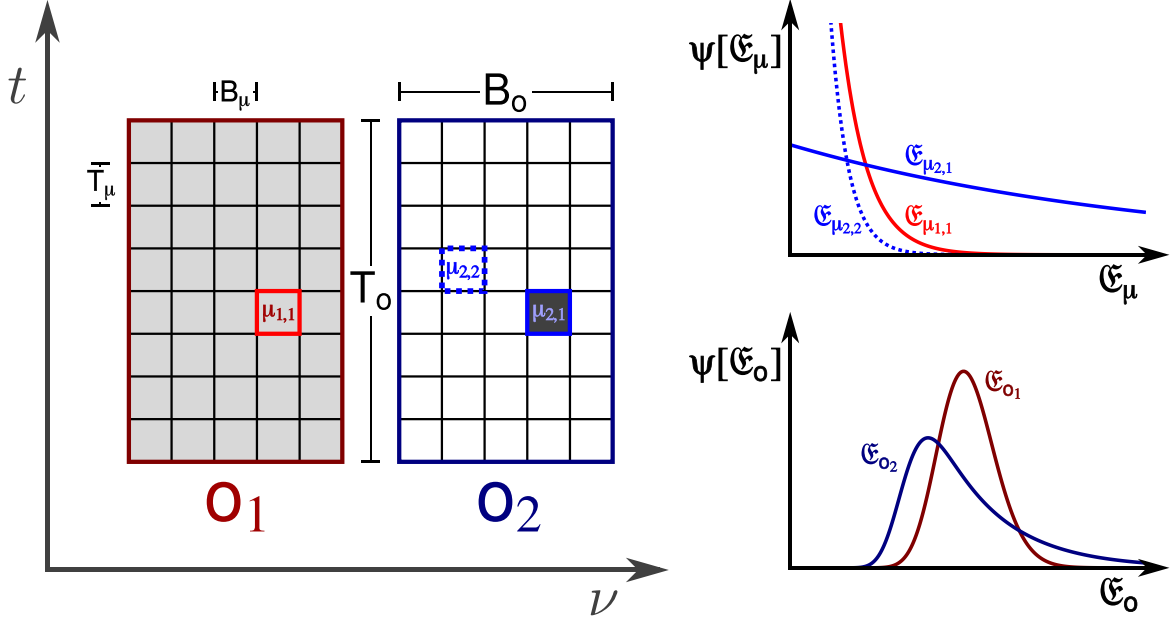


Figure 6. Radio observations (\mathfrak{o}_1 and \mathfrak{o}_2) measure collected energy by summing over the power in a number of modes (amplitudes). A spectrogram on the left shows two broadcasts, one for each observation. The mean total energy intercepted from the shown broadcasts is the same in \mathfrak{o}_1 and \mathfrak{o}_2 , but although the \mathfrak{o}_1 broadcast's energy is spread out among all cells (light shading), the \mathfrak{o}_2 broadcast's energy is concentrated in one cell (dark shading) and the other cells only have background (white). On the right, the resulting probability densities for the energy per mode (top) and energy per observation (bottom) are shown. The noise variance of $\mathfrak{E}_{\mathfrak{o}_2}$ is greater than that of $\mathfrak{E}_{\mathfrak{o}_1}$ despite having the same mean, a result of the heavier PDF tail.

The full variance for incoherent broadcasts is

$$\begin{aligned} \mathbb{V}[\mathfrak{E}_{\mathfrak{o}}] = N_{\mathfrak{o}}^{\mu} & \left[(k_B \mathcal{T}_n + \mathcal{A} \langle Y_{\mu,M}^{B;1} \rangle \langle \dot{\epsilon}_{\mu|B} \rangle_M)^2 + \mathcal{A}^2 \langle Y_{\mu,M}^{B;2} \rangle \left(\langle \dot{\epsilon}_{\mu|B}^2 \rangle_M + \langle N_{\mu,C}^B \rangle_M \langle \dot{\epsilon}_{\mu|B} \rangle_M^2 \right) \right] \\ & + \mathcal{A}^2 \langle Y_{\mathfrak{o},M}^{B;2} \rangle \left(\langle \dot{\epsilon}_{\mathfrak{o}|B}^2 \rangle_M + \langle N_{\mathfrak{o},C}^B \rangle_M \langle \dot{\epsilon}_{\mathfrak{o}|B} \rangle_M^2 \right). \quad (\text{B28}) \end{aligned}$$

For convenience and intuition's sake when calculating the effective signal-to-noise ratio, we can express this in terms of $\check{\mathfrak{s}}[\mathfrak{e}_{\mathfrak{o}|B}]$ (equation 59) to find the generalization of equation 57:

$$\begin{aligned} \frac{\mathbb{V}[\mathfrak{E}_{\mathfrak{o}}]}{N_{\mathfrak{o}}^{\mu} (k_B \mathcal{T}_n)^2} = & \left(1 + \check{\mathfrak{s}}[\mathfrak{e}_{\mathfrak{o}|B}] \sqrt{N_{\mathfrak{o}}^{\mu}} \frac{\langle Y_{\mu,M}^{B;1} \rangle}{\langle y_{\epsilon;B} \chi_{\epsilon;B} \rangle_{\mathfrak{o},M}} \frac{\langle \dot{\epsilon}_{\mu|B} \rangle_M}{\langle \dot{\epsilon}_{\mathfrak{o}|B} \rangle_M} \right)^2 + \check{\mathfrak{s}}[\mathfrak{e}_{\mathfrak{o}|B}]^2 N_{\mathfrak{o}}^{\mu} \frac{\langle Y_{\mu,M}^{B;2} \rangle}{\langle y_{\epsilon;B} \chi_{\epsilon;B} \rangle_{\mathfrak{o},M}^2} \left(\frac{\langle \dot{\epsilon}_{\mu|B}^2 \rangle_M}{\langle \dot{\epsilon}_{\mathfrak{o}|B} \rangle_M^2} + \langle N_{\mu,C}^B \rangle_M \frac{\langle \dot{\epsilon}_{\mu|B} \rangle_M^2}{\langle \dot{\epsilon}_{\mathfrak{o}|B} \rangle_M^2} \right) \\ & + \check{\mathfrak{s}}[\mathfrak{e}_{\mathfrak{o}|B}]^2 \frac{\langle Y_{\mathfrak{o},M}^{B;2} \rangle}{\langle y_{\epsilon;B} \chi_{\epsilon;B} \rangle_{\mathfrak{o},M}^2} \left(\frac{\langle \dot{\epsilon}_{\mathfrak{o}|B}^2 \rangle_M}{\langle \dot{\epsilon}_{\mathfrak{o}|B} \rangle_M^2} + \langle N_{\mathfrak{o},C}^B \rangle_M \right). \quad (\text{B29}) \end{aligned}$$

B.2.1. The box model and incoherent broadcasts

In the box model, the modes form a contiguous window in time and frequency, with $N_{\mathfrak{o}}^{\mu} = |\Pi_{\mathfrak{o}}| T_{\mathfrak{o}} B_{\mathfrak{o}}$. The mean measured energy $\langle \mathfrak{E}_{\mathfrak{o}} \rangle$ can be found with equation B21.

The full expression for the variance is complicated even with the simplifying approximations of the box model. Narrowband emission in the form of lines is coherent and likely to have frequency drift; they are treated with the chord model (Appendix B.3.3). The box model itself is very useful for wideband broadcasts. If $\beta_B \gg B_{\mathfrak{o}}$, the broadcasts are necessarily incoherent.

I scale $\langle N_{x,C}^B \rangle_M$ and $\langle Y_{x,M}^{B;n} \rangle$ in equation B29 under the assumption that the observation only includes one beam, covering the same sky field in all observations. Thus, $\langle Y_{x,M}^{B;n} \rangle = \langle Y_{o,M}^{B;n} \rangle \langle N_{x,M}^B \rangle / \langle N_{o,M}^B \rangle$. The equations include means of the polarization factor $\zeta_{o|B} \equiv \sum_{p \in \Pi_o} \zeta_{p|B}(p; \varpi_B)$ and its square, with $\langle \zeta_{o|B} \rangle_M = |\Pi_o|/2$.

For incoherent pulses ($\tau_B \ll T_o$, $\beta_B \gg B_\mu$),

$$\frac{\mathbb{V}[\mathfrak{E}_o]}{N_o^\mu (k_B \mathcal{T}_n)^2} \approx \left(1 + \frac{\check{\mathfrak{s}}[\mathfrak{e}_{o|B}]}{\sqrt{N_o^\mu}} \frac{\langle Y_{o,M}^{B;1} \rangle}{\langle y_{\epsilon;B} \chi_{\epsilon;B} \rangle_{o,M}} \right)^2 + \check{\mathfrak{s}}[\mathfrak{e}_{o|B}]^2 \frac{\langle Y_{o,M}^{B;n} \rangle}{\langle y_{\epsilon;B} \chi_{\epsilon;B} \rangle_{o,M}^2} \left[\frac{\langle \hat{\epsilon}_{\nu;B}^2 \rangle_M}{\langle \hat{\epsilon}_{\nu;B} \rangle_M^2} \frac{4 \langle \zeta_{o|B}^2 \rangle_M}{|\Pi_o|^2} \left(1 + \frac{\langle \zeta_{\mu|B}^2 \rangle_M |\Pi_o|^2 T_o}{\langle \zeta_{o|B}^2 \rangle_M N_o^\mu T_\mu} \right) + \langle N_{o,C}^B \rangle_M \left(1 + \frac{1}{N_o^\mu} \right) \right]. \quad (\text{B30})$$

Hisses ($\tau_B \gg T_o$, $\beta_B \gg B_o$) include steady continuum sources and have

$$\frac{\mathbb{V}[\mathfrak{E}_o]}{N_o^\mu (k_B \mathcal{T}_n)^2} \approx \left(1 + \frac{\check{\mathfrak{s}}[\mathfrak{e}_{o|B}]}{\sqrt{N_o^\mu}} \frac{\langle Y_{o,M}^{B;1} \rangle}{\langle y_{\epsilon;B} \chi_{\epsilon;B} \rangle_{o,M}} \right)^2 + \check{\mathfrak{s}}[\mathfrak{e}_{o|B}]^2 \frac{\langle Y_{o,M}^{B;2} \rangle}{\langle y_{\epsilon;B} \chi_{\epsilon;B} \rangle_{o,M}^2} \left[\frac{\langle \hat{\rho}_{\nu;B}^2 \rangle_M}{\langle \hat{\rho}_{\nu;B} \rangle_M^2} \frac{4 \langle \zeta_{o|B}^2 \rangle_M}{|\Pi_o|^2} \left(1 + \frac{\langle \zeta_{\mu|B}^2 \rangle_M |\Pi_o|^2}{\langle \zeta_{o|B}^2 \rangle_M N_o^\mu} \right) + \langle N_{o,C}^B \rangle_M \left(1 + \frac{1}{N_o^\mu} \right) \right]. \quad (\text{B31})$$

Lines with $\beta_B \ll B_o$ necessarily have a coherence time $\tau_{c;B} \gg B_o^{-1} \geq T_\mu$ (see section 5.4).¹⁸

B.3. Coherent radio broadcasts

The mean energy in coherent broadcasts is correlated between different times. This leads to a prolonged ‘‘plateau’’ in the covariance where it takes on values of order the variance. In a fully coherent broadcast, there is no variance and thus no covariance. A partially coherent broadcast can be viewed as band-limited Gaussian white noise, the sum of a continuum of small random sinusoids with slightly different frequencies, and so fluctuates with wave noise on long timescales.

B.3.1. Dredrifting, energy conservation, and the chord model

Coherent radio broadcasts are narrowband, immediately suggesting the use of the chord model. The details of how we look for putative signals with incoherent dredrifting complicates this relatively simple picture, however.

A line drifts across $|\delta_B| T_o$ of bandwidth over an observation, a long-term smearing effect. If this is greater than B_o and $T_o/T_d > 1$, the center of the line moves into different frequency channels in different dynamic spectra. Summing along one channel results in the loss of power. The modes are first summed into intermediate data blocks (d), each with the same bandwidth as the channel as a whole ($B_d = B_o$). Each data block d_j is then shifted in frequency by an amount $-(\Theta_{d_j} - \Theta_o) \Delta_o$, ‘‘straightening out’’ the skewed lines on the spectrogram that represent drifting signals. A broadcast that starts out at drift rate δ_B in the inertial frame then is treated as though it has a new drift rate $\delta'_B = \delta_B - \Delta_o$. This simple translate-and-add method splits the window ‘‘box’’ into several boxes strung along a chord with Δ_o in the inertial-frame (raw) spectrogram. As such, the chord model does not actually apply after dredrifting – we have a ‘‘pseudochord’’ model for these observations, as opposed to the ‘‘true chord’’ model that applies when $\Delta_o = 0$.

The amount of time that a broadcast spends in the reconstructed ‘‘box’’ in the dredrifting frame can be shorter or longer than the naive prediction based on δ'_B , a result of ‘‘shadowing’’ effects of the different inertial-frame boxes and the chord running out of the constructed observation window and then reentering it. The effects of the dredrifting can be described by a parameter

$$\xi_{\tau; o|B} \equiv \frac{\langle \tau_{o|B} |\delta_B \rangle_{o,M}}{\langle \tau_{o|B}^{\text{CHORD}} |\delta_B = \delta'_B \rangle_{o,M}} = \langle \tau_{o|B} |\delta_B \rangle_{o,M} \frac{1 + |\delta'_B| T_o / B_o}{T_o}, \quad (\text{B32})$$

where $\tau_{o|B}^{\text{CHORD}}$ is the duration that would apply if we were working in a ‘‘true’’ chord model with $\delta_B = \delta'_B$ and $\Delta_o = 0$.

¹⁸ No signal can meaningfully have $\tau_B \ll T_\mu$ and $\beta_B \ll B_\mu$ simultaneously, so there is no strict blip regime for radio broadcasts.

There are four basic regimes of behavior, as shown in Figure 7. Regime A is closest to the simple chord model, where a chord is not likely to pass straight through the bandwidth of a channel during a single data window. Regime D is also fairly simple – in both the inertial frame and the dedrifted frame, the broadcast has high drift rate, passing through the observation window once and never returning. Regime C represents a relatively successful dedrifted of a high- δ_B broadcast. A well-known issue with this dedrifted method is that the data block’s duration imposes a short-term smearing in frequency: the broadcast enters and leaves the datum’s bandwidth before the next datum can correct, spreading the energy over many channels. Like long-term smearing, this reduces sensitivity. Regime B, however, is not as familiar, because it represents a case where dedrifted *ruins* a broadcast already with low drift rate. In this case, the data block’s duration imposes a minimum “exposure” that is much longer than naively expected from δ'_B – a kind of apparent short-term desmearing. However, it is also possible for a broadcast ostensibly in the frequency range of the dedrifted channel to be “missed” as the data blocks skip over wide intervals in frequency (pink shading in the figure). Although regime B does not apply to a detection, it still comes up when considering the sample variance of the broadcast population.

Both the mean number and typical time the broadcast spend in an observation are affected by the dedrifted process. The product of the two is constant, a fundamental result that is needed for energy conservation. Suppose we had a population of broadcasts, all with the same drift rate and the same luminosity. The mean amount of energy intercepted per window is proportional to $\langle N_{x,M}^B \rangle \langle \dot{\epsilon}_{x|B} \rangle = \langle N_{x,M}^B \rangle \langle \dot{\ell}_B \rangle \langle \zeta_{x|B} \rangle \langle \tau_{x|B} \rangle \propto \langle N_{x,M}^B \rangle \langle \tau_{x|B} \rangle$. Now suppose that the instantaneous bandwidth of the observation is B_x at all times, even though which frequencies are covered can shift from one moment to the next. When averaged over all samples, the mean aggregate emission of a population is unaffected by drift rate, as long as the abundance of lines is approximately constant over the entire bandwidth spanned by the observation. This is a consequence of frequency translation symmetry and conservation of energy. If a larger spread of drift rate resulted in $\langle N_{x,M}^B \rangle$ going down for one channel, then it should do so for the next one, and the one after that, and the one after that, and so on. That would mean that the summed energy over the bandwidth $\gtrsim 2B_x \bar{\delta}_M$ has also decreased. But where could the energy have gone? The broadcasts are still shining as brightly; they merely have shifted around within that bandwidth. Additionally, for every broadcast that leaves the window, we expect one broadcast to enter on average.

Thus, as a general principle,

$$\frac{d \langle N_{x,M}^B \rangle}{d \delta_B} \langle \tau_{x|B} | \delta_B \rangle_M = \langle N_{x,M}^B \rangle \Psi[\delta_B]_{x,M} \langle \tau_{x|B} | \delta_B \rangle_M = \langle N_{x,g}^* \rangle Z_M^B B_x T_x \Psi[\delta_B]_M. \quad (\text{B33})$$

Integrating over drift rate also gives us

$$\langle N_{x,M}^B \rangle \langle \tau_{x|B} \rangle_M = \langle N_{0;o,M}^B \rangle T_x = \langle N_{x,g}^* \rangle Z_M^B B_x T_x. \quad (\text{B34})$$

Finally, putting the luminosity back in, a robust result of energy conservation is

$$\langle N_{x,M}^B \rangle \langle \dot{\epsilon}_{x|B} \rangle_M = \langle N_{0;x,M}^B \rangle \langle \dot{\ell}_B \rangle_M \langle \zeta_{x|B} \rangle_M T_x = \langle N_{0;o,M}^B \rangle \langle \dot{\ell}_B \rangle_M \frac{|\Pi_x| B_x}{2 B_o} T_x. \quad (\text{B35})$$

This average applies also to weighted numbers, like $\langle N_{x,M}^{B;n} \rangle$ and even $\langle Y_{x,M}^{B;n} \rangle$:

$$\langle Y_{x,M}^{B;n} \rangle \langle \dot{\epsilon}_{x|B} \rangle_M = \langle Y_{0;x,M}^{B;n} \rangle \langle \dot{\ell}_B \rangle_M \langle \zeta_{x|B} \rangle_M T_x \text{ and } \langle N_{x,M}^{B;n} \rangle \langle \dot{\epsilon}_{x|B} \rangle_M = \langle N_{0;x,M}^{B;n} \rangle \langle \dot{\ell}_B \rangle_M \langle \zeta_{x|B} \rangle_M T_x, \quad (\text{B36})$$

which can be seen by applying the energy conservation principle to the population in each small region of the galaxy and then adding.

B.3.2. Covariance for coherent broadcasts

For the covariance, I adopt the form (see equation B24)

$$\text{Cov}[\mathbf{e}_{\mu_1|B}, \mathbf{e}_{\mu_2|B}] = [\mathcal{A} \mathcal{I}_{\mathbf{e};\mu}(\boldsymbol{\theta}_B) y_{\epsilon;B} \dot{\ell}_B]^2 \cdot \chi_{\epsilon;\mu_1|B} \tau_{\mu_1|B} \zeta_{\mu_1|B} \cdot \chi_{\epsilon;\mu_2|B} \tau_{\mu_2|B} \zeta_{\mu_2|B} \cdot \left[g_{p;B}^{(2)}(|\Theta_{\mu_1} - \Theta_{\mu_2}|) - 1 \right] \cdot \begin{cases} 1 & \text{if } p(\mu_1) = p(\mu_2) \\ \xi_{pp;B} & \text{if } p(\mu_1) \neq p(\mu_2) \end{cases}. \quad (\text{B37})$$

The coherence function $g_{p;B}^{(2)}(\Delta t) = \langle |\mathbf{a}_B(t)|^2 |\mathbf{a}_B(t + \Delta t)|^2 \rangle_\infty / \langle |\mathbf{a}_B(t)|^2 \rangle_\infty^2$ is well-known in quantum optics, describing the covariance between the intensity of electromagnetic radiation at two different times separated by Δt in a single

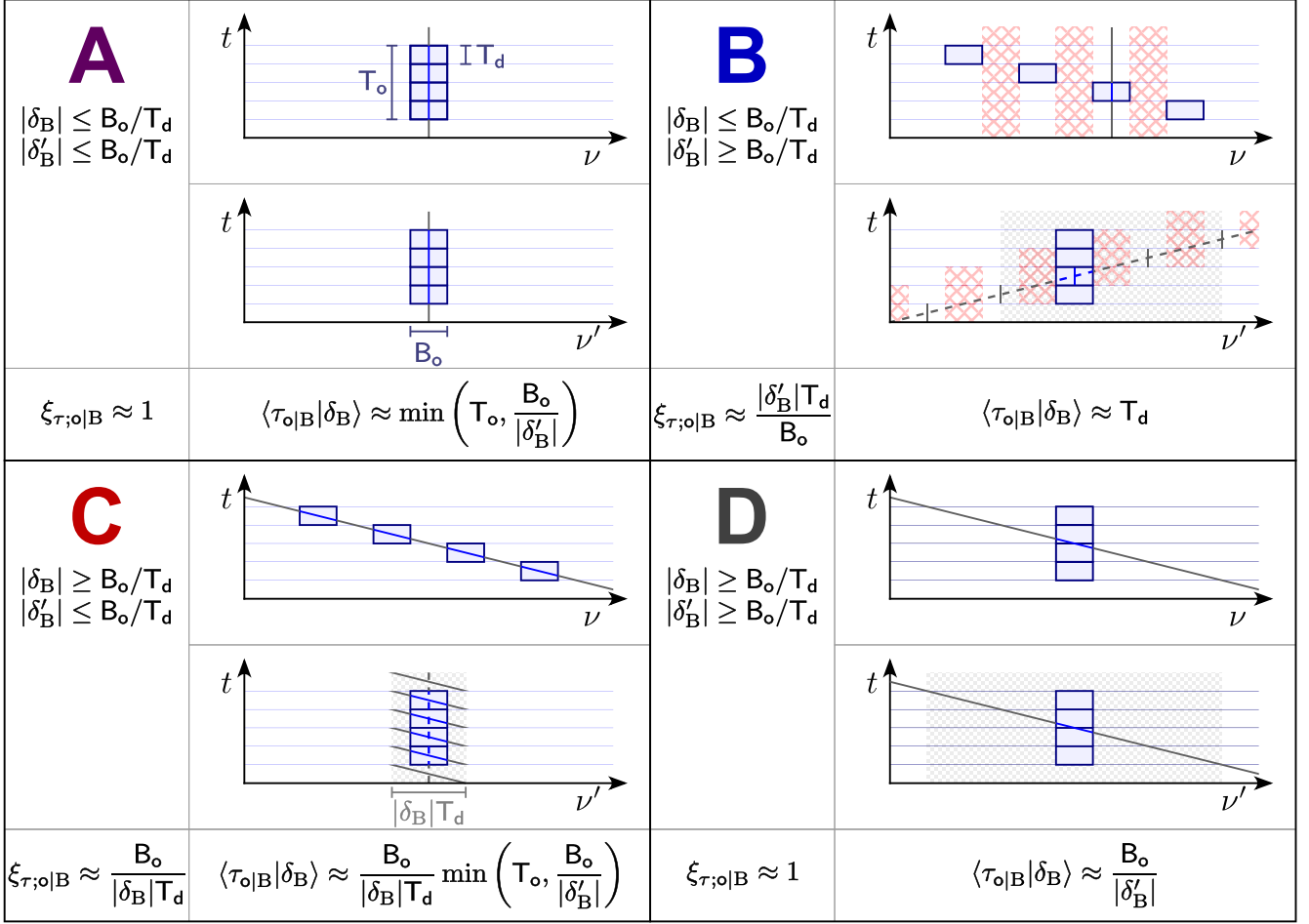


Figure 7. The total energy from a narrowband broadcast sampled by a window, as well as the mean number of broadcasts sampled, depends on both the intrinsic drift rate δ_B and the “observed” drift rate δ'_B . Dedrifting slices up spectrograms into data bins of duration T_d , applying a frequency shift linear in time, inducing an apparent drift rate δ'_B (dotted lines). Within each data bin, however, there is no frequency shift, so the broadcast behaves as if it has the original drift rate δ_B (solid lines). Examples from each of the four regimes are shown. Within each regime, the observation window is constructed from data subwindows (blue boxes). The top spectrogram in each regime sketches the spectrogram before dedrifting is applied; the bottom one shows the spectrogram constructed by dedrifting. In regimes B, C, and D, the line is smeared (grey checkerboard shading). The pink hatched shading for the regime B spectrograms shows where a line is missed by the observation, falling through the gaps despite falling in the nominal bandwidth of the dedrifted channel. A line in one of these gaps would be picked up in one of the neighboring channels. The $\xi_{\tau;o|B}$ factor expresses the ratio between the time the chord spends in the dedrifted observation and the time predicted in the true chord model.

polarization (e.g., Foellmi 2009; Tan et al. 2014; Guerin et al. 2017; Tan & Kurtsiefer 2017; Hippke 2021).¹⁹ As an approximation, I adopt a step function:

$$g_{p;B}^{(2)}(\Delta t) - 1 = \begin{cases} 1 & \text{if } \Delta t \leq \tau_{c;B}/2 \text{ and not perfectly coherent} \\ 0 & \text{if } \Delta t > \tau_{c;B}/2 \text{ or perfectly coherent,} \end{cases} \quad (\text{B38})$$

although the exact form depends on the spectrum of the broadcast (Tan & Kurtsiefer 2017) and is identically zero for a perfectly coherent radiation source. The instantaneous bandwidth $\beta_{t|B}$ of the chord is approximately $\tau_{c;B}^{-1}$. In order

¹⁹ The averaging over the amplitudes and their product is defined to be over a sufficiently long timescale $\gg \tau_{c;B}$, such that the amplitudes fluctuate chaotically. If the averaging is only done over $\ll \tau_{c;B}$, the fluctuations will not be accounted for, and $g_{p;B}^{(2)}$ will appear to be 1 for all sampled Δt , just as for a perfectly coherent source.

for the chord model to be valid, the line needs a coherence time $\gtrsim \mathbf{B}_\circ^{-1}$, though this still leaves open the possibility that $\tau_{c;B} \ll \mathbf{T}_\circ$.

The polarization bears some special discussion. Coherent light is always polarized, and the polarization state remains approximately constant over time intervals shorter than the coherence timescale (Hecht 1998). In this sense, coherent broadcasts are always polarized, when viewed on short enough timescales. On timescales longer than $\sim \tau_{c;B}$, the polarization state may or may not fluctuate, depending on whether the fluctuations in each polarization are correlated. This is what the $\xi_{pp;B}$ factor describes. If the broadcast is unpolarized on long timescales (like a thermal source with a narrow bandpass filter applied), then the fluctuations in one polarization are independent of those in the other on any delay timescale. This is clear when we consider thermal emission, where the two independent polarizations are essentially different messengers. We then set $\xi_{pp;B} = 0$. But if the broadcast has a constant polarization on long timescales (e.g., a linear polarizer is placed in front of the transmitter, and we observe both linear polarizations), then the fluctuations are correlated. For example, if the broadcast is fully linear polarized at an angle 45° , the amplitudes in both polarizations will increase and decrease in tandem. For fully polarized broadcasts, $\xi_{pp;B} = 1$.

Now we must sum over all the modes the broadcast crosses. The modes generally form a grid in time and frequency, with matching points in each polarization. It is clearer to sum along different polarizations first, to bring out all the polarization dependence, before summing along time and frequency. We start by picking one of the polarizations from Π_\circ , dubbed \bar{p} here, and stripping the observation down to that polarization, for a new window $\circ \cap \bar{p}$. The modes in this new window still cover all the time-frequency pairs, and we can use it to define a sum over the time and frequency regions covered by the observation. Equation B37 then is written as

$$\begin{aligned} \sum_{\mu_1, \mu_2 \in \mathcal{S}_\circ^{\mathfrak{H}}} \text{Cov}[\mathbf{e}_{\mu_1|B}, \mathbf{e}_{\mu_2|B}] &= [\mathcal{A}\mathcal{L}_{\mathfrak{E};\mu}(\boldsymbol{\theta}_B) y_{\epsilon;B} \hat{\ell}_B]^2 \sum_{\mu_1, \mu_2 \in \mathcal{S}_{\circ \cap \bar{p}}^{\mathfrak{H}}} \chi_{\epsilon;\mu_1|B} \tau_{\mu_1|B} \cdot \chi_{\epsilon;\mu_2|B} \tau_{\mu_2|B} \left[g_{p;B}^{(2)}(|\Theta_{\mu_1} - \Theta_{\mu_2}|) - 1 \right] \\ &\cdot \sum_{p_1, p_2 \in \Pi_\circ} \zeta_{\mu_1|B} \zeta_{\mu_2|B} (1 \cdot \mathbb{I}[p_1 = p_2] + \xi_{pp;B} \cdot \mathbb{I}[p_1 \neq p_2]). \end{aligned} \quad (\text{B39})$$

Remember, $\zeta_{\mu_1|B}$, $\zeta_{\mu_2|B}$, and $\xi_{pp;B}$ describe the *mean* emission of the broadcast, not the fluctuations – they should be constants in the chord model, regardless of the instantaneous polarization state. The sum over polarizations can be solved explicitly, noting that $\zeta_{p(p_2)|B} = 1 - \zeta_{p(p_1)|B}$ for orthogonal polarizations p_1 and p_2 :

$$\xi_{pp; \circ|B} \equiv \sum_{p_1, p_2 \in \Pi_\circ} \zeta_{\mu_1|B} \zeta_{\mu_2|B} (1 \cdot \mathbb{I}[p_1 = p_2] + \xi_{pp;B} \cdot \mathbb{I}[p_1 \neq p_2]) = \zeta_{\circ|B}^2 - 2\zeta_{\bar{p}|B}(1 - \zeta_{\bar{p}|B})(1 - \xi_{pp;B}) \mathbb{I}[|\Pi_\circ| = 1]. \quad (\text{B40})$$

I write the total sum over all modes as

$$\sum_{\mu_1, \mu_2 \in \mathcal{S}_\circ^{\mathfrak{H}}} \text{Cov}[\mathbf{e}_{\mu_1|B}, \mathbf{e}_{\mu_2|B}] = [\mathcal{A}\mathcal{L}_{\mathfrak{E};\mu}(\boldsymbol{\theta}_B) y_{\epsilon;B} \chi_{\epsilon;B} \hat{\ell}_\circ]^2 \xi_{c; \circ|B}, \quad (\text{B41})$$

with

$$\xi_{c; \circ|B} \equiv \xi_{pp; \circ|B} \frac{1}{\tau_{\circ|B}^2 \zeta_{\circ|B}^2} \sum_{\mu_1, \mu_2 \in \mathcal{S}_{\circ \cap \bar{p}}^{\mathfrak{H}}} \tau_{\mu_1|B} \tau_{\mu_2|B} \left[g_{p;B}^{(2)}(|\Theta_{\mu_1} - \Theta_{\mu_2}|) - 1 \right]. \quad (\text{B42})$$

As in previous sections, I assume that transmittance solely depends on position. All of the complications in the chord running in and out of the window while competing against the finite coherence time are stuffed into this sum. To do a full calculation for all possible cases is beyond the scope of the paper, because of all the different regimes shown in Figure 7. Its value can be calculated in some cases:

- If the broadcast is perfectly coherent, there are no fluctuations to contribute to the covariance, and thus $\xi_{c; \circ|B} = 0$.
- If the coherence time is much longer than $\tau_{\circ|B}$ (which may be longer than the naive $\tau_{\circ|B}^{\text{CHORD}}$, however), then $g_{p;B}^{(2)} - 1$ is always 1 whenever the ‘‘chord’’ is in the observation window, regardless of how dedrifting is affecting things. Then we are simply summing all the $\tau_{\mu|B}$ twice, once for $\tau_{\mu_1|B}$ and once for $\tau_{\mu_2|B}$. Within any chord-like model, $\sum_{\mu \in \mathcal{S}_\circ^{\mathfrak{H}}} \tau_{\mu|B} = \tau_{\circ|B}$, so $\xi_{c; \circ|B} = \xi_{pp; \circ|B} / \zeta_{\circ|B}^2$.
- When $\Delta_\circ = 0$, then we are working in the true chord model, and the broadcast enters and leaves the window once. The inner summation over μ_2 essentially integrates for a duration $\tau_{c;B}$, subject to additional cutoffs when the chord enters and leaves the observational window:

$$\sum_{\mu_2 \in \mathcal{S}_{\circ \cap \bar{p}}^{\mathfrak{H}}} \tau_{\mu_2|B} [g_{p;B}^{(2)}(|\Theta_{\mu_1} - \Theta_{\mu_2}|) - 1] \approx \min(\vartheta_{\circ|B} + \tau_{\circ|B}, \Theta_{\mu_1} + \tau_{c;B}/2) - \max(\vartheta_{\circ|B}, \Theta_{\mu_1} - \tau_{c;B}/2) \approx \min(\tau_{c;B}, \tau_{\circ|B}). \quad (\text{B43})$$

Here $\vartheta_{\circ|B}$ is when the chord enters the observation window, either because the window itself begins or the chord has drifted into the window's bandpass; $\vartheta_{\circ|B} + \tau_{\circ|B}$ is when the chord leaves, either because the window ends or it drifts out of the frequency range. There are two natural limits: when $\tau_{\mu|B} \ll \tau_{c;B} \ll \tau_{\circ|B}$, this sum is usually $\sim \tau_{c;B}$, and when $\tau_{\circ|B} \ll \tau_{c;B}$, it is $\tau_{\circ|B}$. The sum over μ_1 integrates the time the chord spends in the observational window, which is $\tau_{\circ|B}$. Thus,

$$\xi_{c;\circ|B} \approx \frac{\xi_{pp;\circ|B}}{\xi_{\circ|B}^2} \min\left(1, \frac{\tau_{c;B}}{\tau_{\circ|B}}\right). \quad (\text{B44})$$

- If $\tau_{\mu|B} \ll \tau_{c;B} \ll T_d$ for a typical ‘‘datum’’ window d used for dedrifting, then the inner sum over μ_2 is nonzero usually within only one such datum. Hence we have

$$\xi_{c;\circ|B} \approx \frac{\xi_{pp;\circ|B}}{\xi_{\circ|B}^2} \min\left(1, \frac{\tau_{c;B}}{\tau_{d|B}}\right). \quad (\text{B45})$$

B.3.3. Variance for coherent broadcast populations

The full expression for the energy variance is found by taking the weighted mean sum of the covariance terms for all the broadcasts in the sample. Applying Campbell's theorem, the average over broadcast samples for a single society is:

$$\left\langle \sum_{\mathbf{w}_B \in \Sigma_{\circ,C}^B} \sum_{\mu_1, \mu_2 \in S_{\circ}^{\mu}} \text{Cov}[\mathbf{e}_{\mu_1|B}, \mathbf{e}_{\mu_2|B}] \middle| \mathbf{w}_C \right\rangle \approx \langle N_{\circ,C}^B \rangle [\mathcal{A} y_{\epsilon;C} \chi_{\epsilon;C} \mathcal{I}_{\epsilon;\circ}(\boldsymbol{\theta}_C)]^2 \langle \xi_{\circ|B}^2 \rangle_C \langle \xi_{c;\circ|B} \rangle_C \mathbb{I}[\mathbf{w}_C \in W_{\circ}^C]. \quad (\text{B46})$$

Another application of Campbell's theorem for the societal distribution, assuming that societies are interchangeable, gives us the average over all samples,

$$\left\langle \sum_{\mathbf{w}_B \in \Sigma_{\circ}^B} \sum_{\mu_1, \mu_2 \in S_{\circ}^{\mu}} \text{Cov}[\mathbf{e}_{\mu_1|B}, \mathbf{e}_{\mu_2|B}] \right\rangle \approx \mathcal{A}^2 \langle Y_{\circ,M}^{B;2} \rangle \langle \xi_{\circ|B}^2 \rangle_M \langle \xi_{c;\circ|B} \rangle_M. \quad (\text{B47})$$

Finally, we arrive at the total variance:

$$\begin{aligned} \mathbb{V}[\boldsymbol{\epsilon}_{\circ}] \approx N_{\circ}^{\mu} & \left[\left(k_B \mathcal{T}_n + \mathcal{A} \langle Y_{\mu,M}^{B;1} \rangle \langle \dot{\epsilon}_{\mu|B} \rangle_M \right)^2 + \mathcal{A}^2 \langle Y_{\mu,M}^{B;2} \rangle \langle N_{\mu,C}^B \rangle_M \langle \dot{\epsilon}_{\mu|B} \rangle_M^2 \right] \\ & + \mathcal{A}^2 \langle Y_{\circ,M}^{B;2} \rangle \left(\langle \xi_{\circ|B}^2 \rangle_M (1 + \langle \xi_{c;\circ|B} \rangle_M) + \langle N_{\circ,C}^B \rangle_M \langle \dot{\epsilon}_{\circ|B} \rangle_M^2 \right). \quad (\text{B48}) \end{aligned}$$

All of the dependence of the variance on the drift rate distribution comes from the term proportional to $\langle \xi_{\circ|B}^2 \rangle_M (1 + \langle \xi_{c;\circ|B} \rangle_M)$. This sample variance term decreases as the spread of drift rates increases: while more broadcasts are intercepted, the amount of energy caught falls because they cross the window more quickly, and the quadratic dependence on $\dot{\epsilon}_{\circ|B}$ is the stronger effect.

The terms constant and linear in $\langle \dot{\ell}_B \rangle_M \langle \tau_{\mu|B} \rangle_M$ in equation B48 are known (as in Cordes et al. 1997). One noise variance term in the incoherent expression is missing, reflecting the lack of wave noise in a perfectly coherent signal. Despite the lack of self-interference in individual broadcasts, the mutual interference when there is more than one broadcast adds an additional kind of wave noise. Whenever $\langle N_{\mu,M}^B \rangle \gg \langle \dot{\ell}_B^2 \rangle_M / \langle \dot{\ell}_B \rangle_M^2$, equation 61 converges to the incoherent limit of equation 57. This is, of course, what we expect from the central limit theorem. Furthermore, the partially coherent case ($\langle \xi_{c;\circ|B} \rangle_M \sim 1$) adds a term that effectively magnifies the sample variance, and this term can lead to much greater variance than in the incoherent case.

To understand intuitively how the variance is affected by drift rate, it is helpful to write it in terms of the expected number of broadcasts and individual broadcast signal-to-noise ratio if the drift rate is zero ($\check{\mathfrak{s}}_0[\mathbf{e}_{\circ|B}]$; equation 64).

Most of the terms simplify through the application of conservation of energy (equation B35).

$$\frac{\mathbb{V}[\mathbf{c}_o]}{N_o^\mu (k_B \mathcal{T}_n)^2} \approx \left(1 + \frac{\check{\mathfrak{s}}_0[\mathbf{c}_o|B]}{\sqrt{N_o^\mu}} \frac{\langle Y_{0;o,M}^{B;1} \rangle}{\langle y_{\epsilon;B} \chi_{\epsilon;B} \rangle_{o,M}} \right)^2 + \check{\mathfrak{s}}_0[\mathbf{c}_o|B]^2 \frac{\langle Y_{0;o,M}^{B;2} \rangle}{\langle y_{\epsilon;B} \chi_{\epsilon;B} \rangle_{o,M}^2} \left[\frac{4 \langle \zeta_{p|B}^2 \rangle_M \langle \dot{\ell}_B^2 \rangle_M \xi_{\delta;o,M}^B}{|\Pi_o|^2 \langle \dot{\ell}_B \rangle_M^2} \right. \\ \left. (1 + \langle \xi_{c;o|B} \rangle_M) + \langle N_{0;o,C}^B \rangle_M \left(1 + \frac{1}{N_o^\mu} \right) \right], \quad (\text{B49})$$

where $\xi_{\delta;o,M}^B \equiv \langle \tau_{o|B}^2 \rangle_M / [\langle \tau_{o|B} \rangle_M \mathcal{T}_o]$. Paper I presented calculations for $\langle \tau_{o|B}^2 \rangle_M$ in the true chord model ($\Delta_o = 0$)

B.3.4. Serendipitous lines in the chord model

Whether or not we have found a line through a deliberate dedrifting search, there is also be a background of “serendipitous” lines. If all lines have the same intrinsic flux, the “brightest” line will be the one that happens to be closest to being dedrifting by accident for whatever Δ_o is used, the one with the smallest $|\delta'_B|$ if $\mathcal{T}_o \gg \mathcal{T}_d$. This can be roughly estimated by calculating the minimum drift rate magnitude expected in a survey. Using the results of Paper I, the minimum drift rate magnitude in a population sampled by window x is found as

$$F[|\delta'_B|]_{x,M} (\delta_{x;M}^L) = 1 - \frac{1}{\langle N_{x;M}^B \rangle} \ln \left[\frac{1}{2} \left(e^{\langle N_{x;M}^B \rangle} + 1 \right) \right]. \quad (\text{B50})$$

if $N_{x;M}^B$ is Poissonian (which in general requires the diffuse approximation).

Let us suppose the uniform drift rate distribution holds, with the distribution centered at Δ_M^B and having a width $\bar{\delta}_M$ (equation 19). To simplify things further, assume $|\Delta_M^B - \Delta_o| \leq \bar{\delta}_M$, and $\delta_{x;M}^L \leq \bar{\delta}_M - |\Delta_M^B|$, which excludes the possibility that $\delta_{x;M}^L$ spills off the edges of the uniform distribution. It can be shown that

$$\frac{\delta_{x;M}^L}{B_x / \mathcal{T}_x} = \sqrt{\left(\bar{u}_{x;M}^2 + 2\bar{u}_{x;M} + (U'_{x;M})^2 \right) \left(1 - \frac{1}{\langle N_{x;M}^B \rangle} \ln \left[\frac{1}{2} \left(e^{\langle N_{x;M}^B \rangle} + 1 \right) \right] \right) + 1 - 1}. \quad (\text{B51})$$

The scaled quantities $\bar{u}_{x;M} \equiv \bar{\delta}_M \mathcal{T}_x / B_x$ and $U'_{x;M} \equiv (\Delta_M^B - \Delta_o) \mathcal{T}_x / B_x$ express drift rates in “natural units” of B_x / \mathcal{T}_x .

To calculate the “brightest” expected signal from serendipitous lines, we want to consider all lines caught by all observations of the target galaxy. Thus, the appropriate window to use in equation B51 covers each point of the sky for the entire dwell time and the entire bandwidth. Now, the bandwidth in a pointing is generally very large in a radio SETI search, at least a few hundred kilohertz if not many megahertz or gigahertz. The frequency window is large enough that broadcasts drift in or out only at the very edge, and $\bar{u}_{s;M}, |U'_{s;M}| \ll 1$. When $\langle N_{s;M}^B \rangle \gtrsim 1$,

$$\delta_{s;M}^L \approx \frac{\bar{\delta}_M \ln 2}{\langle N_{s;M}^B \rangle}, \quad (\text{B52})$$

with one line with $|\delta'_B| \approx \delta_{s;M}^L$ expected. As the number of background lines increases, the minimum drift rate magnitude falls proportionally. Eventually, we expect some to be dedrifting by chance. For a fixed Δ_o with $\mathcal{T}_o \gg \mathcal{T}_d$, a line is dedrifting when the long-term smearing effect is smaller than the bandwidth of a channel or the short-term smearing effect, $\delta'_B \leq \max(|\Delta_o| \mathcal{T}_d / \mathcal{T}_o, B_o / \mathcal{T}_o)$. On average, this is achieved when

$$\langle N_{s;M}^B \rangle \gtrsim \frac{\bar{\delta}_M \ln 2}{\max(|\Delta_o| \mathcal{T}_d / \mathcal{T}_o, B_o / \mathcal{T}_o)} \text{ implying } \langle N_{0;o,M}^B \rangle \gtrsim \frac{\bar{u}_{o;M} \ln 2}{\max(|\Delta_o| \mathcal{T}_d / B_o, 1)} \frac{B_o \langle N_{o,g}^* \rangle}{B_s \langle N_{s,g}^* \rangle}. \quad (\text{B53})$$

The serendipitous contribution to $N_{o,M}^{B;\text{eff}}$ then proceeds through the sparse and confusion regimes for these “brightest” dedrifting lines.

Although lines may be sparse enough that the typical trial Δ_o has no dedrifting lines, the optimal signal-to-noise is found for a specific Δ_o that matches the δ_B of any specific line. This improvement in performance is modeled with the $I_{o,M}^B$ variable set to 1. This line, by careful dedrifting, achieves an effective bandwidth of $\hat{\beta}_{o;t|B}^{\min} \approx \max(B_o, |\Delta_o| \mathcal{T}_d)$.

But if an observation has intercepted multiple lines, all of equal flux, it is unlikely that any one dedrifted line happens to coincide with the maximum fluctuations in the background of lines. Thus, the optimal signal-to-noise ratio depends on whether the signal-to-noise from an intentionally dedrifted line rises above that of the serendipitous lines.

From these considerations, we have

$$N_{\circ,M}^{\text{B;eff}} \approx \max \left(\frac{I_{\circ,M}^{\text{B}}}{\max(1, |\Delta_{\circ}| T_{\text{d}} / B_{\circ})}, \Delta N_{\circ,M}^{\text{B;eff}} \right) \quad (\text{B54})$$

with the serendipitous contribution

$$\Delta N_{\circ,M}^{\text{B;eff}} = \begin{cases} 0 & \text{if } \mathbb{M} [N_{\text{s},M}^{\text{B}}] = 0 \\ \max \left[\frac{B_{\circ}}{\hat{\beta}_{\circ:t|B}} \right]_{\text{s}|M} \approx \min \left(\frac{\langle N_{\text{s},M}^{\text{B}} \rangle B_{\circ}}{\bar{\delta}_M T_{\circ} (\ln 2)}, 1 \right) & \text{if } \mathbb{M} [N_{\text{s},M}^{\text{B}}] \geq 1 \text{ and } \delta_{\text{s};M}^L \geq \max \left(|\Delta_{\circ}|, \frac{B_{\circ}}{T_{\circ}} \right) \\ \frac{\mathbb{M} \left[\max \left[N_{\circ,M}^{\text{B}} (|\delta'_{\text{B}}| \leq \hat{\beta}_{\circ:t|B}^{\min}) \right] \right] - \langle N_{\circ,M}^{\text{B}} (|\delta'_{\text{B}}| \leq \hat{\beta}_{\circ:t|B}^{\min}) \rangle}{\max(1, |\Delta_{\circ}| T_{\text{d}} / B_{\circ})} & \text{if } \delta_{\text{s};M}^L < \max \left(|\Delta_{\circ}|, \frac{B_{\circ}}{T_{\circ}} \right) \end{cases} \quad (\text{B55})$$

when $T_{\circ} \gg T_{\text{d}}$. When no dedrifting correction is applied ($\Delta_{\circ} = 0$, $\hat{\beta}_{\circ:t|B}^{\min} = B_{\circ}$), and $\bar{u}_{\circ;M} \geq 1$, it can be shown with the results of Paper I, Appendix C that

$$\langle N_{\circ,M}^{\text{B}} (|\delta'_{\text{B}}| \leq \hat{\beta}_{\circ:t|B}^{\min}) \rangle = \langle N_{\circ;M}^{\text{B}} \rangle \frac{3}{2\bar{u}_{\circ;M}}, \quad (\text{B56})$$

keeping $\Delta N_{\circ,M}^{\text{B;eff}} \sim 1$ well past the point at which a low drift rate population would be confused. These effective numbers are defined relative to the brightness of a zero-drift line.

B.3.5. Evaluating sample confusion and sensitivity in surveys for drifting lines

To estimate when sample confusion sets in for a survey, I presuppose $I_{\circ,M}^{\text{B}} = 1$ and ignore the serendipitous contribution. The sample variance gives an upper limit on the signal-to-noise ratio. Under the usual assumptions (diffuse approximation, identical luminosities, two polarizations observed, distant galaxy, $T_{\circ} \gg T_{\text{d}}$),

$$\check{\mathfrak{E}}[\mathfrak{E}_{\circ}] \lesssim \frac{1}{\max(1, |\Delta_{\circ}| T_{\text{d}} / B_{\circ})} \left[\langle N_{0;\circ,M}^{\text{B};2} \rangle \xi_{\delta;\circ,M}^{\text{B}} (1 + \langle \xi_{\text{c};\circ|B} \rangle_M) \right]^{-1/2}. \quad (\text{B57})$$

Thus, confusion necessarily sets in for this particular dedrifted observation when

$$\langle N_{0;\circ,M}^{\text{B};2} \rangle > \left[\bar{\mathfrak{E}}_{\text{s}}^2 \max \left(1, \frac{|\Delta_{\circ}|^2 T_{\text{d}}^2}{B_{\circ}^2} \right) \xi_{\delta;\circ,M}^{\text{B}} (1 + \langle \xi_{\text{c};\circ|B} \rangle_M) \right]^{-1} \quad (\text{B58})$$

Applying equation B51 to the observation window, it can be shown that this roughly corresponds to there being $[\bar{\mathfrak{E}}_{\text{s}}^2 \max(1, |\Delta_{\circ}| T_{\text{d}} / B_{\circ})]^{-1}$ serendipitously dedrifted lines per observation.

The conventional assumption is that broadcasts are extremely rare. Thus, we will need to dedrift observations by an amount $\Delta_{\circ} \approx \delta_{\text{B}}$, typically by $\sim \langle |\delta_{\text{B}}| \rangle_M$, a value that may be high for broad drift rate distributions. Yet when there are many broadcasts, some will happen to have a drift rate near 0 by chance, as long as the drift rate distribution extends to zero and the lines have linear drift.

This has two consequences. First, sample confusion only occurs when there are a lot of broadcasts. Because surveys (generally) are made of many observations, there is likely to be a fortuitously dedrifted broadcast for a $\Delta_{\circ} = 0$ observation well before confusion sets in. Confusion only prevents detection if it prevents detection *at every tried drift rate, including those near zero*. The ‘‘confusion limits’’ on our sensitivities to broadcasts should therefore be evaluated for $\Delta_{\circ} = 0$,

$$\langle N_{0;\circ,M}^{\text{B};2} \rangle > \left[\bar{\mathfrak{E}}_{\text{s}}^2 \xi_{\delta;\circ,M}^{\text{B}} (1 + \langle \xi_{\text{c};\circ|B} \rangle_M) \right]^{-1}. \quad (\text{B59})$$

Accordingly, wider drift rate distributions actually preserve our sensitivity against confusion, because more broadcasts are summed into the background of any one observation.

Second, the EIRP sensitivity of a SETI survey is sensitive to smearing. For narrowband observations with incoherent dedrifting, the sensitivity loss can be significant (Margot et al. 2021) – for a *typical* line. But for high enough values

of $\langle N_{\circ,M}^B \rangle$, a survey is expected to find lines with zero drift, for which the smearing penalty does not apply. Thus, sensitivity loss from drift is dependent on the mean number of broadcasts that are intercepted by the survey. This is basically for the same reason that a survey is more likely to make a detection if there are many broadcasts with a broad luminosity distribution: with so many broadcasts, some will be so far on the high-luminosity tail that they should be detectable.

Lines with significant curvature in their drifts are subject to more smearing, as they do not remain at zero drift for long. This problem would plague even coherent dedrifting and would require more advanced techniques that fit higher-order terms to the drifts. Nonetheless, the same basic points should apply if some lines lack curvature by chance.

C. DERIVATION OF PHOTON COUNTING VARIANCE

This appendix presents a short derivation of the noise variance when counting photons from broadcasts. From equation A12, we find the sample variance

$$\mathbb{V}[\langle \mathfrak{Q}_o | \Sigma_o^B, \Sigma_o^C \rangle] = \mathcal{A}^2 \left[\langle \hat{q}_{o|B}^2 \rangle_M + \langle N_{\circ,C}^B \rangle_M \langle \hat{q}_{o|B} \rangle_M^2 \right] \langle Y_{x,M}^{B;2} \rangle, \quad (\text{C60})$$

where $Y_{\circ,M}^{B;2}$ employs the photon distance $d_q = d_M$. For the noise variance, we start by noting that the total number of collected photons is simply a linear sum, with no cross-interference:

$$\mathfrak{Q}_o = \mathfrak{q}_{o|n} + \sum_{\mathbf{w}_C \in \Sigma_{\circ,M}^C} \sum_{\mathbf{w}_B \in \Sigma_{\circ,C}^B} \mathfrak{q}_{o|B}. \quad (\text{C61})$$

Furthermore, the broadcasts of a society are independent of each other, and the aggregate emission of the societies in the metasociety are also independent; all are independent of the background noise. Hence, it follows from independence that the individual variances add and

$$\mathbb{V}[\mathfrak{Q}_o | \Sigma_o^B, \Sigma_o^C] = \langle \mathfrak{q}_{o|n} \rangle + \sum_{\mathbf{w}_C \in \Sigma_{\circ,M}^C} \sum_{\mathbf{w}_B \in \Sigma_{\circ,C}^B} \mathbb{V}[\mathfrak{q}_{o|B}]. \quad (\text{C62})$$

The background noise is almost certainly Poissonian, but it is possible that the variance in the photon broadcasts is not. Sub-Poissonian photon statistics are possible for artificial transmitters, while artificial modulation can greatly increase the variance of individual broadcasts. But if the broadcasts each have Poissonian photon statistics (as unmodulated lasers do),

$$\mathbb{V}[\mathfrak{Q}_o | \Sigma_o^B, \Sigma_o^C] = \langle \mathfrak{q}_{o|n} \rangle + \sum_{\mathbf{w}_C \in \Sigma_{\circ,M}^C} \sum_{\mathbf{w}_B \in \Sigma_{\circ,C}^B} \langle \mathfrak{q}_{o|B} \rangle. \quad (\text{C63})$$

The noise variance is then the mean over all samples. First, the results of Appendix A apply; equation A4 for photons is

$$\left\langle \sum_{\mathbf{w}_C \in \Sigma_{\circ,M}^C} \sum_{\mathbf{w}_B \in \Sigma_{\circ,C}^B} \langle \mathfrak{q}_{o|B} \rangle \right\rangle = \Xi_M^C \mathcal{A} \langle \hat{q}_{o|B} \rangle_M \langle N_{\circ,C}^B \rangle_M \int_{\mathcal{V}_o} \mathcal{I}_{\Omega; \circ}(\mathbf{r}_*) y_{q;B}(\mathbf{r}_*) \chi_{q;B}(\mathbf{r}_*) \frac{d \langle N_{\circ,g}^* \rangle}{d \mathbf{r}_*} d \mathbf{r}_*, \quad (\text{C64})$$

as long as the societies are interchangeable and extinction depends only on position. Some algebra gives us

$$\mathbb{V}[\mathfrak{Q}_o] = \langle \mathfrak{q}_{o|n} \rangle + \mathcal{A} \langle \hat{q}_{o|B} \rangle_M \langle Y_{\circ,M}^{B;1} \rangle + \mathcal{A}^2 \left[\langle \hat{q}_{o|B}^2 \rangle_M + \langle N_{\circ,C}^B \rangle_M \langle \hat{q}_{o|B} \rangle_M^2 \right] \langle Y_{\circ,M}^{B;2} \rangle, \quad (\text{C65})$$

which can also be expressed as

$$\frac{\mathbb{V}[\mathfrak{Q}_o]}{\langle \mathfrak{q}_{o|n} \rangle} = 1 + \frac{\check{s}[\mathfrak{q}_{o|B}]}{\sqrt{\langle \mathfrak{q}_{o|n} \rangle}} \frac{\langle Y_{\circ,M}^{B;1} \rangle}{\langle y_{q;B} \rangle_M} + \check{s}[\mathfrak{q}_{o|B}]^2 \left(\frac{\langle \hat{q}_{o|B}^2 \rangle_M}{\langle \hat{q}_{o|B} \rangle_M^2} + \langle N_{\circ,C}^B \rangle_M \right) \frac{\langle Y_{\circ,M}^{B;2} \rangle}{\langle y_{q;B} \rangle_M^2} \quad (\text{C66})$$

for convenience when calculating signal-to-noise ratio.

D. MAXIMUM OF MANY POISSON RANDOM VARIABLES

Suppose we have a fixed number N° of independent samples, each containing N^J events, and we would like to estimate the maximum N^J among those N° samples, $\max[N^J]$. The median $\mathbb{M}[\max[N^J]]$ provides a typical estimate. Each N^J has a Poisson distribution with a mean $\langle N^J \rangle$. In particular, for equally bright broadcasts and insignificant background, the maximum \mathfrak{S} achieved is determined by the difference between the maximum number of broadcasts intercepted by an instrument and the mean.

The cumulative mass function (CMF) of the N^J is given by the regularized upper incomplete gamma function, $Q(n+1, \langle N^J \rangle)$. Then, by extreme value theory (Gumbel 1958; Castillo et al. 2005; see Paper I), the maximum of N° independent realizations has $P(n \leq \langle N^J \rangle) = [Q(n+1, \langle N^J \rangle)]^{N^\circ}$. There is no analytic expression for $\langle \max[N^J] \rangle$ that I am aware of, but the median is defined by

$$[Q(\mathbb{M}[\max[N^J]] + 1, \langle N^J \rangle)] = e^{-(\ln 2)/N^\circ} \approx 1 - \frac{\ln 2}{N^\circ}, \quad (\text{D67})$$

with the approximation becoming more precise when $N^\circ \gg 1$.

The Poisson distribution function is discrete, leading to jumps in the CMF. Note also that $Q(n+1, \langle N^J \rangle)$ includes the probability that $N^J = \lfloor n \rfloor$. I use a continuous probability distribution that treats N^J as a continuous quantity.

 D.1. Sparse limit: $\langle N^J \rangle \ll 1$

When the typical observation is expected to be empty, the Poisson probability falls off exponentially with $\langle N^J \rangle$. The CMF starts out near 1 for $N^J = 0$, and each time N^J is incremented, virtually all of the remainder is eliminated. Thus, to a good approximation,

$$P(N^J < n; \langle N^J \rangle) = Q(n, \langle N^J \rangle) \approx 1 - \frac{\langle N^J \rangle^n}{n!}. \quad (\text{D68})$$

By taking advantage of Stirling's approximation, $n! \approx (n/e)^n \sqrt{2\pi n}$, some algebra gives us

$$\mathbb{M}[\max[N^J]] \approx \left[\langle N^J \rangle \exp \left[1 + W_0 \left(\frac{1}{\langle N^J \rangle e} \ln \left[\frac{N^\circ e^{-\langle N^J \rangle - 1}}{\ln 2 \sqrt{2\pi} \langle N^J \rangle} \left(\frac{\mathbb{M}[\max[N^J]] + 1/2}{\mathbb{M}[\max[N^J]]} \right)^{\mathbb{M}[\max[N^J]] + 1/2} \right) \right] \right] - 1/2 \right] \quad (\text{D69})$$

using the principal branch of the Lambert W function, W_0 , and after rounding down because N^J is a discrete variable. The right-hand side depends on $\mathbb{M}[\max[N^J]]$, but the dependence is fairly weak for $\mathbb{M}[\max[N^J]] \gtrsim 1$, approaching \sqrt{e} , giving us

$$\mathbb{M}[\max[N^J]] \approx \left[\langle N^J \rangle \exp \left[1 + W_0 \left(\frac{1}{\langle N^J \rangle e} \ln \left[\frac{N^\circ e^{-\langle N^J \rangle - 1/2}}{\ln 2 \sqrt{2\pi} \langle N^J \rangle} \right] \right) \right] - 1/2 \right]. \quad (\text{D70})$$

Equation D70 is an excellent approximation when $N^\circ \gg 1$. The argument for W_0 is generally quite small, but an adequate approximation is $W_0(x) \approx \ln x + \ln \ln x \cdot (1/\ln x - 1)$ (Roy & Olver 2010). Its argument must be $\geq -1/e$ to be valid. Several terms are needed, however; taking $W_0(x) \rightarrow \ln x$ leads to underestimates of $\mathbb{M}[\max[N^J]]$ (Figure 8).

 D.2. Confusion limit: $\langle N^J \rangle \gg 1$

In the confusion limit, the Poisson distribution approaches a normal distribution with mean and variance $\langle N^J \rangle$. Although this approximation does not necessarily hold far out on the tails of the distribution, it suggests that

$$\mathbb{M}[\max[N^J]] = \langle N^J \rangle + C \sqrt{\langle N^J \rangle}, \quad (\text{D71})$$

with $C \sim 1$, because the normal distribution falls off with each standard deviation and outliers will be rare.

Now, for $x = a + \sqrt{2a}C'$,

$$1 - Q(a+1, x) \approx \frac{1}{2} \operatorname{erfc}(-C') - \frac{1}{3} \sqrt{\frac{2}{\pi a}} (1 + C'^2) e^{-C'^2} \quad (\text{D72})$$

when a is large, with erfc referring to the complementary error function (Paris 2010). In this case, $a \rightarrow \mathbb{M}[\max[N^J]]$ and $x \rightarrow \langle N^J \rangle$, which gives us $C \approx C'/\sqrt{2}$. Furthermore, the second term on the right-hand side is small because

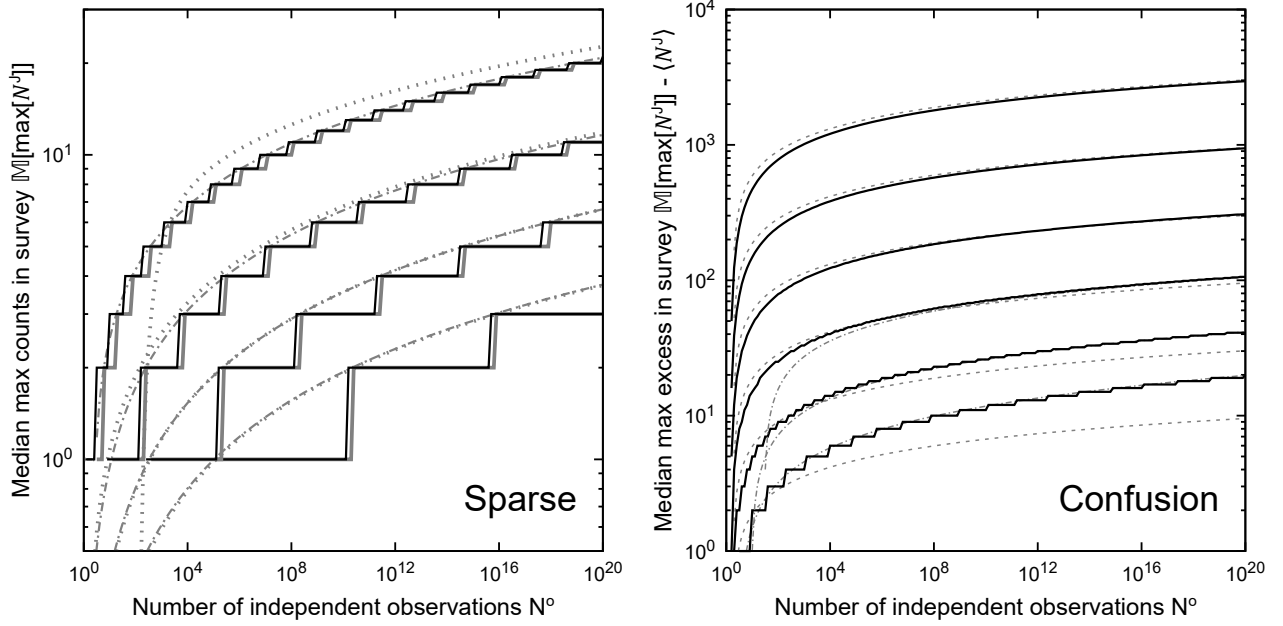


Figure 8. Approximations to $\mathbb{M}[\max[N^J]]$ in the sparse (left) and confusion (right) regimes. On left, the numerically computed value (solid black; equation D67) is compared to estimates (gray): equation D69 (gray solid; without rounding down, dashed-dotted) and equation D70 without rounding down (grey, dotted). On right, the numerical result (solid black) compared to equation D74 (gray dashed) and equation D70 without rounding (gray dashed-dotted). From top to bottom, $\langle N^J \rangle = 1, 10^{-1}, 10^{-2.5}, 10^{-5}$ on the left and $\langle N^J \rangle = 10^5, 10^4, 10^3, 10^2, 10^1, 1$ on the right.

$\mathbb{M}[\max[N^J]] \approx \langle N^J \rangle$ is large by assumption, and it is suppressed rapidly as u increases past 1. Thus,

$$u \approx \sqrt{2} \operatorname{erf}^{-1} \left[2 \left(\frac{1}{2} \right)^{1/N^o} - 1 \right]. \quad (\text{D73})$$

For large N^o , this can be written as $C^2 \approx W_0[N^{o2}/(2\pi(\ln 2)^2)]$. The first term of $W_0(x)$ gives us the relatively simple

$$C \sim \sqrt{2 \ln \frac{N^o}{\sqrt{2\pi \ln 2}}}. \quad (\text{D74})$$

This is a poor approximation when $\langle N^J \rangle \sim 1$, but it does well for large $\langle N^J \rangle$ (Figure 8, dashed lines).

Remarkably, equation D70 also does well in the confusion regime when $N^o \gg 1$ (dash-dotted lines), despite equation D68 being a poor approximation. More accurately, $Q(n+1, \langle N^J \rangle) \approx 1 - \langle N^J \rangle^{n+1} / (n+1)! \cdot C \sqrt{\langle N^J \rangle}$ where $C \leq \sqrt{\pi/2}$ decreases with N^o , but the $\mathbb{M}[\max[N^J]]$ only has a logarithmic dependence on the additional factor.

D.3. Applicability to populations of broadcasts

These approximations are used in this paper to estimate the fluctuations in the number of broadcasts for the signal-to-noise ratio. Broadcasts are not generally Poisson; they are clustered into societies. We can ignore this when the diffuse approximation is applicable ($\langle N_{o,C}^B \rangle \ll 1$). Then, $N_{o,C}^B$ is basically a Bernoulli variable flagging the rare societies that are broadcasting in the o window; the societies of a metasociety are a Poisson point process, and a Poisson sum of Bernoulli variables is itself Poisson. The approximations also apply if the number of societies is fixed: perhaps we posit a single society for a survey covering a single star that we are trying to constrain, much like the single metasociety assumption applying for a target galaxy in this paper.

The approximations also apply in a way for the opposite limit, when $\langle N_{o,C}^B \rangle_M \gg \langle N_{o,M}^C \rangle$ and $\gg 1$, if all societies are interchangeable (with $\langle N_{o,C}^B \rangle = \langle N_{o,C}^B \rangle_M$). Then, there are small deviations in the number of broadcasts per society, but very nearly all societies have the same number. The fluctuations in the signal-to-noise ratio are mostly the result of the varying number of societies, with $\mathbb{M}[\max_{o \in \mathcal{S}_o} N_{o,M}^B] \approx \mathbb{M}[\max_{o \in \mathcal{S}_o} N_{o,M}^C] \langle N_{o,C}^B \rangle_M$. Note, however, that the

number of effective observations is much smaller, roughly the number of nonoverlapping pointings – measurements in different channels and likely even different epochs sample the same societies.

REFERENCES

- Aartsen, M. G., Abraham, K., Ackermann, M., et al. 2017, *ApJ*, 835, 151, doi: [10.3847/1538-4357/835/2/151](https://doi.org/10.3847/1538-4357/835/2/151)
- Abbott, B. P., Abbott, R., Abbott, T. D., et al. 2019, *Physical Review X*, 9, 031040, doi: [10.1103/PhysRevX.9.031040](https://doi.org/10.1103/PhysRevX.9.031040)
- Abbott, R., Abbott, T. D., Abraham, S., et al. 2021, *PhRvD*, 104, 022005, doi: [10.1103/PhysRevD.104.022005](https://doi.org/10.1103/PhysRevD.104.022005)
- Abdollahi, S., Acero, F., Ackermann, M., et al. 2020, *ApJS*, 247, 33, doi: [10.3847/1538-4365/ab6bcb](https://doi.org/10.3847/1538-4365/ab6bcb)
- Abeysekara, A. U., Archambault, S., Archer, A., et al. 2016, *ApJL*, 818, L33, doi: [10.3847/2041-8205/818/2/L33](https://doi.org/10.3847/2041-8205/818/2/L33)
- Ackermann, M., Ajello, M., Allafort, A., et al. 2012, *ApJ*, 755, 164, doi: [10.1088/0004-637X/755/2/164](https://doi.org/10.1088/0004-637X/755/2/164)
- Adelson, R. M. 1966, *Journal of the Operational Research Society*, 17, 73
- Ajello, M., Di Mauro, M., Paliya, V. S., & Garrappa, S. 2020, *ApJ*, 894, 88, doi: [10.3847/1538-4357/ab86a6](https://doi.org/10.3847/1538-4357/ab86a6)
- Annis, J. 1999, *Journal of the British Interplanetary Society*, 52, 19. <https://arxiv.org/abs/astro-ph/9901322>
- Baddeley, A. 2007, in *Stochastic Geometry*, ed. W. Weil (Berlin: Springer), 1–75, doi: [10.1007/978-3-540-38175-4_1](https://doi.org/10.1007/978-3-540-38175-4_1)
- Barbour, A. D., & Chryssaphinou, O. 2001, *Annals of Applied Probability*, 964, doi: [10.1214/aoap/1015345355](https://doi.org/10.1214/aoap/1015345355)
- Bas, E. 2019, *Basics of Probability and Stochastic Processes* (Berlin: Springer), doi: [10.1007/978-3-030-32323-3](https://doi.org/10.1007/978-3-030-32323-3)
- Beck, R., Berkhuijsen, E. M., & Hoernes, P. 1998, *A&AS*, 129, 329, doi: [10.1051/aas:1998187](https://doi.org/10.1051/aas:1998187)
- Bell, E. F. 2003, *ApJ*, 586, 794, doi: [10.1086/367829](https://doi.org/10.1086/367829)
- Brin, G. D. 1983, *QJRAS*, 24, 283
- Brown, M. J. I., Jannuzi, B. T., Floyd, D. J. E., & Mould, J. R. 2011, *ApJL*, 731, L41, doi: [10.1088/2041-8205/731/2/L41](https://doi.org/10.1088/2041-8205/731/2/L41)
- Brzycki, B., Siemion, A. P. V., de Pater, I., et al. 2023, *ApJ*, 952, 46, doi: [10.3847/1538-4357/acdee0](https://doi.org/10.3847/1538-4357/acdee0)
- Calabretta, M. R., Staveley-Smith, L., & Barnes, D. G. 2014, *PASA*, 31, e007, doi: [10.1017/pasa.2013.36](https://doi.org/10.1017/pasa.2013.36)
- Carrigan, Richard A., J. 2009, *ApJ*, 698, 2075, doi: [10.1088/0004-637X/698/2/2075](https://doi.org/10.1088/0004-637X/698/2/2075)
- Carroll-Nellenback, J., Frank, A., Wright, J., & Scharf, C. 2019, *AJ*, 158, 117, doi: [10.3847/1538-3881/ab31a3](https://doi.org/10.3847/1538-3881/ab31a3)
- Castillo, E., Hadi, A. S., Balakrishnan, N., & Sarabia, J. M. 2005, *Extreme Value and Related Models with Applications in Engineering and Science* (Hoboken, NJ: Wiley-Interscience)
- Caves, C. M., & Drummond, P. D. 1994, *Reviews of Modern Physics*, 66, 481, doi: [10.1103/RevModPhys.66.481](https://doi.org/10.1103/RevModPhys.66.481)
- Chabrier, G. 2003, *ApJL*, 586, L133, doi: [10.1086/374879](https://doi.org/10.1086/374879)
- Chiu, S. N., Stoyan, D., Kendall, W. S., & Mecke, J. 2013, *Stochastic Geometry and its Applications: Third Edition* (New York: Wiley), doi: [10.1002/9781118658222](https://doi.org/10.1002/9781118658222)
- Ćirković, M. M. 2015, *Serbian Astronomical Journal*, 191, 1, doi: [10.2298/SAJ1591001C](https://doi.org/10.2298/SAJ1591001C)
- . 2018, *The Great Silence: Science and Philosophy of Fermi's Paradox* (New York: Oxford University Press)
- Ćirković, M. M., & Vukotić, B. 2008, *Origins of Life and Evolution of the Biosphere*, 38, 535, doi: [10.1007/s11084-008-9149-y](https://doi.org/10.1007/s11084-008-9149-y)
- Cocconi, G., & Morrison, P. 1959, *Nature*, 184, 844, doi: [10.1038/184844a0](https://doi.org/10.1038/184844a0)
- Condon, J. J. 1974, *ApJ*, 188, 279, doi: [10.1086/152714](https://doi.org/10.1086/152714)
- . 1992, *ARA&A*, 30, 575, doi: [10.1146/annurev.aa.30.090192.003043](https://doi.org/10.1146/annurev.aa.30.090192.003043)
- Condon, J. J., Cotton, W. D., Greisen, E. W., et al. 1998, *AJ*, 115, 1693, doi: [10.1086/300337](https://doi.org/10.1086/300337)
- Condon, J. J., Cotton, W. D., Fomalont, E. B., et al. 2012, *ApJ*, 758, 23, doi: [10.1088/0004-637X/758/1/23](https://doi.org/10.1088/0004-637X/758/1/23)
- Corbet, R. H. D. 1997, *Journal of the British Interplanetary Society*, 50, 253
- Cordes, J. M., Lazio, J. W., & Sagan, C. 1997, *ApJ*, 487, 782, doi: [10.1086/304620](https://doi.org/10.1086/304620)
- Czech, D., Isaacson, H., Pearce, L., et al. 2021, *PASP*, 133, 064502, doi: [10.1088/1538-3873/abf329](https://doi.org/10.1088/1538-3873/abf329)
- Dale, D. A., Helou, G., Contursi, A., Silbermann, N. A., & Kolhatkar, S. 2001, *ApJ*, 549, 215, doi: [10.1086/319077](https://doi.org/10.1086/319077)
- Daley, D. J., & Vere-Jones, D. 2003, *An Introduction to the Theory of Point Processes. Volume I: Elementary Theory and Methods* (New York: Springer), doi: [10.1007/b97277](https://doi.org/10.1007/b97277)
- Delhaize, J., Smolčić, V., Delvecchio, I., et al. 2017, *A&A*, 602, A4, doi: [10.1051/0004-6361/201629430](https://doi.org/10.1051/0004-6361/201629430)
- Dixon, R. S. 1985, in *IAU Symposium, Vol. 112, The Search for Extraterrestrial Life: Recent Developments*, ed. M. D. Papagiannis (Dordrecht: D. Reidel Publishing Co.), 305–314, doi: [10.1007/978-94-009-5462-5_39](https://doi.org/10.1007/978-94-009-5462-5_39)
- Djorgovski, S. G., Mahabal, A., Drake, A., Graham, M., & Donalek, C. 2013, in *Planets, Stars and Stellar Systems. Volume 2: Astronomical Techniques, Software and Data*, ed. T. D. Oswalt & H. E. Bond (Springer), 223, doi: [10.1007/978-94-007-5618-2_5](https://doi.org/10.1007/978-94-007-5618-2_5)

- Draine, B. T., & Lazarian, A. 1998, *ApJL*, 494, L19, doi: [10.1086/311167](https://doi.org/10.1086/311167)
- Dyson, F. J. 1960, *Science*, 131, 1667, doi: [10.1126/science.131.3414.1667](https://doi.org/10.1126/science.131.3414.1667)
- Embrechts, P., Klüppelberg, C., & Mikosch, T. 2013, *Modelling Extremal Events: for Insurance and Finance*, Vol. 33 (Berlin: Springer), doi: [10.1007/978-3-642-33483-2](https://doi.org/10.1007/978-3-642-33483-2)
- Enriquez, J. E., Siemion, A., Foster, G., et al. 2017, *ApJ*, 849, 104, doi: [10.3847/1538-4357/aa8d1b](https://doi.org/10.3847/1538-4357/aa8d1b)
- Evans, N. J., I., Hills, R. E., Rydbeck, O. E., & Kollberg, E. 1972, *PhRvA*, 6, 1643, doi: [10.1103/PhysRevA.6.1643](https://doi.org/10.1103/PhysRevA.6.1643)
- Foellmi, C. 2009, *A&A*, 507, 1719, doi: [10.1051/0004-6361/200911739](https://doi.org/10.1051/0004-6361/200911739)
- Forgan, D. H. 2019, *Solving Fermi's Paradox* (Cambridge: Cambridge University Press), doi: [10.1017/9781316681510](https://doi.org/10.1017/9781316681510)
- Forward, R. L. 1984, *Journal of Spacecraft and Rockets*, 21, 187, doi: [10.2514/3.8632](https://doi.org/10.2514/3.8632)
- Gajjar, V., Perez, K. I., Siemion, A. P. V., et al. 2021, *AJ*, 162, 33, doi: [10.3847/1538-3881/abfd36](https://doi.org/10.3847/1538-3881/abfd36)
- Garrett, M. A. 2015, *A&A*, 581, L5, doi: [10.1051/0004-6361/201526687](https://doi.org/10.1051/0004-6361/201526687)
- Geringer-Sameth, A., Koushiappas, S. M., & Walker, M. G. 2015, *PhRvD*, 91, 083535, doi: [10.1103/PhysRevD.91.083535](https://doi.org/10.1103/PhysRevD.91.083535)
- Gray, R. H., & Mooley, K. 2017, *AJ*, 153, 110, doi: [10.3847/1538-3881/153/3/110](https://doi.org/10.3847/1538-3881/153/3/110)
- Greggio, L., & Renzini, A. 1990, *ApJ*, 364, 35, doi: [10.1086/169384](https://doi.org/10.1086/169384)
- Griffith, R. L., Wright, J. T., Maldonado, J., et al. 2015, *ApJS*, 217, 25, doi: [10.1088/0067-0049/217/2/25](https://doi.org/10.1088/0067-0049/217/2/25)
- Guerin, W., Dussaux, A., Fouché, M., et al. 2017, *MNRAS*, 472, 4126, doi: [10.1093/mnras/stx2143](https://doi.org/10.1093/mnras/stx2143)
- Gumbel, E. J. 1958, *Statistics of Extremes* (New York: Columbia University Press), doi: [10.7312/gumb92958](https://doi.org/10.7312/gumb92958)
- Haenggi, M. 2013, *Stochastic Geometry for Wireless Networks* (Cambridge: Cambridge University Press), doi: [10.1017/cbo9781139043816](https://doi.org/10.1017/cbo9781139043816)
- Harp, G. R., Richards, J., Tarter, J. C., et al. 2016, *AJ*, 152, 181, doi: [10.3847/0004-6256/152/6/181](https://doi.org/10.3847/0004-6256/152/6/181)
- Harris, M. J. 1986, *Ap&SS*, 123, 297, doi: [10.1007/BF00653949](https://doi.org/10.1007/BF00653949)
- . 2002, *Journal of the British Interplanetary Society*, 55, 383, doi: [10.48550/arXiv.astro-ph/0112490](https://doi.org/10.48550/arXiv.astro-ph/0112490)
- Harwit, M. 1981, *Cosmic discovery: The search, scope, and heritage of astronomy* (New York: Basic Books, Inc.)
- Hecht, E. 1998, *Optics: Fourth Edition* (San Francisco: Addison Wesley)
- Hippke, M. 2018, *Acta Astronautica*, 151, 53, doi: [10.1016/j.actaastro.2018.05.038](https://doi.org/10.1016/j.actaastro.2018.05.038)
- . 2021, *AJ*, 162, 1, doi: [10.3847/1538-3881/abf7b7](https://doi.org/10.3847/1538-3881/abf7b7)
- Hippke, M., & Forgan, D. H. 2017, arXiv e-prints, arXiv:1711.05761, doi: [10.48550/arXiv.1711.05761](https://doi.org/10.48550/arXiv.1711.05761)
- Högbom, J. A. 1974, *A&AS*, 15, 417
- Horowitz, P., & Sagan, C. 1993, *ApJ*, 415, 218, doi: [10.1086/173157](https://doi.org/10.1086/173157)
- Howard, A. W., Horowitz, P., Wilkinson, D. T., et al. 2004, *ApJ*, 613, 1270, doi: [10.1086/423300](https://doi.org/10.1086/423300)
- Isaacson, H., Siemion, A. P. V., Marcy, G. W., et al. 2017, *PASP*, 129, 054501, doi: [10.1088/1538-3873/aa5800](https://doi.org/10.1088/1538-3873/aa5800)
- Jarrett, T. H., Cluver, M. E., Brown, M. J. I., et al. 2019, *ApJS*, 245, 25, doi: [10.3847/1538-4365/ab521a](https://doi.org/10.3847/1538-4365/ab521a)
- Jones, E. M. 1981, *Icarus*, 46, 328, doi: [10.1016/0019-1035\(81\)90136-6](https://doi.org/10.1016/0019-1035(81)90136-6)
- Jugaku, J., & Nishimura, S. 2004, in *Bioastronomy 2002: Life Among the Stars*, ed. R. Norris & F. Stootman, Vol. 213 (San Francisco: Astronomical Society of the Pacific), 437, doi: [10.1017/s0074180900193672](https://doi.org/10.1017/s0074180900193672)
- Kardashev, N. S. 1964, *Soviet Ast.*, 8, 217
- Kashibadze, O. G., Karachentsev, I. D., & Karachentseva, V. E. 2020, *A&A*, 635, A135, doi: [10.1051/0004-6361/201936172](https://doi.org/10.1051/0004-6361/201936172)
- Kingman, J. F. C. 1993, *Poisson Processes* (Oxford: Clarendon Press), doi: [10.1093/oso/9780198536932.001.0001](https://doi.org/10.1093/oso/9780198536932.001.0001)
- Kogan, L. 1999, *PASP*, 111, 510, doi: [10.1086/316345](https://doi.org/10.1086/316345)
- Kudale, S., & Chengalur, J. N. 2017, *Experimental Astronomy*, 44, 97, doi: [10.1007/s10686-017-9547-0](https://doi.org/10.1007/s10686-017-9547-0)
- Kuiper, T. B. H., & Morris, M. 1977, *Science*, 196, 616, doi: [10.1126/science.196.4290.616](https://doi.org/10.1126/science.196.4290.616)
- Kulkarni, S. R. 1989, *AJ*, 98, 1112, doi: [10.1086/115202](https://doi.org/10.1086/115202)
- Lacki, B. C. 2015a, arXiv e-prints, arXiv:1501.07309, <https://arxiv.org/abs/1501.07309>
- . 2015b, arXiv e-prints, arXiv:1503.01509, <https://arxiv.org/abs/1503.01509>
- . 2020, *ApJ*, 905, 18, doi: [10.3847/1538-4357/abc1e3](https://doi.org/10.3847/1538-4357/abc1e3)
- Learned, J. G., Kudritzki, R. P., Pakvasa, S., & Zee, A. 2012, *Contemporary Physics*, 53, 113, doi: [10.1080/00107514.2011.640142](https://doi.org/10.1080/00107514.2011.640142)
- Learned, J. G., Pakvasa, S., Simmons, W. A., & Tata, X. 1994, *QJRAS*, 35, 321
- Lebofsky, M., Croft, S., Siemion, A. P. V., et al. 2019, *PASP*, 131, 124505, doi: [10.1088/1538-3873/ab3e82](https://doi.org/10.1088/1538-3873/ab3e82)
- Lehmer, B. D., Alexander, D. M., Bauer, F. E., et al. 2010, *ApJ*, 724, 559, doi: [10.1088/0004-637X/724/1/559](https://doi.org/10.1088/0004-637X/724/1/559)
- Lehmer, B. D., Xue, Y. Q., Brandt, W. N., et al. 2012, *ApJ*, 752, 46, doi: [10.1088/0004-637X/752/1/46](https://doi.org/10.1088/0004-637X/752/1/46)

- Lehmer, B. D., Basu-Zych, A. R., Mineo, S., et al. 2016, *ApJ*, 825, 7, doi: [10.3847/0004-637X/825/1/7](https://doi.org/10.3847/0004-637X/825/1/7)
- Li, D., Gajjar, V., Wang, P., et al. 2020, *Research in Astronomy and Astrophysics*, 20, 078, doi: [10.1088/1674-4527/20/5/78](https://doi.org/10.1088/1674-4527/20/5/78)
- Licquia, T. C., & Newman, J. A. 2015, *ApJ*, 806, 96, doi: [10.1088/0004-637X/806/1/96](https://doi.org/10.1088/0004-637X/806/1/96)
- Lien, A., & Fields, B. D. 2012, *ApJ*, 747, 120, doi: [10.1088/0004-637X/747/2/120](https://doi.org/10.1088/0004-637X/747/2/120)
- Lingam, M., & Loeb, A. 2021, *Life in the Cosmos: From Biosignatures to Technosignatures* (Cambridge, MA: Harvard University Press), doi: [10.4159/9780674259959](https://doi.org/10.4159/9780674259959)
- Malyshev, D., & Hogg, D. W. 2011, *ApJ*, 738, 181, doi: [10.1088/0004-637X/738/2/181](https://doi.org/10.1088/0004-637X/738/2/181)
- Margot, J.-L., Pinchuk, P., Geil, R., et al. 2021, *AJ*, 161, 55, doi: [10.3847/1538-3881/abcc77](https://doi.org/10.3847/1538-3881/abcc77)
- McConnachie, A. W. 2012, *AJ*, 144, 4, doi: [10.1088/0004-6256/144/1/4](https://doi.org/10.1088/0004-6256/144/1/4)
- Messerschmitt, D. G. 2015, *Acta Astronautica*, 107, 20, doi: [10.1016/j.actaastro.2014.11.007](https://doi.org/10.1016/j.actaastro.2014.11.007)
- Meyer, M. J., Zwaan, M. A., Webster, R. L., et al. 2004, *MNRAS*, 350, 1195, doi: [10.1111/j.1365-2966.2004.07710.x](https://doi.org/10.1111/j.1365-2966.2004.07710.x)
- Mineo, S., Gilfanov, M., & Sunyaev, R. 2012, *MNRAS*, 426, 1870, doi: [10.1111/j.1365-2966.2012.21831.x](https://doi.org/10.1111/j.1365-2966.2012.21831.x)
- Moffett, A. J., Ingarfield, S. A., Driver, S. P., et al. 2016, *MNRAS*, 457, 1308, doi: [10.1093/mnras/stv2883](https://doi.org/10.1093/mnras/stv2883)
- Murphy, E. J., Condon, J. J., Schinnerer, E., et al. 2011, *ApJ*, 737, 67, doi: [10.1088/0004-637X/737/2/67](https://doi.org/10.1088/0004-637X/737/2/67)
- Nityananda, R. 1994, in *IAU Symposium*, Vol. 158, *Very High Angular Resolution Imaging*, ed. J. G. Robertson & W. J. Tango (Dordrecht: Kluwer), 11, doi: [10.1007/978-94-011-0880-5_2](https://doi.org/10.1007/978-94-011-0880-5_2)
- Norris, R. P., Hopkins, A. M., Afonso, J., et al. 2011, *PASA*, 28, 215, doi: [10.1071/AS11021](https://doi.org/10.1071/AS11021)
- Nyland, K., Young, L. M., Wrobel, J. M., et al. 2017, *MNRAS*, 464, 1029, doi: [10.1093/mnras/stw2385](https://doi.org/10.1093/mnras/stw2385)
- Oliver, B. M., & Billingham, J. 1971, *Project Cyclops: A Design Study of a System for Detecting Extraterrestrial Intelligent Life*, Vol. NASA-CR-114445 (Mountain View, CA: NASA Ames Research Center)
- Paris, R. B. 2010, in *NIST Handbook of Mathematical Functions*, ed. F. W. J. Olver, D. W. Lozier, R. F. Boisvert, & C. W. Clark (Cambridge University Press), 173–192
- Price, D. C. 2021, in *The WSPC Handbook of Astronomical Instrumentation*, Volume 1: *Radio Astronomical Instrumentation*, ed. A. Wolszczan (Singapore: World Scientific), 159–179, doi: [10.1142/9789811203770_0007](https://doi.org/10.1142/9789811203770_0007)
- Price, D. C., Enriquez, J. E., Brzycki, B., et al. 2020, *AJ*, 159, 86, doi: [10.3847/1538-3881/ab65f1](https://doi.org/10.3847/1538-3881/ab65f1)
- Radhakrishnan, V. 1999, in *Astronomical Society of the Pacific Conference Series*, Vol. 180, *Synthesis Imaging in Radio Astronomy II*, ed. G. B. Taylor, C. L. Carilli, & R. A. Perley (San Francisco: Astronomical Society of the Pacific), 671
- Raimondo, G., Brocato, E., Cantiello, M., & Capaccioli, M. 2005, *AJ*, 130, 2625, doi: [10.1086/497591](https://doi.org/10.1086/497591)
- Rampadarath, H., Morgan, J. S., Tingay, S. J., & Trott, C. M. 2012, *AJ*, 144, 38, doi: [10.1088/0004-6256/144/2/38](https://doi.org/10.1088/0004-6256/144/2/38)
- Roy, R., & Olver, F. W. J. 2010, in *NIST Handbook of Mathematical Functions*, ed. F. W. J. Olver, D. W. Lozier, R. F. Boisvert, & C. W. Clark (Cambridge University Press), 103–134
- Sabater, J., Best, P. N., Hardcastle, M. J., et al. 2019, *A&A*, 622, A17, doi: [10.1051/0004-6361/201833883](https://doi.org/10.1051/0004-6361/201833883)
- Scheuer, P. A. G. 1957, *Proceedings of the Cambridge Philosophical Society*, 53, 764, doi: [10.1017/S0305004100032825](https://doi.org/10.1017/S0305004100032825)
- . 1974, *MNRAS*, 166, 329, doi: [10.1093/mnras/166.2.329](https://doi.org/10.1093/mnras/166.2.329)
- Schwartz, R. N., & Townes, C. H. 1961, *Nature*, 190, 205, doi: [10.1038/190205a0](https://doi.org/10.1038/190205a0)
- Schwarz, U. J. 1978, *A&A*, 65, 345
- Sheikh, S. Z., Wright, J. T., Siemion, A., & Enriquez, J. E. 2019, *ApJ*, 884, 14, doi: [10.3847/1538-4357/ab3fa8](https://doi.org/10.3847/1538-4357/ab3fa8)
- Shostak, S., Ekers, R., & Vaile, R. 1996, *AJ*, 112, 164, doi: [10.1086/117996](https://doi.org/10.1086/117996)
- Siemion, A. P. V., Demorest, P., Korpela, E., et al. 2013, *ApJ*, 767, 94, doi: [10.1088/0004-637X/767/1/94](https://doi.org/10.1088/0004-637X/767/1/94)
- Silva, L., Granato, G. L., Bressan, A., & Danese, L. 1998, *ApJ*, 509, 103, doi: [10.1086/306476](https://doi.org/10.1086/306476)
- Smith, M. W. L., Gomez, H. L., Eales, S. A., et al. 2012, *ApJ*, 748, 123, doi: [10.1088/0004-637X/748/2/123](https://doi.org/10.1088/0004-637X/748/2/123)
- Speagle, J. S., Steinhardt, C. L., Capak, P. L., & Silverman, J. D. 2014, *ApJS*, 214, 15, doi: [10.1088/0067-0049/214/2/15](https://doi.org/10.1088/0067-0049/214/2/15)
- Spekkens, K., Mason, B. S., Aguirre, J. E., & Nhan, B. 2013, *ApJ*, 773, 61, doi: [10.1088/0004-637X/773/1/61](https://doi.org/10.1088/0004-637X/773/1/61)
- Stappers, B. W., Hessels, J. W. T., Alexov, A., et al. 2011, *A&A*, 530, A80, doi: [10.1051/0004-6361/201116681](https://doi.org/10.1051/0004-6361/201116681)
- Stigler, S. M. 1973, *The Annals of Statistics*, 472, doi: [10.1214/aos/1176342412](https://doi.org/10.1214/aos/1176342412)
- Strong, A. W., Porter, T. A., Digel, S. W., et al. 2010, *ApJL*, 722, L58, doi: [10.1088/2041-8205/722/1/L58](https://doi.org/10.1088/2041-8205/722/1/L58)
- Suazo, M., Zackrisson, E., Wright, J. T., Korn, A. J., & Huston, M. 2022, *MNRAS*, 512, 2988, doi: [10.1093/mnras/stac280](https://doi.org/10.1093/mnras/stac280)

- Subotowicz, M. 1979, *Acta Astronautica*, 6, 213, doi: [10.1016/0094-5765\(79\)90157-7](https://doi.org/10.1016/0094-5765(79)90157-7)
- Sullivan, W. T., I., Brown, S., & Wetherill, C. 1978, *Science*, 199, 377, doi: [10.1126/science.199.4327.377](https://doi.org/10.1126/science.199.4327.377)
- Tamm, A., Tempel, E., Tenjes, P., Tihhonova, O., & Tuvikene, T. 2012, *A&A*, 546, A4, doi: [10.1051/0004-6361/201220065](https://doi.org/10.1051/0004-6361/201220065)
- Tan, P. K., & Kurtsiefer, C. 2017, *MNRAS*, 469, 1617, doi: [10.1093/mnras/stx968](https://doi.org/10.1093/mnras/stx968)
- Tan, P. K., Yeo, G. H., Poh, H. S., Chan, A. H., & Kurtsiefer, C. 2014, *ApJL*, 789, L10, doi: [10.1088/2041-8205/789/1/L10](https://doi.org/10.1088/2041-8205/789/1/L10)
- Tarter, J. 1985, in *IAU Symposium*, Vol. 112, *The Search for Extraterrestrial Life: Recent Developments*, ed. M. D. Papagiannis (Dordrecht: D. Reidel Publishing Co.), 271–290, doi: [10.1007/978-94-009-5462-5_37](https://doi.org/10.1007/978-94-009-5462-5_37)
- Tarter, J. 2001, *ARA&A*, 39, 511, doi: [10.1146/annurev.astro.39.1.511](https://doi.org/10.1146/annurev.astro.39.1.511)
- Temi, P., Brighenti, F., & Mathews, W. G. 2007, *ApJ*, 660, 1215, doi: [10.1086/513690](https://doi.org/10.1086/513690)
- Tonry, J., & Schneider, D. P. 1988, *AJ*, 96, 807, doi: [10.1086/114847](https://doi.org/10.1086/114847)
- Tremblay, C. D., & Tingay, S. J. 2020, *PASA*, 37, e035, doi: [10.1017/pasa.2020.27](https://doi.org/10.1017/pasa.2020.27)
- Vernstrom, T., Scott, D., Wall, J. V., et al. 2014, *MNRAS*, 440, 2791, doi: [10.1093/mnras/stu470](https://doi.org/10.1093/mnras/stu470)
- Voros, J. 2013, arXiv e-prints, arXiv:1412.4011. <https://arxiv.org/abs/1412.4011>
- Wasserman, L. 2004, *All of Statistics: A Concise Course in Statistical Inference* (New York: Springer New York), doi: [10.1007/978-0-387-21736-9](https://doi.org/10.1007/978-0-387-21736-9)
- Webb, S. 2015, *If the Universe Is Teeming with Aliens... Where is Everybody?* (Cham, Switzerland: Springer Cham), doi: [10.1007/978-3-319-13236-5](https://doi.org/10.1007/978-3-319-13236-5)
- Wilson, T. L., Rohlfs, K., & Hüttemeister, S. 2009, *Tools of Radio Astronomy* (Berlin: Springer-Verlag), doi: [10.1007/978-3-540-85122-6](https://doi.org/10.1007/978-3-540-85122-6)
- Wlodarczyk-Sroka, B. S., Garrett, M. A., & Siemion, A. P. V. 2020, *MNRAS*, 498, 5720, doi: [10.1093/mnras/staa2672](https://doi.org/10.1093/mnras/staa2672)
- Worden, S. P., Drew, J., Siemion, A., et al. 2017, *Acta Astronautica*, 139, 98, doi: [10.1016/j.actaastro.2017.06.008](https://doi.org/10.1016/j.actaastro.2017.06.008)
- Wright, J. T., Griffith, R. L., Sigurdsson, S., Povich, M. S., & Mullan, B. 2014a, *ApJ*, 792, 27, doi: [10.1088/0004-637X/792/1/27](https://doi.org/10.1088/0004-637X/792/1/27)
- Wright, J. T., Kanodia, S., & Lubar, E. 2018, *AJ*, 156, 260, doi: [10.3847/1538-3881/aae099](https://doi.org/10.3847/1538-3881/aae099)
- Wright, J. T., Mullan, B., Sigurdsson, S., & Povich, M. S. 2014b, *ApJ*, 792, 26, doi: [10.1088/0004-637X/792/1/26](https://doi.org/10.1088/0004-637X/792/1/26)
- Yamamoto, Y., & Haus, H. A. 1986, *Reviews of Modern Physics*, 58, 1001, doi: [10.1103/RevModPhys.58.1001](https://doi.org/10.1103/RevModPhys.58.1001)
- Yun, M. S., Reddy, N. A., & Condon, J. J. 2001, *ApJ*, 554, 803, doi: [10.1086/323145](https://doi.org/10.1086/323145)
- Zackrisson, E., Calissendorff, P., Asadi, S., & Nyholm, A. 2015, *ApJ*, 810, 23, doi: [10.1088/0004-637X/810/1/23](https://doi.org/10.1088/0004-637X/810/1/23)
- Zheng, H., Tegmark, M., Dillon, J. S., et al. 2017, *MNRAS*, 464, 3486, doi: [10.1093/mnras/stw2525](https://doi.org/10.1093/mnras/stw2525)
- Zmuidzinas, J. 2003, *ApOpt*, 42, 4989, doi: [10.1364/AO.42.004989](https://doi.org/10.1364/AO.42.004989)
- . 2015, *ApJ*, 813, 17, doi: [10.1088/0004-637X/813/1/17](https://doi.org/10.1088/0004-637X/813/1/17)